GENETIC AND BIOCHEMICAL STUDIES OF AROMATIC DIOXYGENASE SUBSTRATE SPECIFICITY IN *ACINETOBACTER* SP. STRAIN ADP1

by

DONALD MATTHEW EBY

(Under the direction of Ellen L. Neidle)

ABSTRACT

This dissertation describes the characterization of anthranilate 1,2-dioxygenase. This enzyme and other dioxygenases play an essential role in aromatic compound catabolism by *Acinetobacter* sp. strain ADP1. Two separate enzymes that constitute anthranilate 1,2-dioxygenase were expressed in *Escherichia coli* and purified to homogeneity: a reductase and a terminal dioxygenase. The electron-transferring and catalytic metal centers were identified and characterized. Furthermore, the size and quantity of anthranilate 1,2-dioxygenase subunits were analyzed, and deduced amino acid sequences were used to evaluate evolutionary relatedness among bacterial aromatic ring hydroxylating dioxygenases. Comprehensive activity measurements were completed for anthranilate 1,2-dioxygenase and a homolog, the benzoate 1,2-dioxygenase from ADP1. In additional studies, an ADP1 derived mutant was used to measure the efficiency of generating random mutations and introducing them into the chromosomal *catA* gene that encodes catechol 1,2-dioxygenase. The conditions for mutagenesis were optimized using two different PCR-based approaches for incorporating random mutations. The optimization procedure took advantage of the natural transformability of ADP1-derived strains and the ability to select mutants directly in which mutations has generated non-functional catechol 1,2-dioxygenase enzymes. These studies lay the foundation for continuing efforts to alter the substrate specificity of catechol 1,2-dioxygenase by random mutation. This dissertation also reports investigations aimed at developing an *Acinetobacter* host system for the synthesis of dioxygenases encoded by genes from diverse microorganisms. An expression vector was constructed containing an engineered *Acinetobacter* promoter to facilitate high-level gene expression without the need for a transcriptional activator. To test the system, the wild-type *pcaHG* genes, encoding protocatechuate 3,4-dioxygenase, were deleted from the ADP1 chromosome. These genes were then expressed in trans from the vector, and the effects were determined with regards to growth on protocatechuate or *p*-hydroxybenzoate as the sole carbon source. Furthermore, the expression vector was used to demonstrate that the *pcaHG* genes from a

marine *Roseobacter* isolate could complement the effect of the engineered deletion in the ADP1-derived host strain. Collectively, these studies constitute the beginning steps into engineering ADP1 as a host for altering the substrate specificity and catalytic activity of aromatic dioxygenases in the effort to generate novel growth phenotypes.

INDEX WORDS: Dioxygenase, Acinetobacter, Aromatic compound degradation, Dissertation, Thesis guidelines, Graduate School, Student, Graduate degree, The University of Georgia

GENETIC AND BIOCHEMICAL STUDIES OF AROMATIC DIOXYGENASE SUBSTRATE SPECIFICITY IN *ACINETOBACTER* SP. STRAIN ADP1

by

DONALD MATTHEW EBY

B.S., Rutgers University, 1996

A Dissertation Submitted to the Graduate Faculty of The University of Georgia in Partial Fulfillment of the Requirements for the Degree

DOCTOR OF PHILOSOPHY

ATHENS, GEORGIA

2002

GENETIC AND BIOCHEMICAL STUDIES OF AROMATIC DIOXYGENASE SUBSTRATE SPECIFICITY IN *ACINETOBACTER* SP. STRAIN ADP1

by

DONALD MATTHEW EBY

Major Professor: Dr. Ellen L. Neidle

Committee: Dr. Donald M. Kurtz, Jr.
Dr. Anne O. Summers
Dr. Timothy Hoover
Dr. Robert A. Scott

Electronic Version Approved:

Maureen Grasso
Dean of the Graduate School
The University of Georgia
December 2002

ACKNOWLEDGMENTS

First of all, I would like to thank Ellen for allowing me the considerable freedom in directing my own education at UGA, yet leading me at the appropriate times. Other members of the Neidle lab also deserve my appreciation: Lauren and Becky for their guidance during my first years as a student and Drew for research-stimulating discussions. A sincere thanks to Don Kurtz, Jr., my co-major professor, for allowing my research to extend into biochemistry. Don and his post-doc, Eric Coulter were excellent mentors. I was fortunate to work along side fellow students Zanna Beharry, Nate Cosper, and Alison Buchan. I hope that more collaboration is in the future with these outstanding researchers. Of course, I owe gratitude to my other committee members, Anne Summers, Tim Hoover, and Bob Scott. They have also been understanding and fair advisors.

A completely different type of thanks goes to my many friends outside the University. Thanks to the "team" -- you know who you are. Y'all have mentored me in a very special way and I love you for it. Thank you Ryan and your boat. Thank you Tilley for the scientific dialog with a twist. Thank you family for your unconditional support.

By leaps and bounds above the rest, I owe all my academic honors to Tina. You taught me the wonderful and powerful feeling of self-worth and gave me confidence to continue in my endeavors. In all honesty, I could not have done it without you. This dissertation is dedicated to you.

TABLE OF CONTENTS

Page

CHAPTER 1

INTRODUCTION AND LITERATURE REVIEW

Purpose of Study

Designing biological methods to remove xenobiotic aromatic compounds from water and soil (bioremediation) and generating useful industrial and pharmaceutical arenes with minimal impact to nature (green chemistry) are paramount for our sustainable environment (131, 150). Microbial aromatic ring dioxygenases perform these two functions (11, 52, 60, 76). These enzymes play an essential role in the aerobic catalysis of aromatic compounds in the environment by performing the initial attack and ultimately cleaving the benzene ring. The reaction products of many dioxygenases are useful chiral molecules that are notoriously difficult to synthesize.

Acinetobacter sp. strain ADP1 uses a variety of different ring-hydroxylating and ring-fission dioxygenases to degrade a wide range of aromatic and cyclic substrates as sole sources of carbon and energy (19, 75, 117, 118, 129). ADP1 is easily culturable and has a natural transformation system that facilitates genetic engineering. These qualities make ADP1 an excellent host to assay native dioxygenase enzymes, as well as to express mutated genes and foreign dioxygenases.

Successful engineering of ADP1 for use in bioremediation and biotransformation demands a multi-faceted approach. These techniques

require knowledge of natural aromatic compound metabolism, dioxygenase catalytic activity, substrate specificity, and mechanisms of regulation and expression that control arene degradative pathways. To understand aspects of this research project, background is provided concerning the source and fate of aromatic compounds in the environment and how dioxygenases play a fundamental role in their degradation. Specific studies were conducted to improve understanding of structure/function relationships and substrate specificity. Evolutionary relatedness is discussed for two ring-hydroxylating dioxygenases in ADP1: anthranilate- and benzoate-1,2-dioxygenase (AntDO and BenDO, respectively). The ring-fission catechol 1,2-dioxygenase (CatDO) was used in a model system for developing efficient mutagenesis and transformation protocols to alter enzyme substrate specificity. Expression of a native and a recombinant protocatechuate 3,4-dioxygenase (PcaDO) was investigated to understand the importance of genetic regulation in vivo and to develop a heterologous gene expression system in ADP1.

The Fate of Aromatic Compounds in the Environment

Aromatic compounds are abundant in the environment. Prevalent in nature as the six-carbon ring benzene, arenes are found as structural and protective components of plants, in certain amino acids and hormones, and as a constituent in fossil fuels (4, 22, 110). Lignin, occurring in nature associated with cellulose and hemicelluloses (known as lignocellulose), is a 3-dimensional lattice of aromatic compounds (96). The tremendous mass of this structural plant

polymer synthesized on the Earth makes for the single most abundant source of aromatic compounds. The highly complex and random nature of polymerized aromatic compounds in lignin makes this substance resistant to degradation, as shown by the durability of wood. Despite its stability, lignin is broken down by microbes and is either utilized as a source of carbon and energy or repolymerized into humic substances.

Lignin biodegradation

Natural cycling of the benzene nucleus in aerobic environments is represented in Figure 1.1. Degradation of lignin is initiated predominantly by brown- and white-rot fungi (basidomycetes), although select bacterial populations are known to utilize lignin (4, 96, 97). Biodegradation of lignin is an oxidative process. Peroxidases from fungi generate oxidizing agents such as superoxide anions and hydrogen peroxide to depolymerize lignin, producing a plethora of dimeric and monomeric phenolic intermediates (Fig. 1.2). These products are then methoxylated to remove methyl or alkyl groups from the ring and further oxidized by mono- and di-oxygenase reactions to form a select few arenes containing at least two hydroxyl groups. These catechols are then used as substrates for ring-fission dioxygenases to produce aliphatic compounds that are further metabolized via microbial pathways.

Benzene ring cleavage by microbial oxidative pathways

Complete mineralization of the benzene nucleus is accomplished by a few known aerobic pathways, which are conserved in a diverse array of bacteria and fungi. Two such pathways are the *ortho* (also known as the β-ketoadipate pathway) and the *meta* cleavage pathways (Fig 1.3, (35, 72, 121)). Both pathways use protocatechuate and catechol as the ring fission substrates and are distinguished by the specific carbon-carbon bond that is cleaved. Intradiol (*ortho*) fission of the benzene nucleus occurs at the bond between adjacent carbons bearing hydroxyl groups. Protocatechuate 3,4- and catechol 1,2-dioxygenases, which are both *ortho* cleavage enzymes, break the ring to form di-carboxy muconates. Modified *ortho* cleavage pathways, that degrade chlorinated aromatic pollutants in the environment, include enzymes that are closely related to those of the β-ketoadipate pathway but can handle halogenated substrates (135).

In *meta* cleavage reactions, protocatechuate and catechol are cleaved by the protocatechuate 4,5- and catechol 2,3-dioxygenases, respectively. Fission occurs at the bond between one carbon carrying the hydroxyl group and the adjacent non-hydroxylated carbon to generate muconate semialdehydes (72). Other ring-fission substrates, which undergo a meta-like attack, are gallate (3,4,5-trihydroxybenzoate) and 3-O-methylgallate. They are cleaved at the 3 and 4 positions on the ring by dioxygenases to produce 3-hydroxy-4-carboxymuconates. Distinct from the *meta* and *ortho* routes, pathways degrading aromatic compounds containing hydroxyl groups *para* to each other

(e.g. gentisate, homogentisate, and 3-methylgentisate) contain dioxygenases that cleave the bond between the carbon carrying a carboxyl group and the adjacent hydroxylated carbon (Fig. 1.3, (96)).

Aromatic compound metabolism by Acinetobacter sp. strain ADP1: the β-ketoadipate pathway

Known aromatic and cyclic compounds degraded by ADP1 are all metabolized through the chromosomally encoded β-ketoadipate pathway (Fig. 1.4, (121)). ADP1 does not have plasmid-encoded *meta* cleavage pathways, although some bacteria do use both *ortho* and *meta* cleavage routes (72). The b-ketoadipate pathway has two branches that allow degradation of a variety of aromatic and cyclic hydrocarbons, known as the catechol and protocatechuate branches. Most substrates degraded by ADP1 through the protocatechuate branch come from sources that provide structural and protective functions in plants (160). The strain's ability to utilize different lignin depolymerization products, suggests ADP1 is a representative member in completing lignin biodegradation in natural environments. Salicylate and other alcohols, esters, and aldehydes of benzoate are utilized by ADP1 through benzoate in the catechol branch (86, 87).

So far, ten distinct operons have been identified that encode the catalytic enzymes of the β-ketoadipate pathway (160). Some of these operons also encode porins and permeases that permit transport of substrates into the cytoplasm (25, 29, 118). Additional clustered genes encode regulatory proteins to control expression. Two genetic clusters encode the β-ketoadipate pathway

on the chromosome of ADP1. Each cluster of genes is responsible for metabolism of substrates through either the protocatechuate or the catechol branch.

Protocatechuate branch: the dca-pca-qui-pob-clg-ppa operons

Genes responsible for the protocatechuate branch of the β-ketoadipate pathway comprise a series of at least 40 genes in six operons (italics in Fig. 1.4, (69)). Chlorogenate, an ester formed by plants for protection from pathogens, is cleaved to form quinate and caffeate by the esterase ClgA (160). Oxidation reactions encoded by the *ppa* genes remove propanoate and propenoate groups from lignin metabolites, generating benzoate compounds. The *van* and *pob* genes are responsible for further catalysis of these intermediates to produce protocatechuate. The *qui* genes encode shikimate and quinate catabolism. Transformations in this branch ultimately form protocatechuate, where the *pca* genes encode enzymes that produce tricarboxylic-cycle intermediates. The only exception are the *dca* genes, which are responsible for degrading aliphatic dicarboxylic acids and do not form protocatechuate as an intermediate (not shown in Fig. 1.4).

Catechol branch: the sal-are-ben-cat operons

Growth of ADP1 on benzyl alcohol, benzyl acetate, and *p*-hydroxy benzyl alcohol depends on the *are* genes (86). In vitro analysis has shown that the substrate preference of each enzyme encoded by the *are* genes is broad,

suggesting that ADP1 may grow on a wider range of aryl esters than presently known (87). The product of possible substrates carrying a *para* hydroxyl group on the ring, presumably *p*-hydroxybenzoate, would then be converted to protocatechuate by the enzyme encoded by the *pobA* gene.

Benzoate is first converted to a non-aromatic *cis* diol by BenDO (118). A dehydrogenase, encoded by *benD*, removes the carboxylate side chain and an adjacent hydrogen on benzoate diol to form catechol. Conversion of anthranilate (*o*-aminobenzoate) to catechol is accomplished by AntDO, which is encoded by the *antABC* genes (19). Similar to BenDO, AntDO dihydroxylates its substrate to form catechol directly. An anthranilate diol intermediate has never been identified (45).

Supraoperonic clustering of genes encoding the protocatechuate and catechol branches of the β-ketoadipate pathway

Genes encoding the catabolic routes that funnel aromatic intermediates through either the protocatechuate or catechol branches are clustered within the chomosome forming the specialized regions known as supraoperonic clusters (Fig. 1.5) (5, 47, 160). Most of the genes encoding enzymes that transform aromatic compounds to protocatechuate are located adjacent to each other in the chromosome. One exception is the *van* genes, which are involved in vanillate catabolism. These genes are separated from the *pca* genes by approximately 800 kb in the chromosome (Fig. 1.5) (143). Nearly 270 kb of chromosomal DNA separates the supraoperonic cluster encoding the protocatechuate branch from

the cluster encoding the catechol branch. The *ant* genes are not adjoining the remaining *are-sal-ben-cat* genes, but are separated by almost 1200 kb in the chromosome of ADP1 (19).

As shown in Fig. 1.4, many aromatic compound transformations within the β-ketoadipate pathway are analogous and catalyzed by homologous enzymes (e.g, benzoate versus anthranilate and protocatechuate versus catechol). The metabolically parallel routes, encoded by the supraoperonic clusters, may be the result of evolutionary divergence from ancient genetic duplications (134, 160). Comparison of similar dioxygenases that evolved from common origins, may give insight to specific sequence elements that affect substrate specificity.

Regulation of the genes involved in β-ketoadipate pathway

Operons in each supraoperonic cluster have distinct regulatory systems. Adjacent to most of the catabolic operons encoding the protocatechuate and catechol branches of the β-ketoadipate pathway is a regulator gene, transcribed divergently from a polycistron encoding enzymes that function in the same catabolic pathway (Fig. 1.6) (28, 42, 58, 59, 88, 137). In most cases, an operon encodes catabolism of a substrate that also acts as an effector molecule, interacting with the regulator to induce expression of the operon.

In the catechol branch, the LysR-type regulatory proteins BenM and CatM control the expression of the *ben* and *cat* genes (25, 28, 137). The regulation of the *ben* and *cat* operons is dependent upon intracellular concentrations of the effectors benzoate and *cis,cis*-muconate. The regulons controlled by BenM and

CatM are not mutually exclusive. For example, CatM and BenM both regulate *benABCDE* expression. CatM induces low-level expression of the *benABCDE* operon. In contrast, BenM responds synergistically to both *cis,cis*-muconate and benzoate to achieve high-level transcription of the operon (18, 25).

In the protocatechuate branch, the *pobA* gene and *pca* operon are expressed as separate RNA transcripts, with their expression controlled by the IclR-type regulators, PobR and PcaU, respectively (Fig. 1.6) (42, 59, 151). Similar to the *ben* and *cat* operons, each regulator gene is divergently transcribed from the catalytic operons they regulate. Expression of the *pob* and *pca* genes is induced by the presence of *p*-hydroxybenzoate and protocatechuate, respectively.

Evidence suggests that some form of catabolite repression is involved when ADP1 is grown in the presence of multiple aromatic substrates (54). For example, ADP1 will preferentially degrade benzoate before *p*-hydroxybenzoate, when the transcriptional regulators BenM or CatM are present. A proposed model suggests that BenM and CatM prevent *pobA* expression by repressing transcription of the *pca* genes, thereby inhibiting the expression of a *p*-hydroxybenzoate transporter (14). The *pobA* gene is not expressed when *p*-hydroxybenzoate is absent in the cell.

Importance of dioxygenases in aromatic compound degradation

The microbial dioxygenases are responsible for destabilizing and cleaving the aromatic nucleus, thereby mediating crucial steps in aerobic catabolic

pathways that involve using arenes as sources of carbon and energy (36, 66). The benzene nucleus is very stable, due to the resonance energy that stabilizes the carbon-carbon bond of the aromatic ring (22, 110). Its aromatic nature, as well as its hydrophobicity, makes benzene relatively unreactive. Persistence of aromatic environmental pollutants is a primary example of benzene resiliency in the environment. Hydroxylation of the aromatic ring by dioxygenases alters the electronic configuration, which creates de-stabilization and polarity. Through the action of oxygenases, hydrophobic aromatic compounds become more water-soluble, increasing their bioavalability (96).

Aromatic ring-hydroxylating dioxygenases (ARHDOs) help funnel different aromatic compounds into a limited number of degradation pathways, where aromatic ring-cleaving dioxygenases break open the aromatic benzene nucleus. In this way, diverse aromatic compounds are funneled into a limited number of microbial pathways through a common intermediate, the ring-cleavage substrate (71).

Aromatic Ring-Hydroxylating Dioxygenases (ARHDOs)

The initial enzymatic step catalyzed by ARHDOs is the regio- and stereospecific (*cis*) dihydroxylation of the aromatic ring (Reaction 1.1)

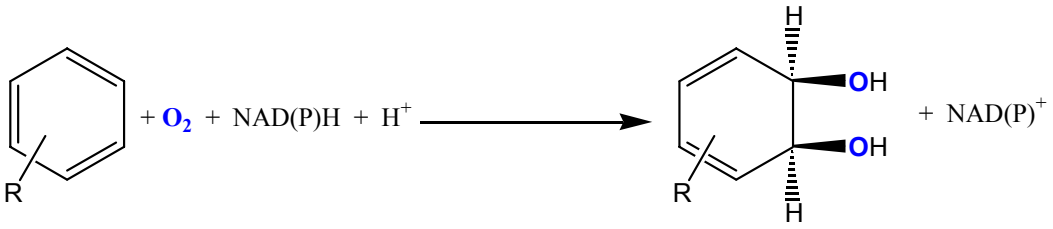

Reaction 1.1 ARHDO-catalyzed dihydroxylation of the aromatic ring

(9, 21). In general, ARHDOs are made up of two or three components. These proteins constitute an electron transfer system to move electrons from NAD(P)H to a terminal dioxygenase, which incorporates O_2 into the aromatic substrate. NAD(P)H is oxidized by a reductase, which contains flavin and sometimes a 2Fe-2S cluster. The reductases, which are mostly monomers, act as oxidoreductases, transferring electrons from NADH to the terminal dioxygenase. In some cases, the electron transfer is direct between the reductase and the terminal dioxygenase (two-component). In others it occurs through an intermediary ferredoxin (three-component, Fig. 1.7).

Terminal dioxygenases are heterologous ($\alpha_x\beta_x$) or homologous (α_x) multisubunit enzymes with the α subunit always containing a Rieske 2Fe-2S cluster and a non-heme mononuclear Fe^{2+} centered at the proposed active site. No prosthetic groups have been found in the β subunits of the bacterial ARHDOs to date (9, 21).

Properties and Proposed Mechanism of AntDO and BenDO

BenDO and AntDO are two-component systems, in which two separate enzymes comprise the ARHDO complex that dihydroxylates the benzene nucleus. A single reductase enzyme transfers electrons directly to a terminal dioxygenase, where catalysis takes place (Fig. 1.8). The BenDO and AntDO terminal dioxygenases have been shown to be similar to the terminal dioxygenase component of the extensively characterized naphthalene 1,2-dioxygenase (NDO) from *Pseudomonas sp*. strain NCIB 9816-4 (30, 94). The crystal structure of the NDO terminal dioxygenase reveals an $\alpha_3\beta_3$ hexamer organized in a "mushroom" shape with the β subunits as the cylindrically shaped "stem" and α subunits as the "cap" (Fig. 1.9). Structural analysis confirms that both the Rieske [2Fe-2S] and non-heme mononuclear catalytic sites reside solely in the α subunits. Two cysteine and two histidine ligands coordinate the diamond-shaped [2Fe-2S] core. Ligands to the mononuclear Fe ion site are a bidentate carboxylate from an aspartate residue,
two nitrogens from hisidine residues, and a solvent molecule. The Fe ion is located towards the C-terminus of the α subunit. To date, the reductase component of NDO has not been as well characterized as the terminal dioxygenase component.

The most detailed analysis of electron transfer in ARHDO reductases has been completed on phthalate dioxygenase reductase (PDR) from *Burkholderia cepacia* DB01, a homolog of benzoate dioxygenase reductase (BDR) and the anthranilate dioxygenase reductase (ADR) (21, 30). Ballou and associates have

determined the structure of PDR with bound NAD, NADH, or pyridine nucleotide analogs and in various redox states by X-ray crystallography (Fig. 1.10, 30, 55, 56). PDR is folded into three domains binding electron transferring centers: FMN binding site at the NH2-terminus, NAD(H) binding near the center of the protein, and [2Fe-2S] center at the COOH-terminus. Structurally, the FMN and NAD(H) binding domains are similar to the corresponding domains in the ferredoxin-NADP+ reductases (FNR) and the [2Fe-2S] domain is closely related to those found in plant-type ferredoxins (56).

Electron transfer mechanism of the reductase

Hydride transfer from NADH to FMN is presumed to occur through a complex in which the nicotinamide stacks alongside the flavin ring (30, 93, 123). The aromatic ring of Phe225 in PDR may act as a gate, which is displaced during electron transfer (Fig. 1.10B). The Phe225 ring is sandwiched between flavin and the nicotinamide group in the structure of NADH-bound, 2-electron reduced PDR. This type of “stacking” contact between flavin and nicotinamide is expected in hydride transfer reactions. (46)

The FMN and [2Fe-2S] prosthetic groups in PDR are arranged so they are in close proximity, near the center of the molecule. Domain packing orients the FMN and [2Fe-2S] moieties so the isoalloxazine rings and the plane of the [2Fe-2S] core are perpendicular. $_1$H nuclear magnetic resonance (NMR) studies on plant ferredoxins suggest that the Fe closest to FMN is reduced by electron transfer from the flavin (44). This Fe is only 7.2 Å from the flavin 8-CH_3, shown

by the structure of PDR (Fig. 1.10B). The short distance between the flavin and ferredoxin affords rapid one electron transfer from the two-electron reduced flavin to the oxidized [2Fe-2S], producing a reduced ferredoxin and flavin in a one-electron reduced semiquinone state. Furthermore, EPR spectra of frozen solutions of PDR reveal an actual interaction between the reduced [2Fe-2S] center and the FMN radical. Two-electron reduced PDR spectrum exhibits g values arising from the existence of both flavin semiquinone and reduced [2Fe-2S]. (30). With PDR in this reduced form, NAD^+ is released and the reductase is ready to transfer electrons to the terminal dioxygenase.

Recently, BDR was purified by Z. M. Beharry and D. M. Eby (92) and the structure solved by Karlsson et al. (92) using X-ray crystallography (Fig. 1.11). The three domains found in PDR are evident in BDR, but are arranged differently. While the flavin and NADH binding domains are in the same relative order, the [2Fe-2S] group is found at the NH_3-terminus in BDR, in contrast to PDR's ferredoxin being at the COOH-terminus. This causes a conspicuous difference between the ferredoxin group positions of PDR and BDR when the flavin and NAD-binding domains are compared (Figs. 1.10A and 1.11A). In BDR, the ferredoxin domain is situated to form hydrogen bonds with both flavin and NAD domains, while the ferredoxin component in PDR interacts exclusively with its flavin domain.

Residues interacting with the flavin and nicotinamide are highly conserved between PDR and BDR, which includes the Phe "gate" (Phe in BDR, Fig. 1.11B). The position of the [2Fe-2S] in BDR is different than in PDR with respect to their

flavins, but the nearest Fe is in close proximity to the 8-CH_3 of the FAD (9.1 Å in BDR), which is similar to the analogous Fe-FMN span in PDR. Because of these similarities, there is likely to be a common electron transfer pathway for PDR and BDR.

In both PDR and BDR, the [2Fe-2S] domain is angled so that space exists for possible binding with their terminal oxygenases. The openings are different in each reductase. BDR leaves space open near the flavin-binding domain while this space in PDR is found on the other side of the protein, between the NAD-binding and ferredoxin domains. The interactions between the reductase and terminal dioxygenase has not been extensively studied in any ARHDO, but it is reasonable to assume a precise association between the enzymes must exist for efficient electron transfer from the reductase ferredoxin to the Rieske ferredoxin in the terminal dioxygenase. Along with the opening found in the quartenary structure of PDR and BDR where the terminal oxygenase may bind and have access to the electron in the reduced [2Fe-2S] center, a prominent indentation on the surface of the α subunits near the Rieske [2Fe-2S] exists in the analogous dioxygenase NDO. This pocket could be a docking point for the ferredoxin component of the NDO system to transfer electron. A similar depression may be found on AntDO and BenDO to interact with their reductases (94). When recombinant BenDO terminal dioxygenase and BDR are expressed and purified together, they form one complex. This multienzyme complex survives anion exchange and size exclusion chromatography, but can be separated by ammonium sulfate precipitation (Beharry et. al, unpublished results). Despite this

tight association, BDR, as well as ADR, can reduce a variety of other proteins. Each reductase can efficiently transfer electrons to either BenDO or AntDO terminal dioxygenases, and also to cytochrome c (7). BDR was used as an oxidoreductase to reduce native and variant recombinant rubrerythrin from *Desulfovibrio vulgaris* (32).

Electron transfer mechanism of the terminal oxygenase

Electron transfer within the terminal oxygenases of AntDO and BenDO begins at the reduced Rieske [2Fe-2S] cluster. Two different types of Rieske clusters have been observed in proteins. They are distinguished by their reduction potentials, which is also a defining characteristic of their biological electron-transfer function. The "structural" Rieske clusters found in cytochrome bc_1/bf_6 complexes have higher reduction potentials (E_m = +150 to +490 mV) than the bacterial multicomponent terminal oxygenase "functional" Rieske clusters (E_m = -150 to –50 mV) (13, 101, 105, 106, 136). X-ray absorption spectroscopy (XAS) of oxidized and reduced Rieske center of AntDO (E_m = -125 mV, estimated from redox potentials of 2-halobenzoate 1,2-dioxygenase and phthalate dioxygenase) was completed by Nate Cosper using prepared samples, made by myself (31). These spectra were compared to XAS of oxidized and reduced forms of two archaeal Rieske ferredoxins (ARF, *Sulfolobus solfataricus* with a E_m = -155 mV, and Sulredoxin ARF from *Sulfolobus sp*. strain 7 with a E_m = +200 mV) (82 and unpublished results). The results suggest that, when reduced, the Fe-N_{imid} bond distance in the Rieske centers of AntDO and *S. solfataricus* ARF

increased by an average of 0.17 Å, compared to a 0.08 Å lengthening in the Fe-N_{imid} bond distance in the Sulredoxin ARF with the higher redox potential (31 and unpublished results). The coordination environment between the structural and functional Rieske centers is identical and is also spectroscopically similar. The difference in the structural changes observed with XAS of oxidized and reduced forms of these ferredoxins may be significant in defining their redox potentials.

Before the structure of NDO was solved, there lacked a plausible pathway for electron transfer from the Rieske center to the mononuclear Fe at the active site within an α subunit. The intrasubunit distance between these metal centers is about 43.5 Å. The α subunits are associated together to position the mononuclear Fe of one subunit only 12 Å away from the Rieske [2Fe-2S] in the adjacent subunit. These results indicate that electron transfer occurs between subunits, which is consistent with an estimated minimum separation of 10 Å between the same redox centers for PDO (56, 94).

Reaction mechanism at the catalytic site of the terminal dioxygenase

The mechanism of aromatic dihydroxylation catalyzed by ARHDOs has not been fully elucidated. A hypothetical model has been proposed for oxygen activation and reaction with the benzene nucleus, based upon the cytochrome P450 reaction cycle, spectroscopic studies, and single turnover chemistry of ARHDO enzymes (Fig. 1.13, (7, 94, 133, 155, 156)). In single turnover studies, complete dihydroxylation of the aromatic substrate can occur when the reductase or ferredoxin is absent, confirming that the terminal dioxygenase is solely

responsible for aromatic ring dihydroxylation. The mononuclear Fe must be reduced and substrate bound to the enzyme in order to bind dioxygen, suggesting that the binding of the aromatic substrate somehow influences electron transfer between the terminal dioxygenase metal centers. This could be a safety mechanism to prevent oxygen activation in the absence of a aromatic substrate. BenDO and NDO single turnover chemistry has shown that only two electrons are needed to produce a dihydroxylated product, but the terminal dioxygenase must be reduced by two more electrons for product release (155, 156).

Dioxygen reduction to hydrogen peroxide is observed when alternative substrates are used by native dioxygenases (dashed arrows, Fig. 1.13). This substrate-dependent uncoupling reaction is presumed to occur by sub-optimal binding of native substrate analogs in the catalytic pocket. Uncoupling is also observed when using enzymes where site-directed mutations have altered the environment of the mononuclear Fe center (7, 104, 127). This could present a problem when engineering ARHDOs to catalyze alternative substrates. Mutant dioxygenases with increased activity on other aromatic compounds, expressed in the cell, may generate levels of peroxide that would damage cellular processes or the enzyme itself.

Comparison of AntDO and BenDO to Other ARHDOs

Sequence comparisons indicate that the genes encoding AntDO and BenDO are homologous to each other, to genes of AntDO and BenDO in

Pseudomonas species, and to several two-component ARHDOs involved in the degradation of substituted benzoates (33). Homologous dioxygenases involved in degrading environmental pollutants include the *Burkholderia cepacia* 2-halobenzoate 1,2-dioxygenase (CbdABC) (64) and 2,4,5-trichlorophenoxyacetic oxygenase (TftAB) (38), and the *Pseudomonas putida* toluate 1,2-dioxygenase (XylXYZ) (67). The *cbd* and *xyl* genes are located on large conjugative plasmids, and it is often suggested that these catabolic plasmids evolved from chromosomal genes encoding degradative pathways for natural aromatic compounds. The presence of xenobiotic compounds in the environment may have put selective pressure on bacteria to acquire novel catabolic activities. These substituted benzoates can be generated as intermediates in the biodegradation of pollutants such as toluene and xylenes. The presence of these compounds in the environment may have led to the selection of a BenDO with enhanced activity on toluate. Comparisons between the ARHDOs that utilize metabolites from environmental pollutant degradation could assist in engineering the dioxygenases of ADP1 to act on xenobiotic aromatic compounds.

It has been proposed that there is a tradeoff between catalytic efficiency and substrate specificity. This hypothesis is supported by studies of biphenyl dioxygenases that suggest that these enzymes can be categorized in two groups: those that have a broad substrate range of poly-chlorinated biphenyls (PCBs) but relatively weak activity towards these substrates, and those that degrade a much narrower range of PCBs but have strong activity against certain di-*para*-substituted congeners (111). Enzymes with broad specificity may be less

efficient and may explain why the catabolic genes on plasmids have not evolved to replace their efficient chromosomal counterparts. For example, the TOL plasmids that carry the *xylXYZ* genes encoding a possibly broader substrate specific toluate dioxygenase usually reside in bacterial strains that have the *benABC* genes on the chromosome, even though the XylXYZ enzyme is sufficient to initiate benzoate degradation (67). Recent studies have shown that the XylXYZ enzyme prefers *meta*- and *para*-substituted chlorobenzoates and toluates to the *ortho*-substituted counterparts (57). Unfortunately, many hypotheses concerning the substrate specificities of these enzymes have not been sufficiently tested with purified enzymes.

In *Acinetobacter* sp. ADP1, conclusions about the substrate specificities of the similar, yet distinct AntDO and BenDO, have been based on the growth characteristics of wild-type and mutant strains. The wild-type strain can use either benzoate or anthranilate as the sole carbon source. In a mutant strain lacking ADR, the BDR reductase can functionally replace ADR (19). This is consistent with other reports in the literature suggesting that reductases can function with terminal dioxygenases other than their cognate partners. In contrast, BenDO terminal dioxygenase cannot replace AntDO terminal dioxygenase to allow growth on anthranilate, even under conditions that allow high *ben*-gene expression (Eby, unpublished results). It therefore seems likely that BenDO is unable to convert anthranilate to catechol at a rate sufficient for growth. In mutant strains lacking BenDO, AntDO does not allow for growth on benzoate. In this case, it is unclear whether the limitation is due to problems with

gene expression or due to the inability of the AntDO to utilize benzoate as an efficient substrate.

Relevant studies of altering the substrate specificity of other ARHDOs

Gibson and his colleagues have investigated substrate specificities of the NDO, 2-nitrotoluene-, and 2,4-dinitrotoluene-dioxygenases by creating hybrid enzymes (124, 125). These three-component enzymes are very similar at the level of nucleic acid and deduced amino acid sequence, yet they have different substrate oxidation profiles. Exchanging C-terminal regions in the α subunits of these enzymes clearly demonstrated the importance of this subunit in substrate specificity. More recent studies have identified specific residues in NDO that affect activity on naphthalene, 2-nitotoluene, and 2,4-dinitrotoluene (23, 126, 128). These residues are found within a hydrophobic cleft on the surface of the enzyme, surrounding the mononuclear Fe catalytic site. This pocket is most likely where the hydrophobic aromatic ring of naphthalene can bind.

A similar study using hybrid enzymes of the homologous tetrachlorobenzene (Tec) and toluene (Tod) dioxygenases also demonstrated that the α subunits of these dioxygenases determine substrate specificity (8). The Tec dioxygenase is able concomitantly to oxygenate and dechlorinate its substrate whereas the wild-type Tod enzyme has no dehalogenating activity. Studies of the hybrid Tec-Tod enzymes demonstrated that a protein region near the mononuclear Fe ligands is important for dehalogenation activity. Furthermore, a single amino acid substitution gave dehalogenase activity to the

Tod α subunit. Manipulations of biphenyl dioxygenases from two *Pseudomonas* strains have similarly demonstrated that a single amino acid change in a dioxygenase α subunit can alter substrate specificity (95, 111).

There have been reports in the literature suggesting that ARHDO β subunits may play a role in substrate specificity (53, 149). In one study, both the α and β subunits of biphenyl dioxygenases appeared to influence substrate specificity (79). In contrast, the hybrid enzyme studies of Parales et al. described above, suggested that this subunit does not influence substrate specificities (124, 125). Results from different studies, therefore have led to different conclusions concerning the role the β subunits. It is possible that the role of this small subunit differs among the various ARHDOs, and further investigation is needed. An early genetic study of the toluate dioxygenase identified a mutant β subunit that affected substrate preferences, although no biochemical work was carried out on the mutant enzyme (68). More recently, Jiang, et. al (85) found that while the β subunit is essential for catalysis, this subunit is not required for the α subunit of toluene dioxygenase from *Pseudomonas putida* F1 to accept electrons from its reduced ferredoxin counterpart. These results support a structural role for the β subunit. This toluate dioxygenase is more closely related to AntDO and BenDO than any of the biochemically well-characterized enzymes, and it will be of interest to determine the role in substrate specificity, if any, of the β subunit of AntDO and BenDO.

Methods of Mutagenesis to Alter Enzyme Catalytic Function and Substrate Specificity

Two methodologies can be used to mutate genes for the purpose of altering the catalytic activity or substrate specificity of their enzyme products. Site-directed mutagenesis allows for specific substitutions of residues that are predicted to be important in the function or substrate preference of an enzyme. Many easy-to-use kits can be purchased to facilitate a small number of residue changes by nucleotide substitutions on a gene within plasmid DNA. Alternatively, random mutagenesis of the gene may be used to generate mutations that affect substrate specificity. Classical methods of nucleotide modification by chemical means (e. g. hydroxylamine mutagenesis) or UV damage have been replaced by procedures that employ the polymerase chain reaction (PCR, (84, 139)). These include generating hybrid enzymes by "shuffling" fragments of DNA encoding two or more homologous enzymes, altering conditions of PCR to increase nucleotide mis-incorporations by polymerases, and using mutated polymerases that lower the fidelity of DNA replication (26, 65, 112, 113, 144).

DNA Shuffling or Sexual PCR

DNA shuffling is an in vitro method to generate recombinant genes and then to select genes optimized for a specific function. It is performed by fragmenting a group of related DNA sequences into a pool of random DNA fragments that are then reassembled to create a collection of hybrid DNA

molecules. A fragment pool is created first by the random cutting of DNase I. Reassembly occurs during PCR, where homologous fragments from different genes anneal and create a template for polymerization. A new hybrid gene can then be screened for novel characteristics that were not encoded by the original genes. This process is repeated until an optimized activity is obtained. This process mimics the gene exchange or "recombination" that occurs during sexual reproduction.

Optimized DNA shuffling method: Random Chimeragenesis on Transient Templates (RACHITT)

The RACHITT method, designed by Coco and associates (26), is an improved DNA shuffling method that allows “fine resolution” recombination between homologous parental alleles. RACHITT differs from conventional sexual PCR in that it uses no thermocycling methods, but employs the trimming, gap filling, and ligation of gene fragments annealing to a transient DNA template. A complete parental gene is used as the initial template, where a pool of random gene fragments from the family of homologous genes hybridize onto it. Gaps between the fragments are filled in during polymerization and “flaps”, or overhangs from the overlapping fragments on the template are cleaved by the flap endonuclease activity of thermal-stable polymerases, respectively (*Taq* or *Pfu*). *Taq* DNA ligase then binds the nicks on the newly formed strand. The hybrid gene can then be used as the template in subsequent reactions. This method allows for several-fold higher levels of recombination in one hybrid gene

than other DNA shuffling techniques. Also, smaller fragments can be joined together than in sexual PCR. Therefore, more genetically diverse genes can be generated than sexual PCR can for gene family shuffling.

DNA shuffling offers a good method when characteristics of two or more genes are to be combined, such as genes encoding enzymes with similar catalytic activity, but different substrate specificities. One pitfall is the genes in the family must be very similar, usually having a nucleotide sequence identity of greater than 70%. If the genes are too dissimilar, or only one gene exists that can be altered to perform a desired function, other random mutagenic methods are needed.

Random mutagenesis using modified PCR conditions or mutated polymerases

Error prone PCR is a random mutagenesis technique for generating amino acid substitutions in proteins by introducing mutations into a gene during PCR. When buffer conditions are sub-optimal or template, nucleotide or polymerase concentrations are incorrect, accuracy of the polymerase to copy DNA diminishes. Higher concentrations of $MgCl_2$ stabilize non-complementary nucleotide pairs. The addition of $MnCl_2$ diminishes template specificity of the polymerase, presumably by incorporation of Mn ions in the polymerase. Different individual dNTP concentrations are used to promote mis-incorporation during polymerization. Increasing the concentration of the polymerase causes chain extension beyond the position of base mismatch (81).

Recently, Stratagene, Inc. has engineered a thermal-stable polymerase used in PCR amplifications, known as Mutazyme. Mutazyme has a high intrinsic error rate compared to *Taq* polymerase, although the nature of this characteristic is a trade secret. The rate of polymerized sequence errors of Mutazyme is approximately 1000-fold over the same rate inherent to *Taq* polymerase. The degree of mutagenesis is controlled by the initial concentration of the template in PCR. For the same PCR yield, DNA amplified from a lower amount of initial template undergoes more duplications than DNA amplified from high concentrations of template DNA. The more times a template is replicated, the more errors will be incorporated by the mutant polymerase. Mutazyme and *Taq* polymerase, under error prone conditions, generate all possible nucleotide substitutions. Both polymerases favor transitions over transversions. Mutazyme preferentially replaces Gs or Cs with As or Ts, while error-prone *Taq* polymerase conditions tend to replace As and Ts with Gs and Cs. Classic chemical mutagenesis methods, such as hydroxylamine mutagenesis, have a tendency to bias a specific nucleotide substitution, and these methods are difficult to use for altering substrate specificity of enzymes. A combination of different error-prone PCR methods can generate a pool of randomly mutated genes that vary widely in quality and quantity of base-pair substitutions.

Known applications of random mutagenesis to alter aromatic ring dioxygenase substrate preference and catalytic activity

Dioxygenases have lately been manipulated to improve their potential for environmental pollutant degradation (52, 60). In most cases, site-directed mutagenesis, in vitro DNA shuffling, and subunit or domain exchange between dioxygenase homologs have been the applied techniques used to alter substrate specificity. These studies have been successfully performed primarily upon several homologous biphenyl dioxygenases, and between the naphthalene-, 2,4-dinitrotoluene-, and 2-nitrotoluene-dioxygenases (see "Relevant studies of altering the substrate specificity of other ARHDOs" section for a summary of these experiments). The methods of mutagenesis used to generate hybrid and variant enzymes of the above dioxygenases have been successful because of the high nucleotide and amino acid sequence identity between them.

Most applied random mutagenesis procedures have identified functionally or catalytically important residues in aromatic ring dioxygenases by generating mutations, which either completely eliminate activity, or produce unstable, temperature-sensitive enzymes. DNA from PCR amplification (35 cycles) of the *Pseudomonas putida xylE* gene, encoding the catechol 2,3-dioxygenase, was transformed, recombined into the chromosome, and expressed in an *Acinetobacter* strain (100, 159). This was completed by using a vector and ADP1-derived recipient that allows for homologous recombination of the PCR-amplified DNA fragments into a specific chromosomal recombination site from which *xylE* can be expressed. PCR-amplified *xylE* donor DNA produced 30% of

transformants that failed to express a functional catechol 2,3-dioxygenase at 37^{o}C, although about 10% expressed the gene when grown at 22^{o}C.

Random mutagenesis was also completed upon the *xlnE* gene, encoding gentisate 1,2-dioxygenase from *Pseudomonas alcaligenes* NCIB 9867 (24). Two different random mutagenesis methods were employed. Error-prone PCR was performed using a non-proof reading DyNAzyme© II *Taq* polymerase (Finnzymes, Finland). Plasmid-borne *xlnE* was randomly mutated while replicating in an *E. coli* strain deficient in certain *mut* DNA repair genes (*XL-1 Red* from Stratagene, Inc.) Mutated *xlnE* genes were expressed in *E. coli* and specific activity measured from cell-free extracts. Mutations corresponding to a conserved central core region of the enzyme resulted in the complete loss of enzyme activity, whereas mutations corresponding to the flanking regions yielded a range of reduced activities compared to wild-type.

Sakamoto and associates were able to utilize error-prone PCR mutagenesis to generate toluene dioxygenase enzymes that had increased activity toward the toluene analog, 4-picoline (138). 30 nmol of $MnCl_2$ was added to 50 μl PCR reactions amplifying the *todC1* gene, encoding the toluene terminal dioxygenase. Resulting amplicons were ligated into plasmids for expression in *E. coli* and subsequent determination of specific activity of the enzymes acting upon either toluene or 4-picoline. One enzyme exhibited 5.6 times higher activity toward 4-picoline and greater activity towards toluene than wild-type toluene dioxygenase. The mutated gene contained five nucletotide substitutions, three of which resulted in amino acid changes and one, which changed the stop codon

(TGA) to Arg (CGA), thereby enlarging the protein by 4.4 kDa. The approach to modify a single gene by accumulating beneficial mutations was used to investigate how readily a toluene dioxygenase adapts to the heterocyclic substrate, 4-picoline. As described in this dissertation, random mutagenesis was used to alter the catA gene, encoding catechol 1,2-dioxygenase (Chapter 3).

Figure 1.1. Global cycling of aromatic compounds in aerobic environments (4, 96, 97).

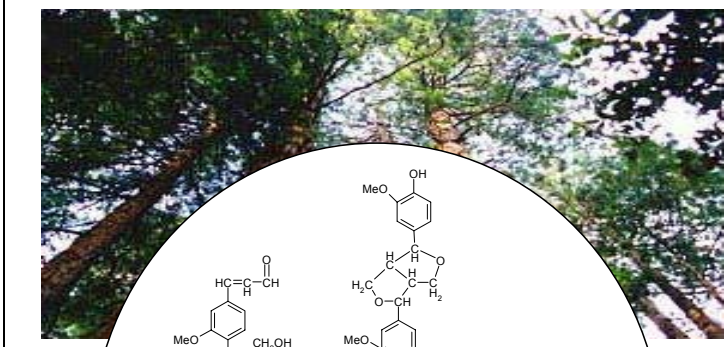

humic compounds

lignolytic activity performed by wood-rotting fungi

& combustion

repolymerization by spontaneous and microbial oxidative reactions

lignocellulose complex

single and poly-aromatics (PAH)
phenolics, aromatic acids, aromatic alcohols

environmental pollutants
pesticides, industrial chemicals

plant cell wall synthesis

transformation by bacteria and fungi

biological components
amino acids, quinones, hormones, alkaloids, flavinoids

biosynthesis

aliphatic and inorganic carbon
TCA cycle intermediates, CO_2

bacterial oxygenase reactions

single aromatics
benzoates, catechols, amino-substituted arenes

Figure 1.2. Aerobic metabolism of lignin biodegradation products to dihydroxy aromatic substrates for ring-fission. Substrates for ring cleavage pathways are boxed. Products of ring-fission are shown below with their designated pathway (*ortho* or *meta*) and the enzyme responsible for ring cleavage, if known (adapted from 96). Microbes each possess only some of these catabolic capabilities.

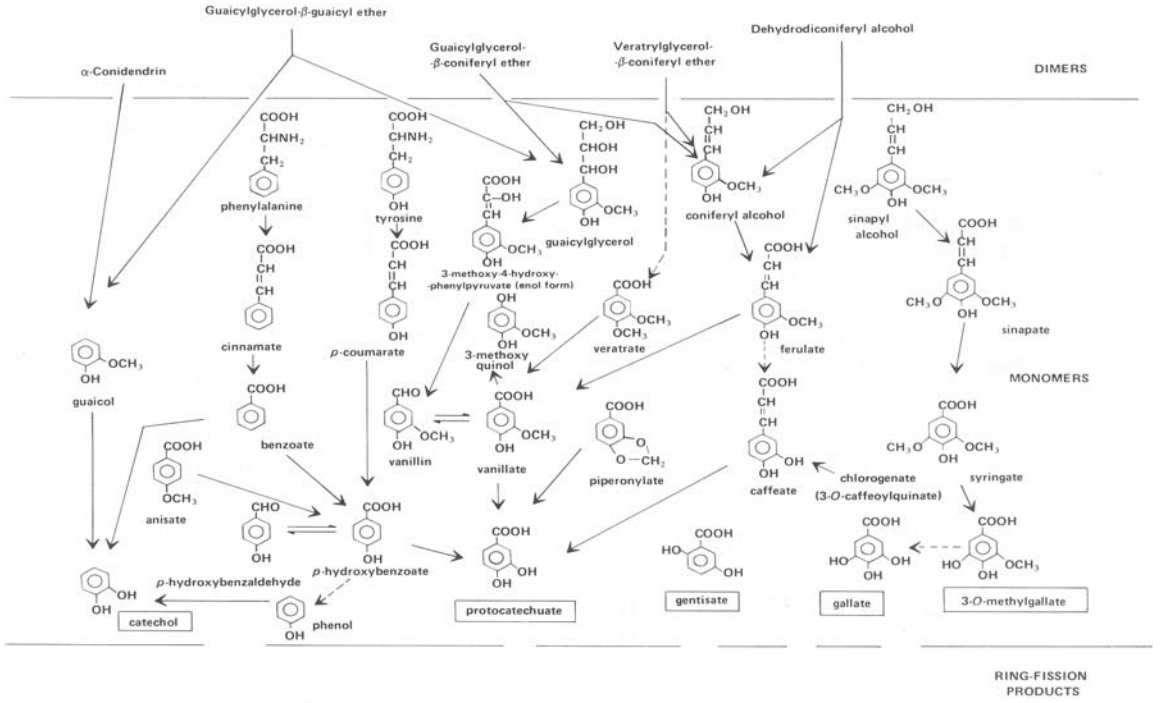
Guaicylglycerol-β-guaicyl ether
α-Conidendrin
Guaicylglycerol-
-β-coniferyl ether
Veratrylglycerol-
-β-coniferyl ether
Dehydrodiconiferyl alcohol
DIMERS
phenylalanine
tyrosine
guaicylglycerol
coniferyl alcohol
sinapyl
alcohol
3-methoxy-4-hydroxy-
-phenylpyruvate (enol form)
cinnamate
p-coumarate
3-methoxy
quinol
veratrate
ferulate
sinapate
guaicol
MONOMERS
benzoate
vanillin
vanillate
piperonylate
caffeate
chlorogenate
(3-O-caffeoylquinate)
syringate
anisate
p-hydroxybenzaldehyde
p-hydroxybenzoate
catechol
phenol
protocatechuate
gentisate
gallate
3-O-methylgallate
RING-FISSION
PRODUCTS

Figure 1.3. Known metabolic routes of aromatic ring-fission and subsequent conversion to tri-carboxylic acid cycle intermediates by aerobic microorganisms. The pathways represented are the bacterial *ortho* cleavage (identical to the known fungal *ortho* cleavage pathway except where denoted by the dashed arrows) (A), the *meta* cleavage (including modified-*meta* gallate and 3-O-methylgallate pathways) (B), gentisate, homogentisate, and 3-methylgentisate pathways (C) (35, 72, 96).

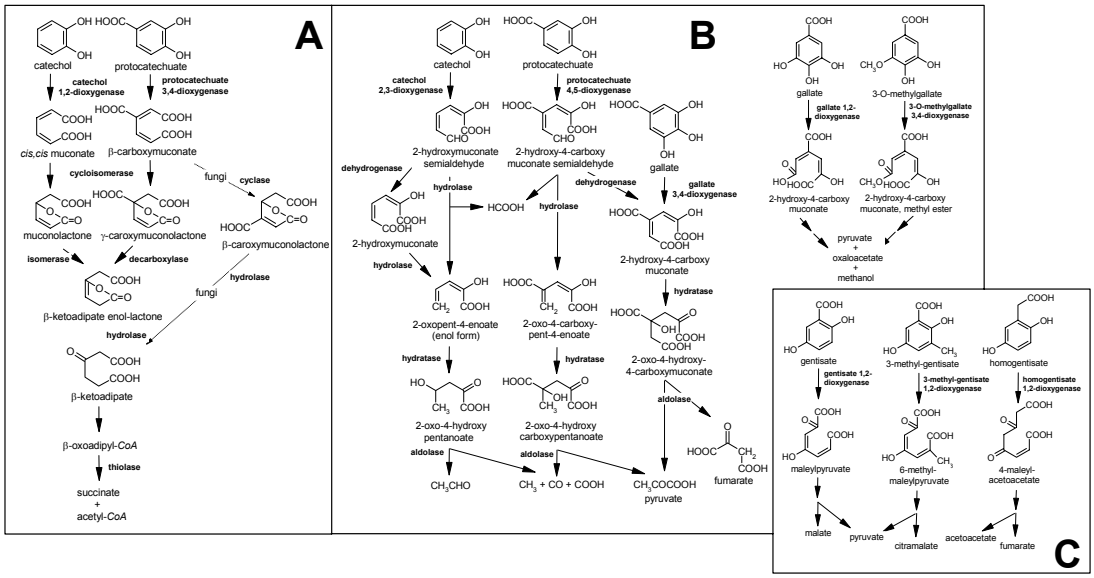
A
catechol
protocatechuate
catechol 1,2-dioxygenase
protocatechuate 3,4-dioxygenase
cis,cis muconate
β-carboxymuconate
cycloisomerase
fungi
cyclase
muconolactone
γ-caroxymuconolactone
β-caroxymuconolactone
isomerase
decarboxylase
hydrolase
fungi
β-ketoadipate enol-lactone
hydrolase
β-ketoadipate
β-oxoadipyl-CoA
thiolase
succinate
+
acetyl-CoA
B
catechol
protocatechuate
catechol 2,3-dioxygenase
protocatechuate 4,5-dioxygenase
2-hydroxymuconate semialdehyde
2-hydroxy-4-carboxy muconate semialdehyde
gallate
dehydrogenase
hydrolase
dehydrogenase
gallate 3,4-dioxygenase
2-hydroxymuconate
HCOOH
hydrolase
2-hydroxy-4-carboxy muconate
hydrolase
hydratase
2-oxopent-4-enoate (enol form)
2-oxo-4-carboxy-pent-4-enoate
2-oxo-4-hydroxy-4-carboxymuconate
hydratase
hydratase
aldolase
2-oxo-4-hydroxy pentanoate
2-oxo-4-hydroxy carboxypentanoate
aldolase
aldolase
CH3CHO
CH3 + CO + COOH
CH3COCOOH
pyruvate
fumarate
gallate
3-O-methylgallate
gallate 1,2-dioxygenase
3-O-methylgallate 3,4-dioxygenase
2-hydroxy-4-carboxy muconate
2-hydroxy-4-carboxy muconate, methyl ester
pyruvate
+
oxaloacetate
+
methanol
C
gentisate
3-methyl-gentisate
homogentisate
gentisate 1,2-dioxygenase
3-methyl-gentisate 1,2-dioxygenase
homogentisate 1,2-dioxygenase
maleylpyruvate
6-methyl-maleylpyruvate
4-maleyl-acetoacetate
malate
pyruvate
citramalate
acetoacetate
fumarate

Figure 1.4 Aromatic compound catabolism by *Acinetobacter* sp. strain ADP1. General genetic designations responsible for each catalytic reaction are shown.

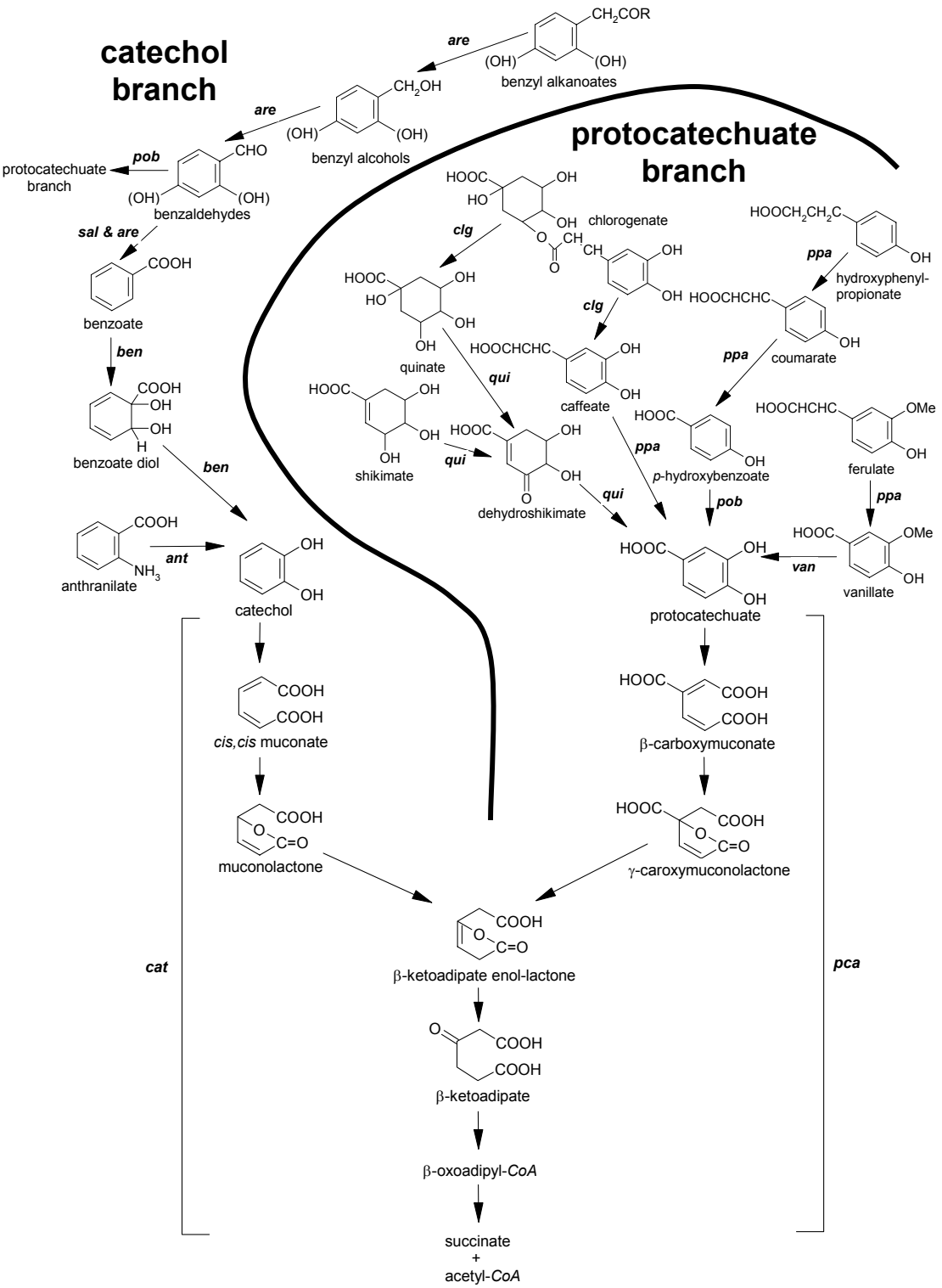
catechol branch
protocatechuate branch
are
pob
protocatechuate branch
benzaldehydes
benzyl alcohols
benzyl alkanoates
sal & are
benzoate
ben
benzoate diol
ben
anthranilate
ant
catechol
cis,cis muconate
muconolactone
cat
clg
quinate
chlorogenate
clg
caffeate
qui
shikimate
qui
dehydroshikimate
qui
ppa
p-hydroxybenzoate
pob
protocatechuate
β-carboxymuconate
γ-caroxymuconolactone
ppa
hydroxyphenyl-propionate
ppa
coumarate
ppa
ferulate
van
vanillate
pca
β-ketoadipate enol-lactone
β-ketoadipate
β-oxoadipyl-CoA
succinate
+
acetyl-CoA

Figure 1.5. Map of the ADP1 chromosome designating the genes responsible for the β-ketoadipate pathway. Digestion by *Not*I restriction enzyme separates the chromosome in 6 fragments labeled A through F (63).

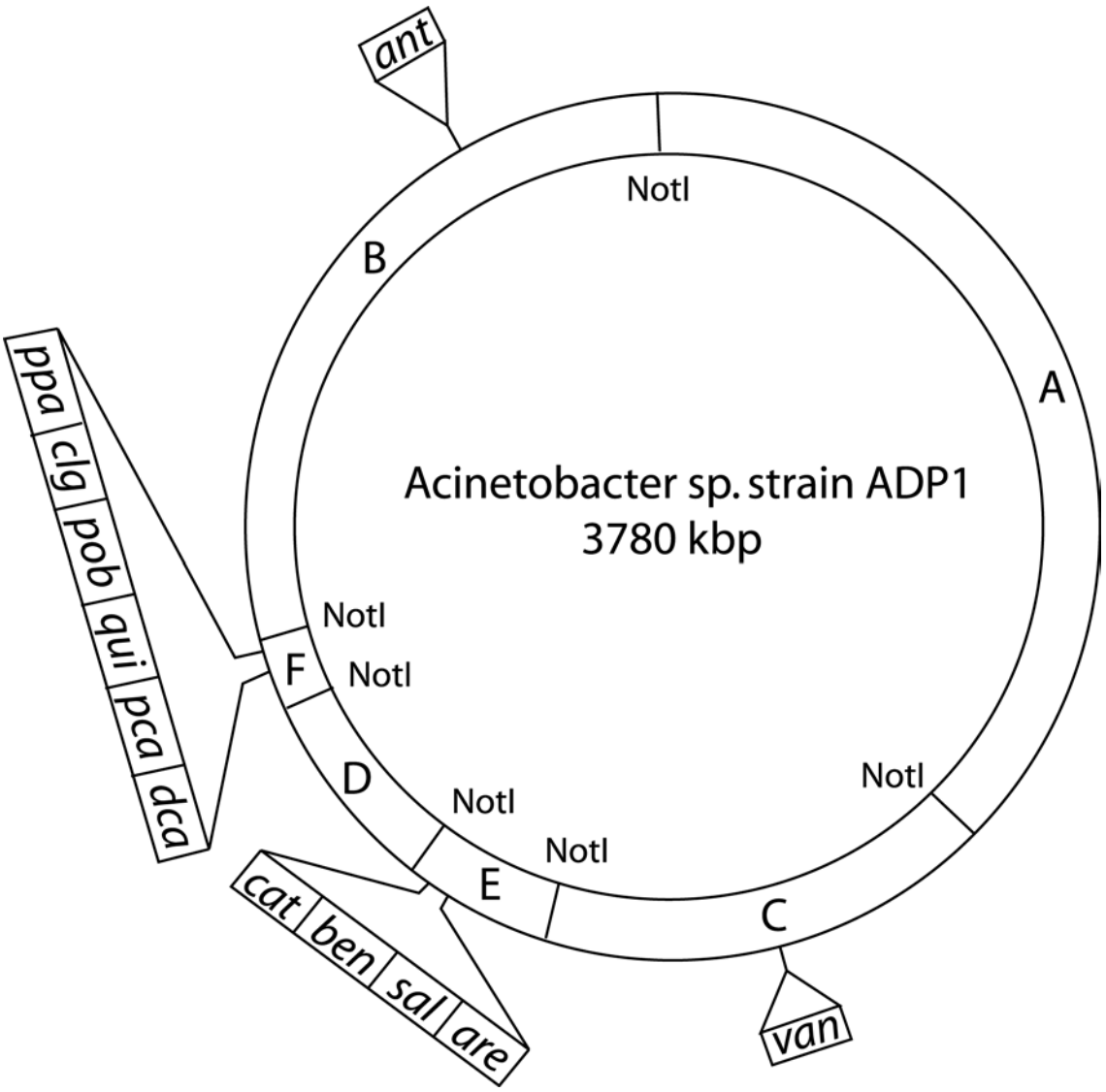
ant
NotI
B
A
ppa
clg
pob
qui
pca
dca
Acinetobacter sp. strain ADP1
3780 kbp
NotI
F
NotI
D
NotI
NotI
E
C
cat
ben
sal
are
van

Figure 1.6. Organization of the *pca, pob, ben* and *cat* operons in the chromosome of ADP1. Primary activators and effector molecules are shown above the operon that they are known to induce expression. *Cis,cis*-muconate is designated as ccm.

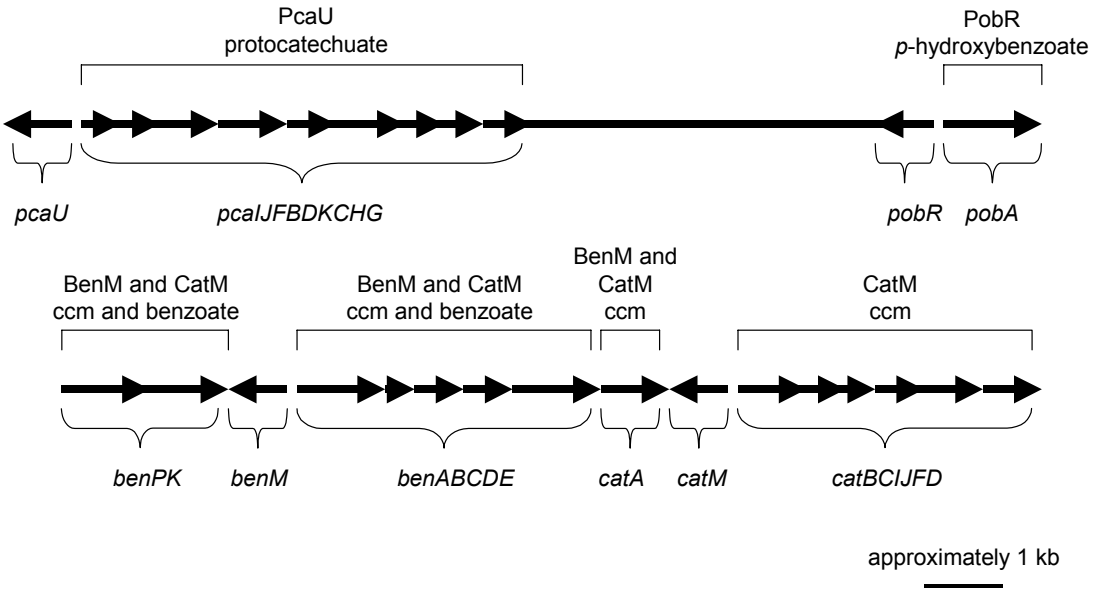
PcaU
protocatechuate
PobR
p-hydroxybenzoate
pcaU
pcaIJFBDKCHG
pobR
pobA
BenM and CatM
ccm and benzoate
BenM and CatM
ccm and benzoate
BenM and
CatM
ccm
CatM
ccm
benPK
benM
benABCDE
catA
catM
catBCIJFD
approximately 1 kb

Figure 1.7. Electron transfer by ARHDOs. A reductase protein transfers two electrons from NAD(P)H to the terminal dioxygenase directly or through an intermediary ferredoxin. In some cases, the ferredoxin protein has a Rieske [2Fe-2S]. Hydroxylation of the aromatic substrate takes place at the mononuclear Fe center within the terminal dioxygenase (9).

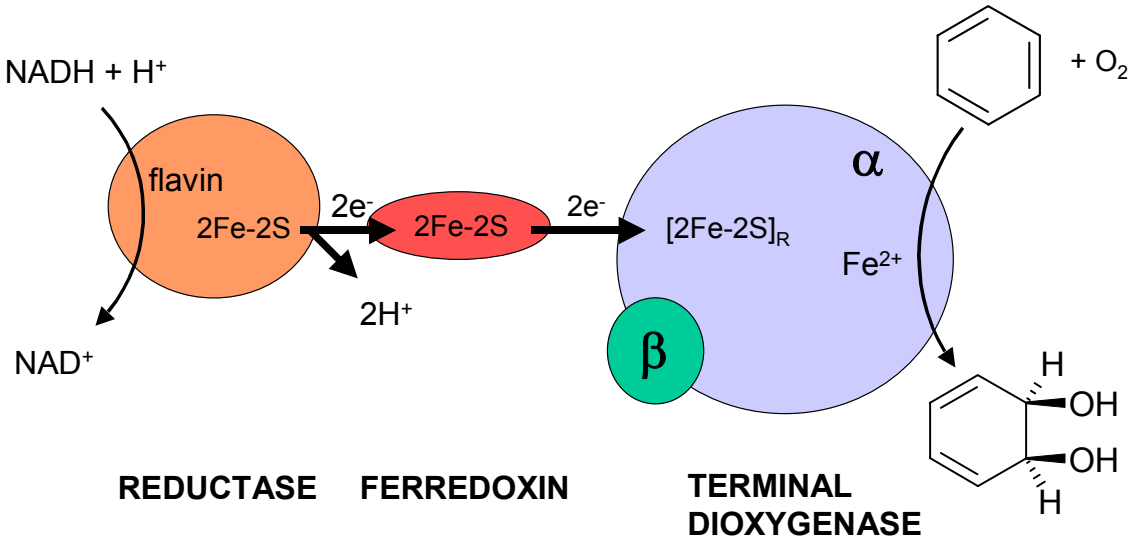
NADH + H+
flavin
2Fe-2S
2e-
2Fe-2S
2e-
[2Fe-2S]R
α
Fe2+
β
+ O2
2H+
NAD+
H
OH
OH
H
REDUCTASE
FERREDOXIN
TERMINAL
DIOXYGENASE

Figure 1.8. The terminal dioxygenase components of AntDO and BenDO (AntAB and BenAB, respectively) catalyze the insertion of molecular oxygen into the aromatic substrate after receiving electrons from the reductase component (ADR or BDR) (45). The reaction catalyzed by BenDO is represented in the green dashed box. In the AntDO-catalyzed reaction of anthranilate to catechol, an anthranilate diol is presumed not to form.

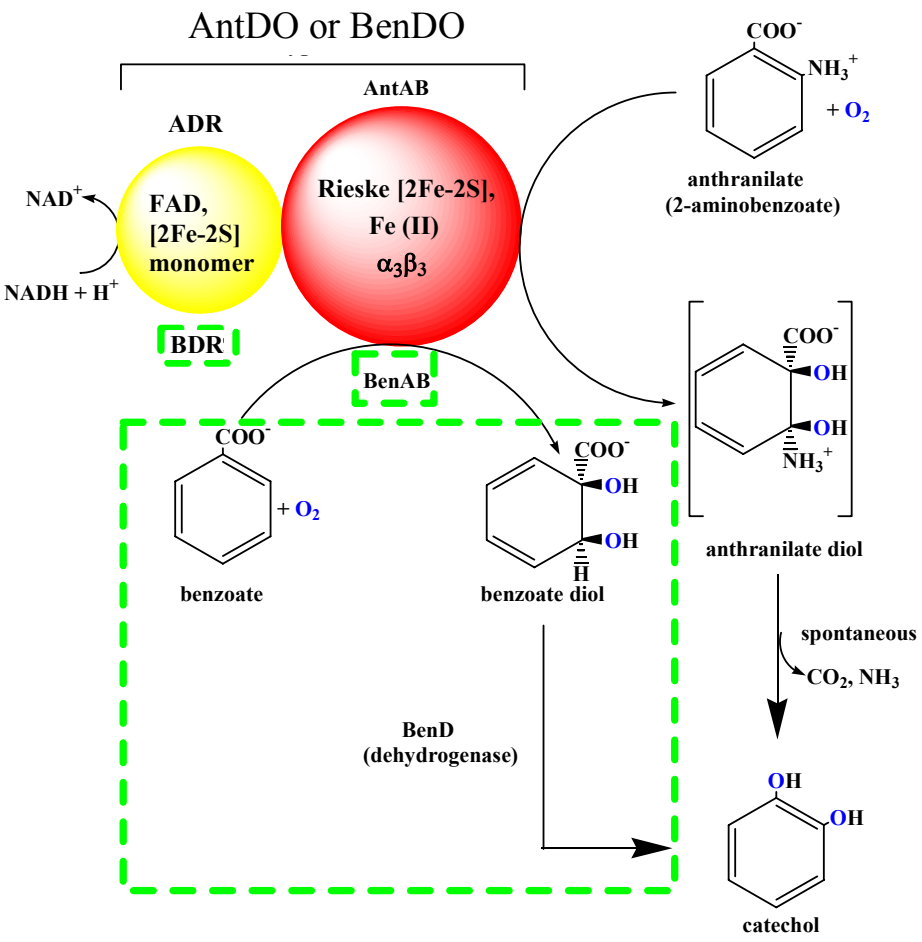
AntDO or BenDO
AntAB
ADR
FAD,
[2Fe-2S]
monomer
Rieske [2Fe-2S],
Fe (II)
α3β3
NAD+
NADH + H+
BDR
BenAB
COO-
NH3+
+ O2
anthranilate
(2-aminobenzoate)
COO-
OH
OH
NH3+
anthranilate diol
COO-
+ O2
benzoate
COO-
OH
OH
H
benzoate diol
spontaneous
CO2, NH3
BenD
(dehydrogenase)
OH
OH
catechol

Figure 1.9. Structure of the naphthalene 1,2-dioxygenase from *Pseudomonas* sp. strain NCIB 9816-4 (94). The $\alpha_3\beta_3$ hexameric complex is colored to show each subunit. α subunits are light blue, pink , and green and β subunits are purple, dark blue, and brown. Iron and sulfur atoms of the metal centers are orange and yellow, respectively (A). View along the molecular three-fold rotation axis with the β subunits underneath the α subunits (B). Models were created using Protein Explorer (www.proteinexplorer.com).

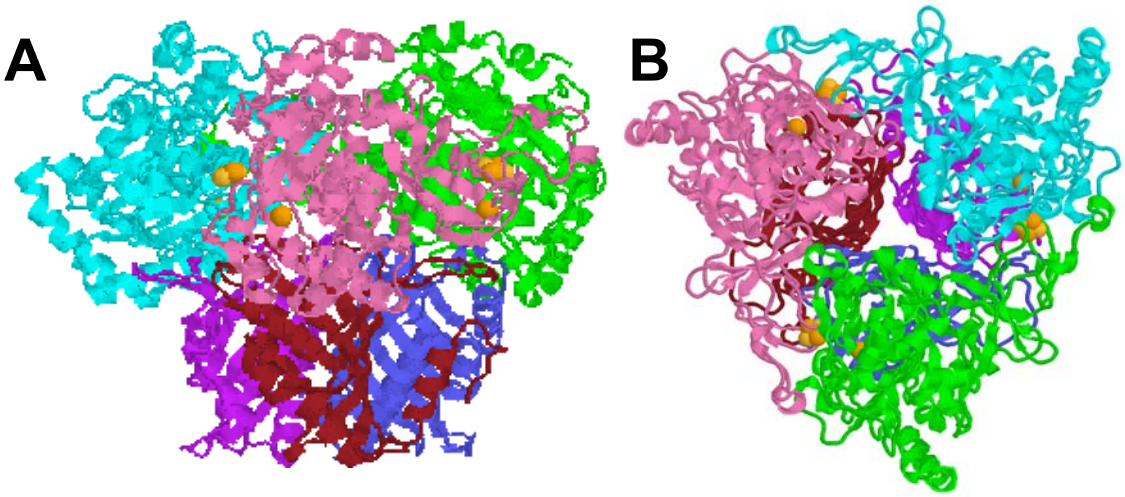
A
B

Fig. 1.10. Crystal structure of the phthalate dioxygenase reductase from *Burkholderia cepacia* DB01 (A). Ligands bound to the [2Fe-2S] (iron is orange and sulfur is yellow) and the Phe225 “gate” with FMN (CPK colored) is shown in (B). Models were created using Protein Explorer (www.proteinexplorer.com).

Phthalate Dioxygenase Reductase

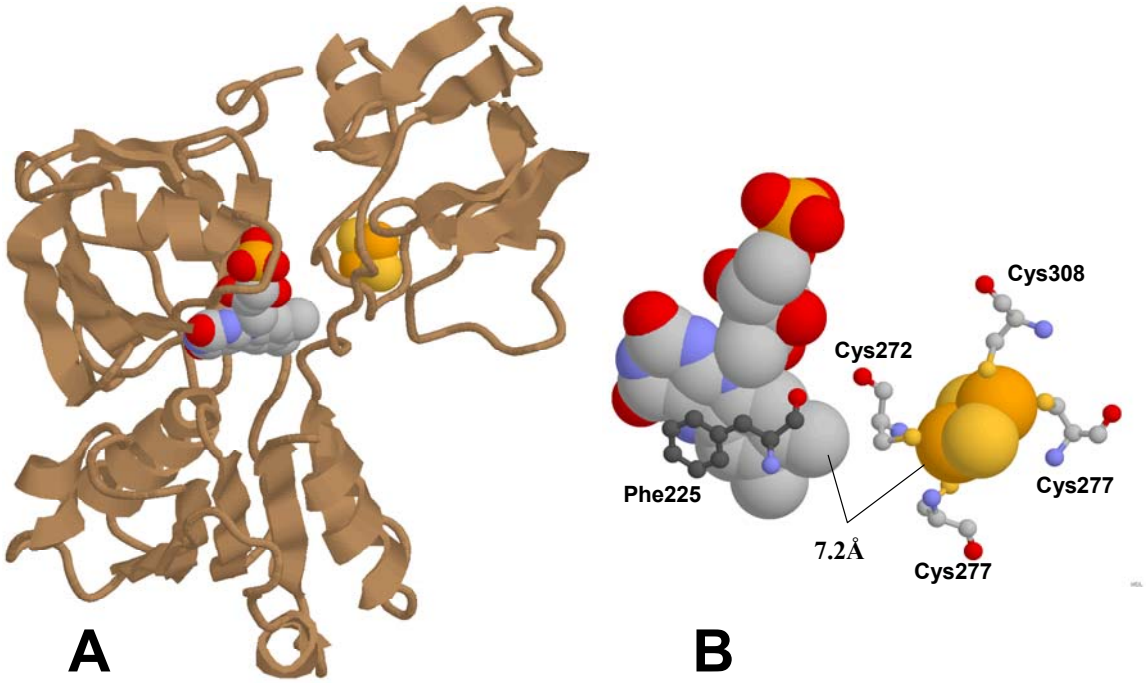

Figure 1.11. Crystal structure of the benzoate dioxygenase reductase from *Acinetobacter* sp. strain ADP1 (A). Ligands bound to the [2Fe-2S] (iron is orange and sulfur is yellow) and the Phe335 “gate” with FAD (CPK colored, nucleotide portion of FAD is tan) is shown in (B) (92). Models were created using Protein Explorer (www.proteinexplorer.com).

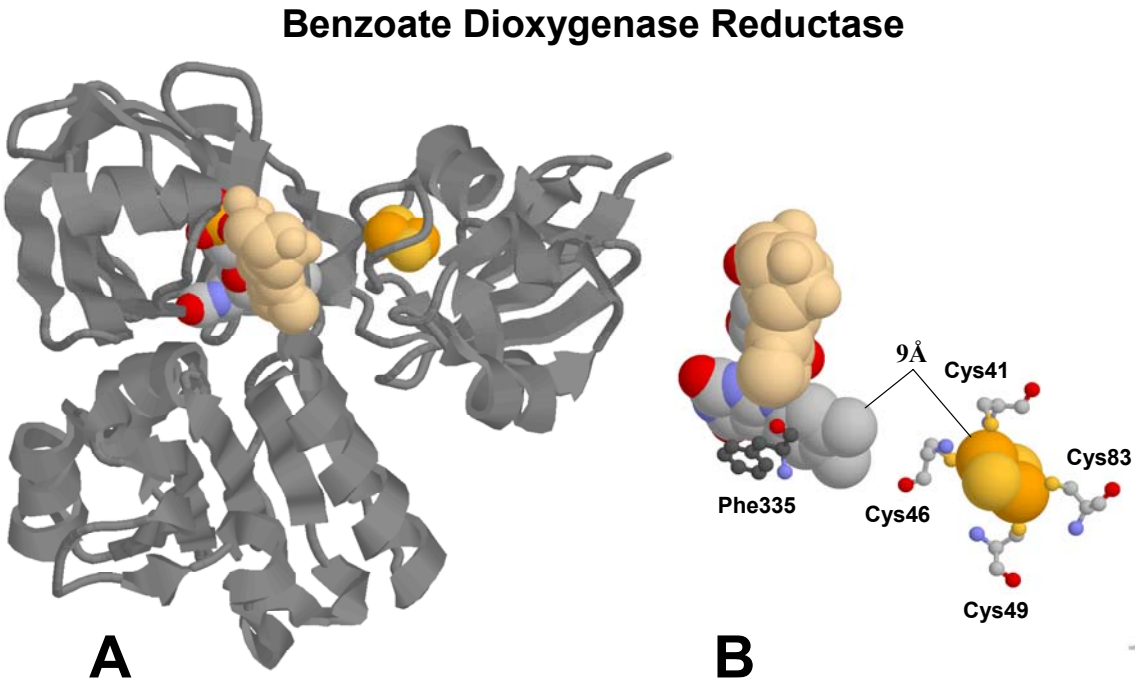
Benzoate Dioxygenase Reductase
9Å
Cys41
Cys83
Phe335
Cys46
Cys49
A
B

Figure 1.12. Proposed inter-subunit electron transfer between α subunits of ARHDOs (NDO residues shown). The Rieske [2Fe-2S] site of one α subunit (α_1) is shown adjacent to the catalytic Fe site of another α subunit (α_2) (adapted from 94). The closest bond distance between the metal centers is 12Å.

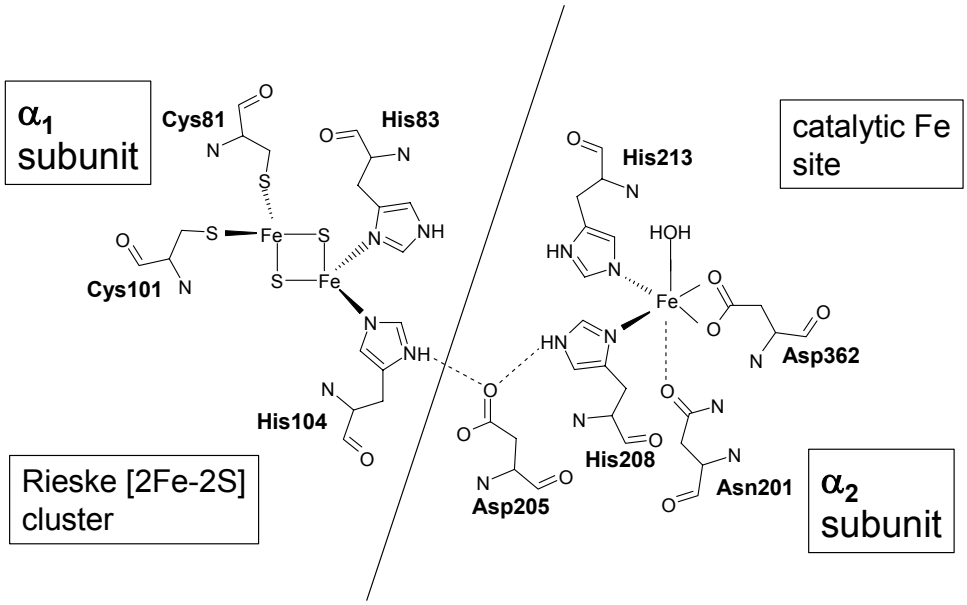
α1 subunit
Cys81
His83
Cys101
His104
Rieske [2Fe-2S] cluster
catalytic Fe site
His213
HOH
Asp362
His208
Asp205
Asn201
α2 subunit

Figure 1.13. Schematic representation of the proposed ARHDO reaction cycle (adapted from 7, 94, 155, 156). Solid arrows show tight coupling of dioxygen and electron incorporation to the aromatic substrate. Dashed arrows designate uncoupling pathways (unc-1 and unc-2) leading to the formation of H_2O_2 or H_2O.

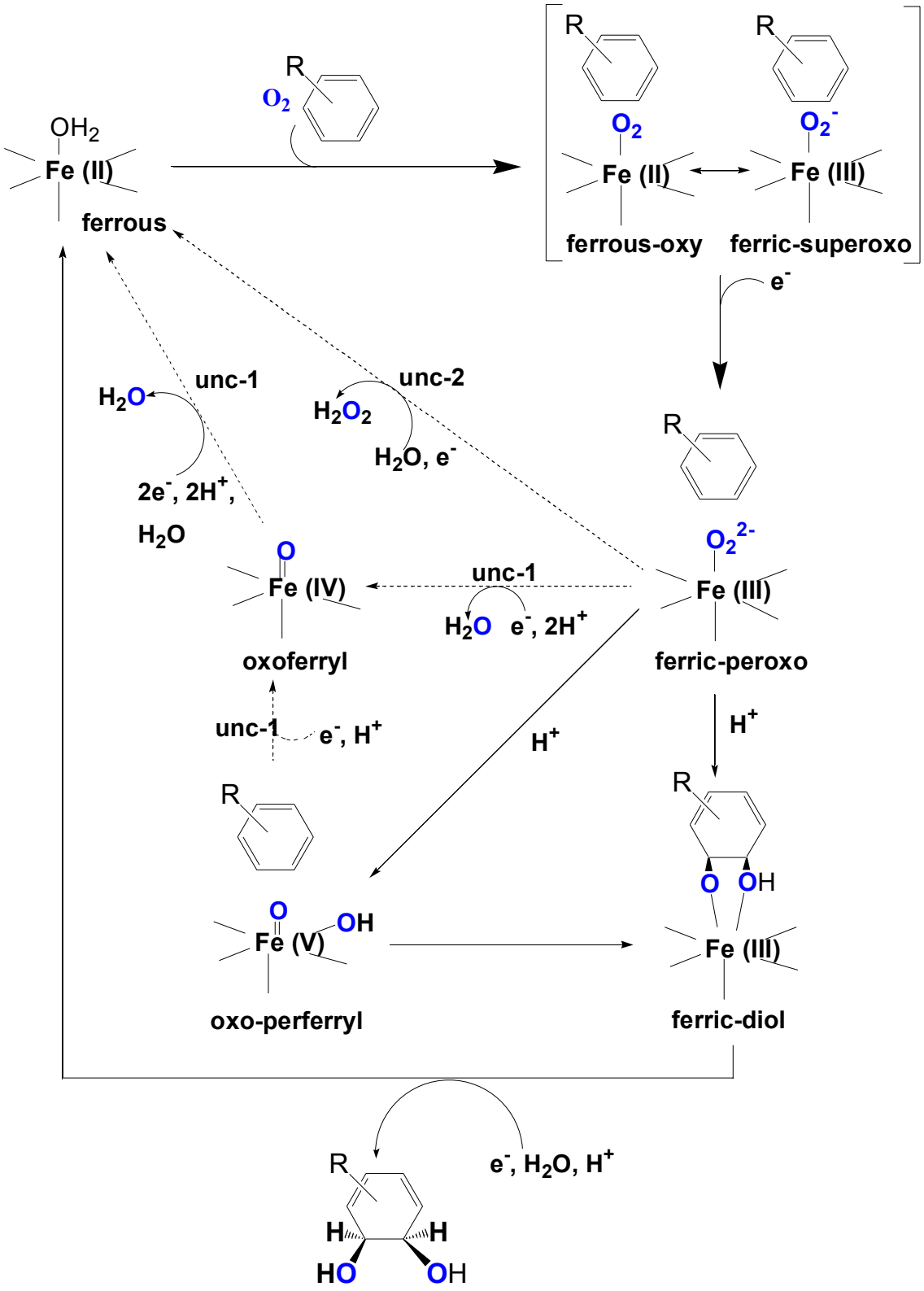
OH2
Fe (II)
ferrous
R
O2
R
R
O2
O2-
Fe (II)
Fe (III)
ferrous-oxy
ferric-superoxo
e-
unc-1
H2O
2e-, 2H+,
H2O
unc-2
H2O2
H2O, e-
R
O
Fe (IV)
oxoferryl
unc-1
H2O
e-, 2H+
O2 2-
Fe (III)
ferric-peroxo
unc-1
e-, H+
H+
H+
R
R
O
OH
O
Fe (V)
OH
oxo-perferryl
Fe (III)
ferric-diol
e-, H2O, H+
R
H
H
HO
OH

CHAPTER 2

CHARACTERIZATION AND EVOLUTION OF ANTHRANILATE 1,2-DIOXYGENASE FROM *ACINETOBACTER* SP. STRAIN ADP1[1]

---

[1]Eby, D.M., Z.M. Beharry, E.D. Coulter, D.M. Kurtz, Jr., and E.L. Neidle. To be submitted to *Journal of Bacteriology*.

Abstract

The two-component anthranilate 1,2-dioxygenase of the bacterium *Acinetobacter* sp. ADP1 was expressed in *Escherichia coli* and purified to homogeneity. This enzyme converts anthranilate (2-aminobenzoate) to catechol with insertion of both atoms of O_2 and consumption of one NADH. The terminal oxygenase component formed an $\alpha_3\beta_3$ hexamer of 54- and 19-kDa subunits. Biochemical analyses demonstrated one Rieske-type [2Fe-2S] center and one mononuclear non-heme iron center in each large oxygenase subunit. The reductase component, which transfers electrons from NADH to the oxygenase component, contained one flavin adenine dinucleotide and one ferredoxin-type [2Fe-2S] center per 39-kDa monomer. Activities of the combined components were measured as rates and quantities of NADH oxidation, substrate disappearance, product appearance, and O_2 consumption. Anthranilate conversion to catechol was stoichiometrically coupled to NADH oxidation and O_2 consumption. The substrate analog benzoate was converted to a non-aromatic benzoate 1,2-diol with similarly tight coupling. This latter activity is identical to that of the related benzoate 1,2-dioxygenase. A variant anthranilate 1,2-dioxygenase was purified containing a methionine-to-lysine change in the large oxygenase subunit that conveys temperature sensitivity in vivo. Independent of temperature, however, the variant did not hydroxylate anthranilate or benzoate. The wild-type anthranilate 1,2-dioxygenase did not efficiently hydroxylate methylated- or halogenated-benzoates but is similar to broad-substrate specific dioxygenases that do. Phylogenetic trees of these dioxygenases that act on

natural and xenobiotic substrates indicated that the subunits of each terminal oxygenase evolved from a common ancestral two-subunit component. Comparisons of the phylogenetic trees for the oxygenase and reductase components revealed slight variations in the branching patterns.

Introduction

Bioremediation efforts have focused attention on the bacterial degradation of xenobiotic methyl- and halogen-substituted benzoates by plasmid-encoded pathways of broad substrate specificity (3, 150). These catabolic routes may have evolved from narrow substrate-specific chromosomally-encoded pathways for degrading natural compounds. The first step in the bacterial catabolism of benzoate or substituted benzoates is dihydroxylation of the aromatic ring (61). Metabolites are subsequently funneled into the tricarboxylic acid cycle. The aromatic ring hydroxylating dioxygenases (ARHDOs) that initiate this sequence belong to a large enzyme family that operates on diverse substrates (9, 103, 109). Although several dozen ARHDOs have been characterized, most of these enzymes catalyze reactions with xenobiotic substrates.

Anthranilate (2-aminobenzoate) is a naturally occurring compound that is formed during bacterial tryptophan degradation (73). In the early 1960s, it was shown that crude cell extracts of some *Pseudomonas* species convert anthranilate to catechol via insertion of both atoms of O_2 into the aromatic ring (80). Despite this long history and its metabolic significance, the enzyme responsible for this activity, anthranilate 1,2-dioxygenase (AntDO; Fig. 2.1) has

not been characterized beyond the studies cited above. The genes encoding AntDO, *antABC*, are known from only one microbe, namely, the soil bacterium, *Acinetobacter* sp. ADP1 (19). A mutant able to grow on anthranilate at 22 ^{0}C but not 39 ^{0}C was used to isolate *antABC* from the ADP1 chromosome. The temperature sensitivity of the mutant resulted from a point mutation in the 43rd codon of *antA*, resulting in a variant gene product with lysine rather than methionine (M43K AntA).

The high degree of sequence similarity between *antABC* and *benABC*, the latter encoding benzoate 1,2-dioxygenase (BenDO) from the same organism (116), suggests a common evolutionary origin for both sets of genes. In fact, the pathways using these ARHDOs converge at catechol (Fig. 2.1). AntDO and BenDO are also closely related to several ARHDOs, encoded by mobile catabolic genes, which act on xenobiotics. These include the *xylXYZ*-encoded toluate (methylbenzoate) dioxygenase of *Pseudomonas putida*, the *cbdABC*-encoded halobenzoate dioxygenase of *Burkholderia cepacia*, the *abs*-encoded aminobenzene sulfonate dioxygenase from *Alcaligenes* sp. strain 0-1, and the *tft*-encoded 2,4,5-trichlorophenoxyacetic acid oxygenase of *B. cepacia* (Table 2.1) (38, 40, 50, 64, 67, 107, 154).

Sequence comparisons with better-characterized ARHDOs (9, 109) led to the inferred functions and prosthetic groups for the reductase (AntC) and oxygenase (AntAB) components of AntDO (Fig. 2.1; Table 2.1). Each α-subunit of the oxygenase component was predicted to contain one Rieske-type [2Fe-2S] center and one mononuclear center (Fe^{2+}, in Fig. 2.1). The mononuclear center

is presumed to be the site of O_2 activation for insertion into the aromatic substrate. The reductase component was predicted to contain flavin adenine dinucleotide (FAD) and one [2Fe-2S] center (19).

As described in this report, we induced the *Acinetobacter* sp. ADP1 AntDO and the variant M43K AntDO in *Escherichia coli* and purified the enzymes to homogeneity. The oligomeric state of AntDO was determined, and metal and prosthetic groups were identified. Previous studies suggest that in ADP1, AntDO and BenDO act efficiently in vivo only on anthranilate and benzoate, respectively, despite the similar structures of these substrates and the sequence similarity of the enzymes (19, 116). We compared anthranilate and benzoate as substrates for AntDO in vitro. The reaction products were identified to confirm that dihydroxylation of anthranilate results in spontaneous conversion to catechol by loss of ammonia and carbon dioxide, whereas dihydroxylation of benzoate yields a stable non-aromatic diol (Fig. 2.1) [6, (118). To help understand the relationship of AntDO to plasmid-encoded ARHDOs of broad substrate specificity, several halogenated- and methylated-benzoates were tested as substrates of AntDO. Recent sequencing of the *Pseudomonas aeruginosa* PAO1 genome also allowed us to identify the putative sequences of AntDO and BenDO from that bacterium and to compare sequence conservation among related enzymes.

Materials and Methods

Reagents and General Procedures.

Substrates were purchased from Sigma. Enzymatically produced 1*R*,2*S*-1,2-dihydroxycyclohexa-3,5-diene carboxylate (benzoate 1,2-diol) was a gift from Dr. Albey M. Reiner (Univ. of Massachusetts, Amherst). Oligonucleotides were synthesized by Integrated DNA Technologies. Nucleotide sequencing was done at the University of Georgia Molecular Genetics Instrumentation Facility (ABI373 sequencer, Applied Biosystems). Molecular biology procedures not detailed below followed standard protocols (140). Plasmid-bearing *E. coli* strains were cultured in Luria-Bertani (LB) medium with 100 μg/ml ampicillin. Protein purity was judged by sodium dodecyl sulfate-polyacrylamide gel electrophoresis (SDS-PAGE) (12.5% polyacrylamide gels) with Coomassie blue staining (141).

Plasmids for high-level ant-gene expression.

Genes of *Acinetobacter* sp. ADP1 (also known as BD413 (90)) were PCR-amplified with *Pfu* polymerase (Stratagene) from the template pBAC103 (19), and placed under control of the inducible P_{tac} promoter of the pCYB1 vector (New England Biolabs). A 1,912-bp *antAB* amplicon was generated with the primers: ANTAnde, 5′ ggacttcatATGACTGCACGTAACCTCGC-3′ and ANTBtaa, 5′-ataatagctcttccgcaTTAGACGTGATAGAAATCGAGTAC-3′ (sequences at the 5′ end of *antA* and the 3′ end of *antB*, respectively, are capitalized; added *Nde*I and *Sap*I restriction sites are underlined). A 1,031-bp *antC* amplicon was similarly

made with primers ANTCnde, 5´ ggggaccatATGAATCATTCTGTTGCACTCAA-3´ and ANTCtaa, 5´-attatagctcttccgcATTAAGTTTTTGCGGTATTACTTTG-3´. After digestion with *Nde*I and *Sap*I, the amplicons were each ligated into pCYB1 to yield pBAC209 (*antAB*) and pBAC208 (*antC*). The nucleotide sequences of the plasmid-borne *ant* regions were confirmed to be the same as in Genbank AF071556.

Site-directed mutagenesis to produce M43K AntA.

An *antA* gene encoding lysine at residue 43 was constructed with the QuikChange Site Directed Mutagenesis kit (Stratagene). Plasmid pBAC209, which contains the wild-type *antAB*, was the template for the complementary mutagenic oligonucleotide primers, 5´-TTTGAACTTGAAAAAGAACTCATTTTTG-3´, and 5'-CAAAAATGAGTTCTTTTTCAAGTTCAAA-3´ (the mutated codon is underlined). The mutated *antAB* DNA of the resulting plasmid, pDMK3, was verified by sequencing.

Induction of AntDO and preparation of cell-free extract.

One-liter cultures of *E. coli* strains DH5α (Gibco BRL) or TOP10F' (Invitrogen) carrying plasmids with *antAB* (pBAC209) or *antC* (pBAC208), respectively, were grown aerobically at 37 ºC until OD_{600} ~0.6. The temperature was then reduced to 30 ºC, and ferrous ammonium sulfate (0.5 mg/ml) was added, followed by isopropyl α-D-thiogalactopyranoside (100 μg/ml) to induce expression of the plasmid-borne *ant* genes. After overnight incubation at 30 ºC

(~18 hrs), cells were harvested by centrifugation and washed once with 20 mM potassium phosphate buffer, pH 7.5 (buffer A). Approximately 25 g of cells from six one-liter cultures were suspended in 25 ml of buffer A containing 0.1 mM phenylmethylsulfonyl fluoride, 1 mg Dnase (Boehringer Mannheim) and 5% (v/v) glycerol. The suspended cells were sonicated on ice with a Branson sonifier cell disrupter 350 with a 0.5-inch probe tip for 2 min at 30-sec intervals at 20 kHz. Cell debris was removed by centrifugation (12,000 x *g* for 30 min) at 4 ºC, resulting in red-brown or yellow-orange supernatants containing AntAB or AntC, respectively. Because M43K AntAB was predicted to be temperature sensitive, cells for its purification were grown at 25 ^{0}C.

Purification of AntAB.

The procedure below was carried out at 4 ºC. The cell-free extract (35 ml) from 6-liters of cells was applied to a Whatman DE52, anion-exchange column (4 cm X 10 cm) equilibrated in buffer A containing 100 mM NaCl (buffer B). The column was washed with 200 ml buffer B, and bound AntAB was eluted with a 250 ml linear NaCl gradient (0.1-0.4 mM) in buffer A at a flow rate of 2.0 ml/min. Active fractions (assayed as described below) were pooled and concentrated by ultrafiltration in a 50-ml Amicon cell (YM-10 membrane) to 10 ml. Filtered 4 M $(NH_4)_2SO_4$ was added with stirring to a final concentration of 1 M. The resulting precipitate was removed by centrifugation (12,000 x *g* for 15 min) and the supernatant was applied to a butyl Sepharose column (2 cm X 11.5 cm, Pharmacia) equilibrated in buffer A containing 1 M $(NH_4)_2SO_4$. AntAB was eluted

at 2.0 ml/min with a 250-ml linear gradient of decreasing $(NH_4)_2SO_4$ concentration (1-0 M) in buffer A. Active fractions were pooled and concentrated by ultrafiltration to 2 ml and equilibrated in 50 mM HEPES containing 200 mM KCl, pH 7.3 (buffer C). The concentrated sample was applied to a Sephacryl S300 column (1.6 cm X 60 cm, Pharmacia) equilibrated in buffer C and eluted in the same buffer at a flow rate of 0.5 ml/min. Active fractions were pooled and concentrated by ultrafiltration. The purified AntAB was frozen in 25 μl aliquots and stored at –80 ºC.

Purification of AntC.

Purification was carried out at 4 ºC under low light conditions to minimize loss of flavin. Cell-free extract from 6 liters of AntC-induced cells (30 ml) was applied to the same DE52 anion-exchange column as for AntAB purification. The column was washed with 200 ml of buffer A. Bound AntC was eluted with a 250-ml linear gradient of Na_2SO_4 (0-250 mM) in buffer A at 2.0 ml/min. Active fractions (assayed as described below) were pooled and concentrated by ultrafiltration to 10 ml. Filtered 4 M $(NH_4)_2SO_4$ was added to a final concentration of 1 M. The precipitate was removed by centrifugation (12,000 x *g* for 15 min), and the supernatant fluid was applied to a butyl Sepharose column (2 cm X 11.5 cm, Pharmacia) equilibrated in 100 mM potassium phosphate buffer (pH 7.5) containing 1 M $(NH_4)_2SO_4$ (buffer D). AntC was eluted with a 250 ml linear gradient of decreasing $(NH_4)_2SO_4$ concentration (1-0 M) at 2.0 ml/min in 100 mM potassium phosphate buffer (pH 7.5). Active fractions were pooled and

concentrated by ultrafiltration to 10 ml and equilibrated in 50 mM N-tris(hydroxymethyl)ethyl-3-aminopropanesulfonic acid, pH 7.0. Samples were dialyzed against the same buffer containing 5% (v/v) glycerol (4 l X 12 hrs) and 1 mM FAD. The sample was concentrated by ultrafiltration, applied to a Sephacryl S200 column (1.6 cm X 60 cm, Pharmacia) equilibrated in buffer C, and eluted at a flow rate of 0.5 ml/min. Purified AntC was frozen in 25 μl aliquots and stored at -80 ºC.

Purification of benzoate 1,2-dioxygenase (BenDO) and benzoate diol dehydrogenase (BenD).

Purification of the benzoate 1,2-dioxygenase reductase (BenC), the terminal dioxygenase (BenAB), and the benzoate diol dehydrogenase (BenD) from ADP1 has been previously described (7). Each enzyme was recombinantly expressed in *E. coli* and purified to homogeneity.

Analyses.

Protein was quantitated by the method of Bradford (12) with bovine serum albumin as the standard (Bio-Rad). The native molecular weights of proteins were determined by gel filtration using a calibrated Sephacryl S300 column (1.6 cm X 60 cm, flow rate 0.5 ml/min, Pharmacia) equilibrated in buffer C. The calibration proteins were ferritin (M_r 450,000), catalase (240,000), aldolase (158,000), bovine serum albumin (68,000), hen egg albumin (45,000), chymotrypsinogen A (25,000) and cytochrome *c* (12,500). Iron content was

assessed with a colorimetric ferrozine method based on that of Batie et al. (6). A 200-μl protein sample (approx. 10 μM) was added to a polystyrene tube containing 250 μl 0.02% ascorbic acid, 30 μl 6 M HCl and 25 μl of a 5 mg/ml solution of ferrozine. The sample was mixed by vortexing and 1 ml of 8 M guanidine-HCl was added. Saturated ammonium acetate (200 μl) was added and A_{562} was measured. A standard curve with a ferrous ammonium sulfate solution was used to determine the molar extinction coefficient for the ferrous iron-ferrozine complex to be determined as 28,000 $M^{-1}cm^{-1}$.

Flavin cofactor in AntC.

Flavin was extracted by boiling a concentrated 1-ml sample of AntC for 10 min. Denatured protein was removed by centrifugation. Thin-layer chromatography was used to identify the flavin, with silica gel coated glass plates and a mobile phase of butanol: acetic acid: water (4:1:4 volume ratio). Samples were visualized with a hand-held UV light. After identification as FAD, the amount was quantitated spectrophotometrically (ε_{450}=11,300 $M^{-1}cm^{-1}$; ε_{375}=9,300 $M^{-1}cm^{-1}$) (50).

Oxygen consumption and NADH oxidation assays.

Substrate-dependent O_2 consumption catalyzed by AntDO was monitored with a Yellow Springs Instruments Model 5300 biological oxygen monitor equipped with a Clark electrode. NADH oxidation was determined spectrophotometrically at 23 ºC by measuring the decrease in A_{340} (ε_{340}=6300 M^{-}

$^{1}cm^{-1}$). Unless stated otherwise, assays were carried out in 50 mM 2-(N-morpholino) ethanesulfonic acid (MES) (pH 6.3), 100 mM KCl, 0.5 mM substrate, 100 μM NADH, 0.5 μM purified AntAB (or a suitable amount of a crude enzyme preparation), and 0.18 μM of reductase in a final volume of 1 ml for NADH oxidation assays or 2.5 ml for O_2 consumption assays. Rates were corrected for a small background NADH oxidation or O_2 consumption in the absence of substrate. In spectrophotometric assays, corrections were made for the absorbance of anthranilate (ε_{340}=1050 M^{-1} cm^{-1}). Reactions were monitored for 5 min, at which point 1000 U bovine liver catalase (Sigma) was added to the reaction in the oxygraph. Hydrogen peroxide was quantified by the amount of O_2 generated due to the disproportionation of H_2O_2 by catalase. Oxygen consumption and NADH oxidation activity was measured for BenDO under similar conditions and described elsewhere (7).

NADH-cytochrome c reductase activity.

The AntC-catalyzed reduction of cytochrome *c* by NADH was detected by an increase in A_{550} (ε_{550}= 19,500 $M^{-1}cm^{-1}$ for reduced minus oxidized cytochrome *c*). The assay mixture contained 20 μM cytochrome *c* (horse heart type 6; Sigma), 100 μM NADH, 0.5 μM pure AntC (or a suitable amount of a crude enzyme preparation) in 100 mM potassium phosphate buffer, pH 7.

Detection of catechol and diol products with substituted benzoates as substrates.

BenD was used to detect diol product formation in the activity assays of BenDO and AntDO. Conversion of diol products to catechol by BenD was monitored as the increase in A_{340} (ε_{340}= 6.22 $mM^{-1}cm^{-1}$) due to the reduction of NAD^+ to NADH. After consumption of NADH in the BenDO NADH oxidation assays, BenD (either 5 mM or a suitable amount of crude enzyme preparation) was added and monitored at A_{340} for 2 min (7). Catechol products were detected by the addition of Gibb's reagent (2,6-dichloroquinone-4-chloroimide) following AntDO- and BenDO-dependent NADH oxidation reactions and reaction where a detectable increase at A_{340} was observed after addition of BenD (7). Positive reactions were identified by the formation of a blue to purple color.

Optimization of AntDO activity.

A mixed buffer system was used to determine the optimal conditions for assaying AntDO activity. This buffer system contained 50 mM total of equimolar amounts of the following six buffers: MES (pK_a 6.1), N-tris(hydroxymethyl), ethyl-3-aminopropanesulfonic acid (pK_a 7.2), HEPES (pK_a 7.5), N-tris(hydroxymethyl)methyl-3-aminopropanesulfonic acid (pK_a 8.4), 2-(N-cyclohexylamino)ethanesulfonic acid (pK_a 9.3), and 3-(cyclohexylamino)-2-hydroxy-1-propanesulfonic acid (pK_a 10.4). Individual NADH oxidation assays were carried out at pH 5.5, 6.0, 6.5, 7.0, 8.0, and 9.0, using the assay conditions described above. After determining the optimal pH for NADH oxidation, assays

were repeated in MES buffer pH (6.3) at four different ionic strengths (0, 50, 100, or 150 mM KCl).

Monitoring reaction substrates and products by high performance liquid chromatography (HPLC).

Samples from AntDO- and BenDO-catalyzed reactions (1 ml) were separated by HPLC and monitored by absorbance at 210 nm (Bio-Rad automatic sampling system model AS-100, solvent delivery system 2800, detector uv-1806, and peak integration software). Compounds were eluted at a rate of 0.8 ml/min from a reverse-phase C_{18} column (Columbus 5 μm, 250 X 4.6 mm) with a mobile phase of 30% (v:v) acetonitrile:water containing 0.1% phosphoric acid. Substrates and products were identified and quantified by comparison to known standards.

Spectroscopy.

Electron paramagnetic resonance (EPR) spectra were recorded on a Bruker ESP-300E spectrometer equipped with an ER-4116 dual-mode cavity and an Oxford Instrument ESR-9 flow cryostat. Ultraviolet-visible absorption spectra were obtained in 1-cm pathlength quartz cuvettes on a Shimadzu UV2101-PC scanning spectrophotometer. To obtain absorption spectra of reduced [2Fe-2S] centers, oxidized proteins (250 μM) were reduced by anaerobic addition of an excess of sodium dithionite or catalytically by addition of AntC and excess

NADH. Samples for spectroscopy were in 25 mM N-tris(hydroxymethyl), ethyl-3-aminopropanesulfonic acid buffer, pH 7.3.

Putative AntDO and BenDO sequences of Pseudomonas aeruginosa PAO1 and construction of phylogenetic trees.

The ADP1 BenDO and AntDO sequences were compared to 6-phase translations of the complete genome sequence of *P. aeruginosa* PAO1 (http:// www.pseudomonas.com) using the BLAST program of the National Center for Biotechnology Information (http:// www.ncbi.nlm.nih.gov). Putative *antABC* and *benABC* sequences at approximate positions 2829398 and 2835988 were identified on the basis of similarity to ADP1 sequences (52 to 70 % identity between homologous deduced protein sequences), restriction site analyses of *Eco*RI and *Kpn*I recognition sequences from previous studies, and the relative position of *cat, ant,* and *ben* genes determined by previous investigations of mutants and mapping studies of mutant loci (161, 162)

Deduced amino acid sequences of ARHDOs were aligned with the Pileup program of the Genetics Computer Group package (41). Trees were generated by applying the neighbor-joining method from a distance matrix created with PROTDIST using the Kimura algorithm of the Phylip program package (University of Washington, Seattle, WA; version 3.52c for UNIX). The SeqBoot program was used for bootstrap analyses. Alternate algorithms for generating trees (Fitch and Kitch) and distance matrices (Dayhoff/PAM and parsimony) produced similar results.

Results

Expression and purification of AntDO.

Genes encoding the ADP1 oxygenase (*antAB)* or reductase (*antC)* components were expressed from plasmids in *E. coli*, a bacterium with no known AntDO genes or activity. The oxygenase and reductase components were each purified to homogeneity by anion-exchange chromatography, hydrophobic interaction chromatography and finally, size-exclusion chromatography. Active AntAB in *E. coli* could be detected by a color change upon addition to the cultures of anthranilate and ferrous iron. The medium gradually turned a dark purple, an identical color to that resulting from addition of catechol and iron to medium with no bacteria. As observed for other oxygenase components (108), AntAB appeared to use an endogenous source of electrons in *E. coli* to catalyze hydroxylation without its native reductase. This color development, presumably due to catechol formation, was a convenient visual indicator of AntAB activity. No dark color developed in the absence of anthranilate or when anthranilate and ferrous iron were added to medium without bacteria.

The *antA* and *antB* genes, adjacent in ADP1 (19), were co-expressed in *E. coli.* This yielded high levels of two proteins corresponding approximately in size to the deduced sequences of the α (54 kDa) and β (19 kDa) subunits, respectively, of AntDO (Fig. 2.2, lanes 2 and 3). Size-exclusion chromatography of the pure AntAB revealed a single oligomer of approximately 220 kDa, which indicates that AntAB is an $\alpha_3\beta_3$ hexamer (Table 2.2). The pure AntAB had a

distinctive red-brown color. Using the extinction coefficient determined at 454 nm (see below), approximately 12.5 mg of pure AntAB were obtained per liter of *E. coli* culture containing the *antAB* plasmid.

Independent expression of *antC* in *E. coli* resulted in abundant production of a protein of a size close to that predicted for the AntDO reductase component (Fig. 2.2, lanes 5 and 6). Initial attempts to isolate and purify AntC resulted in loss of flavin, a process that was visually evident during anion exchange chromatography as a yellow-colored fraction eluting prior to the AntC protein. By minimizing its exposure to light during purification, AntC could be purified with retention of the majority of its flavin (see below). SDS-PAGE and gel filtration indicated that the purified AntC was a monomer of 39 kDa. Approximately 12.5 mg of pure AntC were obtained per liter of *E. coli* culture containing the *antC* plasmid.

Purification of the M43K variant dioxygenase.

A plasmid was expressed in *E. coli* with the *Acinetobacter* wild-type *antB* downstream of the *antA5024* allele (19), which encodes the M43K AntA. The mutant *antAB* did not yield the color change indicative of catechol formation after anthranilate and iron were added to cultures grown at 25 ^{0}C or 37 ^{0}C. Nevertheless, the variant dioxygenase could be purified by the same methods as for wild-type AntAB. In *E. coli*, the mutant genes yielded more AntA that was insoluble compared to the wild-type genes. The insoluble AntA, which was removed by centrifugation following cell sonication, appeared in the pellet (Fig.

2.2, lane 9). In the supernatant from which a low yield of the M43K oxygenase was purified, there was more AntB relative to AntA than with the wild-type oxygenase (Fig. 2.2, lane 8). The subunit sizes of the variant dioxygenase, however, were as expected (Fig. 2.2). The purified component migrated identically to the wild type AntAB on the same size-exclusion column and was, therefore, also inferred to be an $\alpha_3\beta_3$ hexamer. SDS-PAGE of purified M43K AntAB showed α and β bands of approximately the same relative intensities as for the wild-type component (not shown).

Quantitation of the flavin in AntC.

The flavin in the recombinant AntC was identified as FAD by comparison to FAD and flavin mononucleotide standards using thin layer chromatography. When isolated under low-light conditions, AntC contained 0.7 mol FAD per mol of AntC monomer. The reductase activity of AntC could be increased by reconstitution with excess FAD followed by passage over a Sephadex G-25 column to remove unbound FAD. When reconstituted in this fashion, AntC had 1.5 mol FAD per mol AntC (Table 2.2). Further addition of FAD did not increase AntC activity. The AntC isolated in normal room light had less than 4% of the flavin in the low-light-isolated AntC on a per protein basis. The FAD-depleted AntC, when substituted for a comparable level of FAD-enriched AntC, had no detectable catalytic activity.

Iron content in AntDO.

AntC contained 2.3 ± 0.5 mol iron/mol AntC monomer, consistent with the prediction of one [2Fe-2S] center (21, 109). AntAB contained 8.8 ± 1 mol iron/mol protein based on a molecular weight of 220,000 (Table 2.2). Considering the $\alpha_3\beta_3$ subunit composition, the iron analysis is consistent with the prediction of one [2Fe-2S] center and one mononuclear center per α subunit (21, 109). The purified M43K AntAB had 8.1 ± 0.2 mol iron/mol protein, perhaps indicating one empty mononuclear site.

Spectroscopic properties of AntDO.

The absorption spectra of oxidized and enzymatically-reduced recombinant wild-type AntAB are shown in Fig. 2.3A. The absorption maximum of the oxidized AntAB at 454 nm (ε = 14,400 $M^{-1}cm^{-1}$) and the shoulder at 555 nm are typical of Rieske-type $[2Fe\text{-}2S]^{2+}$ centers (6, 21, 49, 109). Upon anaerobic reduction with a catalytic amount of AntC and excess NADH, the absorption spectrum of AntAB resembled those of other reduced (i.e., $[2Fe\text{-}2S]^{+}$) Rieske-type centers, with a general decrease in absorbance throughout the visible region and shoulders at ~520 and 400 nm. Resting oxygenase components of other ARHDOs (21, 94, 153) invariably have their mononuclear centers in the Fe(II) oxidation state, and this reduced mononuclear center is not expected to contribute to either the oxidized or the reduced visible absorption spectrum. Also shown in Fig. 2.3A (inset) is the absorption spectrum of the M43K AntAB. This

spectrum is consistent with a perturbation, but not destruction of the oxidized Rieske center.

The visible absorption spectrum of low-light purified FAD-enriched AntC (Fig. 2.3B) and that of FAD-depleted AntC isolated under normal room light show that AntC has both FAD and a ferredoxin-type $[2Fe\text{-}2S]^{2+}$ center (21, 77). The maxima at ~425 and 460 nm and shoulder at ~550 nm in the absorption spectrum of flavin-depleted AntC are characteristic of ferredoxin-type $[2Fe\text{-}2S]^{2+}$ centers. The ratios of absorption intensities at 330 or 370 nm relative to that at 450 nm in the FAD-enriched reductase are higher than those for the phthalate 4,5-dioxygenase reductase component, which also contains one flavin and one $[2Fe\text{-}2S]^{2+}$ chromopohore (6) (56). Presumably, the excess FAD (1.5 mol/mol AntC) is responsible for the altered absorption intensities of AntC.

The 10-K EPR spectra of the dithionite-reduced AntAB and AntC (Fig. 2.4) confirm the presence of [2Fe-2S] centers. The AntAB EPR spectrum, with g_{avg} = 1.91 and derivative peak at g = 2.01, is characteristic of Rieske-type $[2Fe\text{-}2S]^{+}$ centers (152), and the AntC spectrum with g_{avg} = 1.97, is characteristic of ferredoxin-type $[2Fe\text{-}2S]^{+}$ centers. EPR signals in the g = 4-6 region, which are expected for a mononuclear high spin Fe(III) site in a low-symmetry coordination sphere of oxygen and nitrogen ligands, were not observed in the recombinant wild-type AntAB. Thus, the mononuclear site is most likely in the Fe(II) oxidation state, which is not expected to show an EPR spectrum under these conditions.

Catalytic Properties of AntDO.

AntDO activity was measured by monitoring anthranilate-dependent consumption of NADH. The optimal conditions of pH and salt concentration for this activity were pH 6.3 and 100 mM KCl. This optimization was accomplished with saturating NADH, aromatic substrate, and O_2 (typically 100 μM, 1 mM, and ~0.25 mM, respectively), 0.5 μM AntAB (hexamer) and 0.18 μM AntC. These reagent concentrations were chosen for convenience in monitoring NADH consumption via absorbance at 340 nm. Unless otherwise noted, these conditions were used for all reported results. Under these non-saturating AntC conditions, the turnover number of AntAB, measured as the rate of NADH consumption, was 63 min^{-1} on a per mononuclear site basis.

The K_m of AntAB for AntC was determined with 0.01 μM AntAB and variable amounts of AntC from 0.1 to 2 μM. All other conditions were standard. A Lineweaver-Burk plot was used to estimate a K_m for AntC of 1.4 ± .1 μM. Under saturating (2 μM) AntC, 0.01 μM AntAB and 100 μM NADH, a turnover number of 1300 min^{-1} was observed. Activity levels did not decrease when the anthranilate concentration was reduced to1 μM. The small absorbance change for NADH consumption at < 1 μM anthranilate precluded accurate rate measurements below this concentration. Therefore, the K_m of AntDO for anthranilate was inferred to be <1 μM. An analogous determination under the same conditions gave a K_m for benzoate of ~12 μM.

Activities of AntDO with anthranilate and benzoate.

Table 2.3 summarizes the activities of the purified recombinant AntDO and M43K AntDO with anthranilate and benzoate, as well as quantitations of substrate consumption and product formation. Several considerations circumscribe interpretation of the data in Table 2.3. These activities were measured under conditions that had been optimized for anthranilate as substrate. The relative activities listed in the second column are for initial rates of NADH consumption only; for reasons discussed below, these activities do not necessarily correlate with or even signify consumption of the aromatic carboxylate (as can be seen from the data in the fifth column). To avoid significant background consumption of NADH and O_2 and to allow simultaneous measurements of consumption of several substrates on a reasonable time scale, a non-saturating concentration of AntC was used.

Under conditions optimized for anthranilate turnover, benzoate was a good substrate for AntDO, resulting in 70% of the activity rate as with anthranilate (Table 2.3). Benzoate allowed tight coupling of NADH, O_2 and substrate consumption (i.e. 1:1:1 mol ratio) with no evidence for inactivation of the enzyme. No H_2O_2 was detected in these reactions. Together with the tight coupling, this indicates that all O_2 consumed was incorporated into the substrate. The product of AntDO catalysis with benzoate was the same non-aromatic diol as that formed by the similar *Acinetobacter* sp. ADP1 BenDO [33]. Since AntDO can efficiently convert benzoate to the non-aromatic diol under these conditions but apparently does not do so in vivo, we investigated the effect of lowering the

substrate concentrations. When substrate concentrations were decreased 100-fold to 5 μM, a value still saturating for anthranilate but not for benzoate, NADH oxidation with anthranilate remained identical to that previously observed. However, NADH oxidation with 5 μM benzoate decreased by 45% to a value 23% that of anthranilate-dependent oxidation. Thus, the relative activities of AntDO towards anthranilate and benzoate are modulated by their different apparent K_ms.

Activity of the variant M43K AntAB.

While the soluble yield was much lower, the characterization of the M43K AntAB described above indicated that its overall structure and metal centers are not grossly altered compared to the wild-type protein. M43K AntAB had approximately 25% of the NADH oxidation and O_2 consumption activity of recombinant wild type using anthranilate as substrate at 23 C°. No change in NADH consumption activity was observed with benzoate as substrate. However, this activity, while substrate dependent, was completely uncoupled from substrate hydroxylation. All NADH and O_2 consumed in the reaction could be accounted for by the generation of H_2O_2. No organic product with either anthranilate or benzoate as substrate was detected. Supplementing M43K AntAB with 5, 10, or 100 μM Fe (II) did not increase activity.

In our assays, neither wild-type nor M43K AntDO had any activity at 39 ^{0}C. Samples of AntAB or M43K AntAB were incubated at 39 ^{0}C for 10 min and allowed to cool to room temperature. The heat-treated AntAB exhibited 20% less

activity than a non heat-treated sample, and the stoichiometry of NADH:O_2 consumption was still 1:1 with no detectable H_2O_2. The heat-treated M43K AntDO had comparable activities to a non heat-treated sample, but NADH consumption remained uncoupled from substrate hydroxylation, with H_2O_2 formation accounting for all the NADH and O_2 consumed.

Substrate range of AntDO.

Since ADP1 cannot grow on halobenzoates, methoxybenzoates, or methylbenzoates, it seemed likely that AntDO would have a substrate range narrower than the broad-substrate-specific benzoate dioxygenases. We tested a set of these substituted benzoate as substrates for AntDO (Table 2.4). Aromatic substrate consumption was detected predominately when benzoates with an *ortho* substituent other than hydrogen were used as substrates. The compounds *o*-fluorobenzoate, *o*-chlorobenzoate, and *o*-toluate, as well as anthranilate and benzoate, are good substrates for tightly-coupled hydroxylation reactions catalyzed by the *cbdABC*-encoded 2-halobenzoate 1,2-dioxygenase from *Burkholderia cepacia* (50) (64). Under the assay conditions with 100 μM NADH, described in Table 2.3, HPLC analyses indicated that no *o*-chlorobenzoate, and only 18 μM and 13 μM *o*-fluorobenzoate or *o*-toluate were consumed, respectively. With each of these substrates, more than 40 μM NADH was consumed indicating that electron transfer was uncoupled from substrate hydroxylation.

Putative AntDO and BenDO sequences from Pseudomonas aeruginosa.

Sequence comparisons were used to address the evolutionary relationships among various ARHDOs. Previous studies of catabolic mutants and the relative positions of genetic loci (161, 162) allowed us to identify the putative AntDO and BenDO sequences of *P. aeruginosa*. In pairwise comparisons of the deduced sequences of AntDO from *Acinetobacter* sp. ADP1 and *P. aeruginosa* PAO1, identities and similarities were, respectively, 74% and 81% for the α subunits, 54% and 64% for the β subunits, and 60% and 68% for the reductases. These sequences were also compared to that of BenDO from *Pseudomonas putida* PRS2000 (34). Phylogenetic trees (Fig. 2.5) were generated from multiple sequence alignments of these ARHDOs and others that degrade xenobiotics, which have previously been characterized as class IB based on similarity among all components (Table 2.1). Sequences of the α-subunits of two well-characterized ARHDOs of different classes were also aligned. These α-subunits were NdoB and Pht3 of the class III naphthalene 1,2-dioxygenase (NDO) and the class IA phthalate dioxygenase, respectively (Table 2.1 and Fig. 2.5A). The sequences of other proteins of these latter two dioxygenases were not included in the phylogenetic trees because of relatively poor alignment. The sequences are not known for the reductase of the 2,4,5-trichlorophenoxyacetic acid oxygenase nor for that of the aminobenzene sulfonate dioxygenase. Only the sequence of the α-subunit (AbsA) of the latter enzyme is available.

Discussion

Different enzymes can catalyze the first step in aerobic pathways for anthranilate catabolism. In eukaryotic microbes, anthranilate is first hydroxylated to form 2,3-dihydroxybenzoate by anthranilate hydroxylase. This enzyme is a flavoprotein monooxygenase in *Trichosporon cutaneum* (132) but contains only non-heme iron as a prosthetic group in *Aspergillus niger* (147, 148). Another enzyme, 2-aminobenzoate-CoA ligase, initiates anthranilate degradation in a denitrifying *Pseudomonas* species (1). The AntDO described in this report is distinct from the previously mentioned enzymes and allows aerobic bacteria to use anthranilate as a source of carbon and energy. AntDO had not previously been purified to homogeneity from any organism.

Characterization of AntDO.

The AntDO oxygenase component (AntAB) of *Acinetobacter* sp. ADP1 contains both mononuclear non-heme iron and Rieske-type [2Fe-2S] centers as do all other known ARHDOs. The presumed ligands of the mononuclear and Rieske centers are well conserved among AntDO and other ARHDO oxygenase components (Fig. 2.6). The results reported here also confirm that AntDO can be classified as a two-component class IB ARHDO (9, 109). The key features for this classification are the presence of both FAD and a [2Fe-2S] center in the reductase component (AntC), and the lack of a separate ferredoxin in the electron transfer chain (Table 2.1).

Gel-filtration chromatography indicates that AntDO is an $\alpha_3\beta_3$ hexamer. This same oligomeric structure was found for the dioxygenase component of NDO, a class III ARHDO (Table 2.1). NDO is the only such component for which an x-ray crystal structure has been solved (94). The dioxygenase components of NDO and AntDO appear to share a common evolutionary origin (Fig. 2.5A) and presumably common structure-function relationships. Alignment of nine class IB α-subunit sequences, including AntA, shows that all of the residues furnishing iron ligands in NdoB are conserved (Fig. 2.6). Two class IB dioxygenases, BenDO from *Pseudomonas putida (arvilla*) C-1 and the 2-halobenzoate 1,2-dioxygenase from *Burkholderia cepacia* were also shown to be $\alpha_3\beta_3$ hexamers (50, 157). These latter two enzymes have pH optima in a range similar to that determined here for AntDO, pH 6.3 (50, 157). As found for AntDO, all of these analogous ARHDOs appear to have a monomeric reductase component.

Temperature sensitivity and the M43K AntDO variant dioxygenase.

Our results do not directly explain the temperature-sensitive phenotype of the *Acinetobacter* mutant that encodes M43K AntDO (19). Although a low yield of a stable $\alpha_3\beta_3$ hexamer of this variant enzyme could be purified, the recombinant enzyme did not hydroxylate anthranilate at either the permissive (22 ^{0}C) or non-permissive (39 ^{0}C) temperature for growth of the mutant on anthranilate. Since a majority of the recombinant M43K AntA was insoluble, it is possible that the temperature sensitivity lies in instability of the □-subunit prior to its assembly into the hexamer. Our studies of the soluble recombinant M43K

AntDO provided no evidence that the basis for temperature sensitivity in *Acinetobacter* involves dissociation of the hexamer. The M43 residue is in a highly conserved region of the N-terminal domains of the class IB ARHDOs. In the alignment used to generate Fig. 2.5A, 8 of the 9 class IB sequences contained a methionine corresponding to the 43rd residue of the ADP1 AntA. The exception was AbsA in which a lysine is normally present rather than methionine, consistent with active dioxygenases tolerating this amino acid substitution under some conditions.

Substrate preferences of AntDO.

The purified AntDO catalyzed the conversion of anthranilate to catechol in a well-coupled reaction. The recombinant AntDO also catalyzed the tightly coupled conversion of benzoate to benzoate 1,2-diol, as does BenDO. The inability of ADP1 strains lacking functional structural genes encoding BenDO to grow on benzoate may reflect the inability of benzoate to induce AntDO, insufficient production of the *benD*-encoded benzoate diol dehydrogenase in vivo, and/or problems with the rate of benzoate diol formation by AntDO (118) (19). The lower apparent K_m of AntDO for anthranilate versus benzoate suggests that intracellular substrate levels also contribute to growth specificities. The apparent K_m for anthranilate of < 1 μM indicated a high affinity of AntDO for this substrate. To date, the best-characterized BenDO is from *Pseudomonas putida (arvilla)* C-1, for which an apparent K_m for benzoate of approximately 4 μM was reported (157). Since the latter enzyme also has a higher turnover number for its

substrate, approximately 4-fold higher than that of AntDO for anthranilate, the specificity constants (k_{cat}/K_m) for these two enzymes might be comparable. The ARHDO encoded by the *cbdABC* genes, appears to have a lower affinity for its substrate with an apparent K_m for 2-chlorobenzoate of 22 μM (50). This enzyme, unlike AntDO, has an extremely broad substrate range and can efficiently hydroxylate a variety of *ortho*-substituted benzoate analogs. The relatively low affinity of the halobenzoate 1,2-dioxygenase for 2-chlorobenzoate might indicate that the broad substrate specificity evolved at the expense of catalytic efficiency.

Substrate range of AntDO compared to BenDO

The relative activities of the purified recombinant BenDO with benzoate, anthranilate, and other benzoate analogs are summarized in Table 2.5. The tight coupling of the BenDO-catalyzed hydroxylation of benzoate to electron transfer is confirmed by the stoichiometry of the substrates (NADH, dioxygen, and benzoate) consumed to the formation of benzoate diol: 1:1:1:1. Tightly coupled reactions were also observed when AntDO used either anthranilate or benzoate as a substrate.

When anthranilate was used as the substrate for BenDO, the amount of anthranilate consumed to catechol formed was greater then 1:1, although the consumption of each substrate was approximately 1:1:1. The less than complete conversion of anthranilate to catechol contrasts to the substrate:product stoichiometry of the AntDO-catalyzed hydroxylation of either benzoate or anthranilate, where conversions of both substrates to products were tightly

coupled (Table 2.4). There is the possibility that BenDO converts some anthranilate to an anthranilate diol, but no such product has ever been isolated from these reactions. Anthranilate may bind in the substrate pocket of BenDO with ring carbons 1 and 6 positioned to be hydroxylated. Carbons 1 and 6 of anthranilate are regio-homologous to carbons 1 and 2 of benzoate (Reaction 2.1).

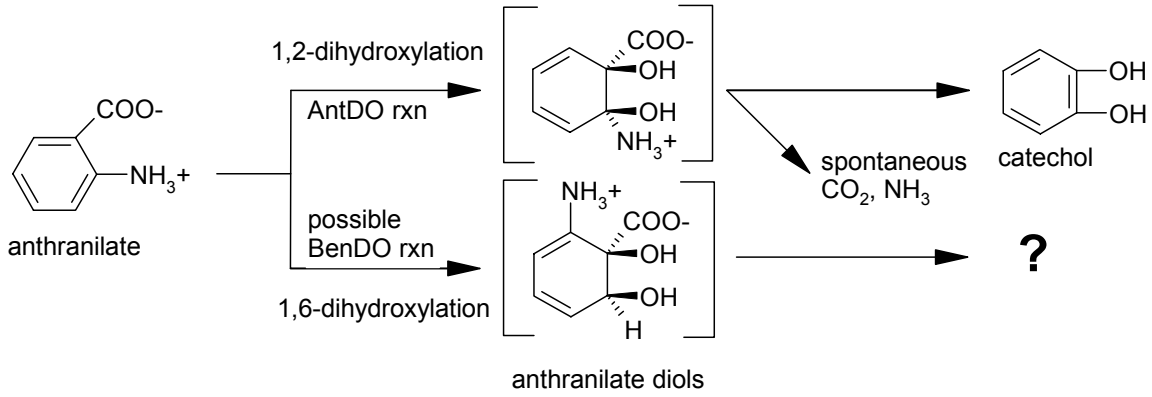

Reaction 2.1 Hypothetical 1,6-dihydroxylation of anthranilate by BenDO

With many other substituted benzoate, the AntDO- and BenDO-dependent oxidation of NADH and the consumption of O_2 led to the production of H_2O_2. This uncoupling of electron transfer from substrate hydroxylation occurs when some or all of the electrons from NADH are used to reduce O_2 without dihydroxylation of the aromatic compound (7, 62, 91, 104). The uncoupling of electrons in oxygenase reaction leads to the formation of H_2O_2 and/or H_2O. In our studies, H_2O_2 can be detected using the catalase reaction, while formation of H_2O cannot be detected directly (7). Reduction of 1 mol O_2 to 1 mol H_2O_2 requires 2 mol electrons or 1 mol NADH, while twice as many electrons are

required to reduce O_2 to H_2O. The BenDO-catalyzed reduction of O_2 in the presence of *p*-methylbenzoate and *o*-methoxybenzoate, and in the AntDO-catalyzed reduction of O_2 in the presence of *p*-methoxybenzoate, all electrons from NADH oxidation were used to produce H_2O_2 (Tables 2.4 and 2.5).

In most cases, either a diol or catecholic product was detected in reactions using AntDO. *o*-chlorobenzoate, *p*-methoxybezoate and *p*-hydroxybenzoate were the only three substrate used in AntDO-catalyzed reactions that did not produce a detectable product. All other benzoate analogs, other than anthranilate, produced a detectable diol or catecholic product during uncoupled reactions, where a larger amount of NADH was oxidized compared to O_2 and aromatic substrate consumption. Some of the excess electrons were used in each of these reactions to produce H_2O_2.

Because AntDO is able to act upon many of the benzoate analogs and especially, with some of the *ortho*-substituted benzoates converted to catechol, this enzyme may be a good candidate to alter its substrate specificity to allow ADP1 to degrade novel substrates. The fact that *o*-fluorobenzoate and *o*-methoxybenzoate are converted to catechol directly by AntDO could suggest ADP1 could utilize these substrates as carbon and energy, if expression in the strain would allow sufficient activity to support growth. *o*-hydroxybenzoate, which is also converted to catechol by AntDO, can be used a carbon source by ADP1 via the *sal* and *ben* genes.

BenDO showed a preference for *meta* substituted benzoates with the exception of the methoxy- and hydroxybenzoates. The amount of NADH

oxidized in these reactions did not necessarily parallel diol or catechol formation. In some cases, electron transfer was diverted from substrate hydroxylation to reduce some (*m*-aminobenzoate) or all (*p*-methylbenzoate and *o*-methoxybenzoate) of the O_2 consumed to H_2O_2 in uncoupled reactions. In reactions with BenDO-catalyzed ortho-substituted benzoates, which produced detectable diol product, it is uncertain if dihydroxylation occurs at carbon 1 and 2, carrying the carboxylate and ortho substituent, or at carbons 1 and 6, which would be similar to dihydroxylation of benzoate, where carbon 2 is bonded to a hydrogen. Studies directed to identification of these diol products will resolve this question.

Evolution of the class IB ARHDOs.

In previous studies, evolutionary relationships among the α-subunits of ARHDOs of different classes have been established [29, (108). In this report, the identification of the likely AntDO and BenDO sequences from *P. aeruginosa* PAO1 and the recent availability of the BenDO sequence from *P. putida* PRS2000 (34) made it possible to examine relationships among all components of the class IB ARHDOs. The branching patterns of the phylogenetic trees for the α- and β-subunits of the class IB terminal oxygenases are nearly identical. The matched branching patterns are consistent with the class IB ARHDOs having evolved from an ancestral two-subunit oxygenase component. The CbdAB component that hydroxylates halobenzoates may be more closely related to BenAB than to AntAB. The plasmid-encoded XylXY component, which

hydroxylates methylbenzoates, appears to have diverged relatively recently from BenAB. The AbsA α-subunit component was as distantly related to the other class IB ARHDOs as was the NdoB of the class III NDO, consistent with the Abs dioxygenase being an atypical Class IB enzyme (107).

Phylogenetic comparisons of the reductases (Fig. 2.5C) demonstrate that the *Acinetobacter* and *Pseudomonas* AntC homologs, like the corresponding AntA and AntB homologs, are closely related to each other. In contrast, the BenC reductase of ADP1 was not as closely related to its *Pseudomonas* homologs as were the BenA and BenB proteins. This greater divergence may reflect the relaxed requirement of oxygenase components for specific reductases. For example, the *Acinetobacter* AntAB dioxygenase component does not require its cognate reductase for activity but appears to function both with BenC in vivo [6], and, as shown here, in a heterologous expression system with an unidentified *E. coli* reductase. During evolution, the reductases may tolerate more amino acid substitutions than the oxygenases. Additionally, the recruitment and association of different oxygenase- and reductase-components may occur. The newly available BenDO sequences demonstrate the tight clustering of XylZ with the *Pseudomonas* BenC reductases. Thus the broad-substrate-specific toluate dioxygenase, encoded by the *xylXYZ* genes of a *Pseudomonas* plasmid (68) (3), may have evolved from a *Pseudomonas* BenDO rather than from the BenDO of ADP1 to which it has previously been compared (67).

Acknowledgements

We thank Alison Buchan and Barny Whitman for helpful discussions on phylogenetic trees and Ish Dhawan for assistance in obtaining EPR spectra.

This work was supported by the National Institutes of Health Grant GM59818-01 (E.L.N. and D.M.K.), National Science Foundation Grant MCB-9808784 (E.L.N.), and National Science Foundation Research Training Grant BIR9413235 (support for D.M.E. and Z.M.B).

This chapter is an adaptation to the following publication: Eby, D. M., Z. M. Beharry, E. D. Coulter, D. M. Kurtz, Jr., and E. L. Neidle. 2001. Journal of Bacteriology. 183(1):109-118. The information contained in this dissertation from the published article is reprinted with permission of publisher.

TABLE 2.1. Classification of selected ARHDOs.

Enzyme[a]	Genes	Enzyme class[c]	Characteristics of class
Anthranilate 1,2-dioxygenase (AntDO) Benzoate 1,2-dioxygenase (BenDO) 2-Aminobenzenesulfonate dioxygenase 2-Halobenzoate 1,2-dioxygenase Toluate 1,2-dioxygenase 2,4,5-Trichlorophenoxyacetic acid oxygenase	*antABC* *benABC* *absA*[b] *cbdABC* *xylXYZ* *tftAB*[b]	class IB	Two components **Reductase component:** FAD ferredoxin-type [2Fe-2S] **Oxygenase component:** Rieske-type [2Fe-2S] mononuclear Fe(II)
Phthalate dioxygenase	*pht3, pht2*	class IA	Two components **Reductase component:** Flavin mononucleotide ferredoxin-type [2Fe-2S] **Oxygenase component:** Rieske-type [2Fe-2S] mononuclear Fe(II)
Naphthalene 1,2-dioxygenase (NDO)	*ndoBAC*[b]	class III	Three components **Reductase component:** FAD Ferredoxin-type [2Fe-2S] **Ferredoxin component:** Rieske-type [2Fe-2S] **Oxygenase component:** Rieske-type [2Fe-2S] mononuclear Fe(II)

[a] Abbreviations for dioxygenases are in parentheses.
[b] Genes encoding some components are not yet identified.
[c] According to the classification of Batie et al (21, 109).

TABLE 2.2. Molecular and spectroscopic properties of recombinant *Acinetobacter* sp. ADP1 AntDO

component	molecular weight (M_r)			iron content (mol/mol protein)	flavin content (mol/mol protein)	Absorption maxima (λ[$mM^{-1}cm^{-1}$])
	calc'd from sequence	SDS-PAGE	gel filtration			
AntAB (oxygenase)	53,942 (α) 19,333 (β)	52,000 (α) 21,500 (β)	220,000	8.8±1[a]	0	320(31)[ae] 454(14.4)[a] 555(7)[ae]
M43K AntAB (oxygenase)	53,939 (α) 19,333 (β)	52,000 (α) 21,500 (β)	220,000	8.1±0.2	0	320[e] 454 555[e]
AntC (reductase)	38,553	39,000	45,000	2.3±0.5	0.7[b], 1.5[c]	330 (25)[c] 370 (23)[c] 450 (22)[c] 410,462[d]

[a] Per $\alpha_3\beta_3$ hexamer, as-isolated (oxidized Rieske center, reduced mononuclear center).

[b]As FAD from low-light isolation.

[c]After reconstitution with FAD as described in Materials and Methods.

[d]Low-flavin form; ε not determined (cf. Fig. 3).

[e]Peak shoulder

TABLE 2.3. Activities and reaction stoichiometries of recombinant *Acinetobacter* sp. ADP1 AntDO and M43K AntDO with anthranilate and benzoate[a]

	Aromatic Substrate	**Activity (%)[b]**	**Stoichiometries in NADH-limited reactions (μM)[c]**			
			Substrate Consumed			Product formed, identity
			NADH	O_2	Arom. Sub.	
AntDO	Anthranilate	100	95 (10)	100(7)	91(2)	87(2), catechol
	Benzoate	69(4)	89(9)	86(8)	83(9)	NQ[d], benzoate 1,2-diol
M43K AntDO	Anthranilate	24(2)	23(4)	24(2)	None	14(3), H_2O_2
	Benzoate	24(3)	23(3)	22 (5)	None	16(4), H_2O_2

[a]Assay conditions: 100 μM NADH, 0.25 μM O_2, 500 μM aromatic carboxylate, 0.5 μM AntAB, 0.18 μM AntC, and in 50 mM MES, 100 mM KCl (pH 6.3) at room temperature (~23 ºC). Values (SD) listed are the averages of three determinations. Small background consumptions of NADH and O_2 in the absence of aromatic carboxylates were subtracted in each case.

[b]Initial rate of NADH oxidation (A_{340}/min) expressed as a percentage of recombinant wild type AntDO with anthranilate as substrate (40 ± 1 μM NADH oxidized/min/μM AntAB hexamer) under the assay conditions listed in footnote a.

[c]Measured by: ε_{340} = 6,300 $M^{-1}cm^{-1}$ (NADH), oxygen electrode (O_2), or HPLC using known standards (aromatic substrate and product formed). Assay conditions are listed in footnote a.

[d]Not quantitated because the compound was not well resolved by HPLC.

Table 2.4. Activities, reaction stoichiometries and product formation of recombinant *Acinetobacter* sp. ADP1 AntDO with various benzoate derivatives.[a]

	Substrate consumed (μM/5 min)			Product formed (μM/5 min)		
Substrate	NADH[b]	O_2[b]	Aromatic substrate[c]	H_2O_2	Diol product[d]	Catechol product[e]
anthranilate	100±6	102±7	101±3	n.d.[f]	-	+, 96±2[g]
benzoate	89±9	86±8	80±11	n.d.[f]	+, 80±5[h]	-
m-aminobenzoate	47±10	47±10	n.d.[f]	5	-	+
p-aminobenzoate	21±5	11±1	6±2	2	+	+
o-fluorobenzoate	47±9	40±9	18±2	5	+	+, 12±2[g]
m-fluorobenzoate	36±6	33±6	+	5	+	-
p-fluorobenzoate	45±8	42±6	+	2	+	-
o-chlorobenzoate	42±9	30±9	n.d.[f]	3	-	-
m-chlorobenzoate	48±7	43±2	+	15	+	-
p-chlorobenzoate	32±5	23±5	+	13	+	-
o-methylbenzoate	47±7	39±6	13±2	5	+	+
m-methylbenzoate	48±6	36±7	+	5	+	-
p-methylbenzoate	28±4	19±9	+	7	+	-
o-methoxybenzoate	43±4	42±5	23±4	3	+	+,19±3[g]
m-methoxybenzoate	57±3	43±7	ND	7	+	-
p-methoxybenzoate	12±7	10±4	ND	12	-	-
o-hydroxybenzoate	63±4	60±8	48±4	5	-	-[i]
m-hydroxybenzoate	42±5	30±3	ND	5	-	+
p-hydroxybenzoate	20±3	18±7	ND	7	-	-
M43KAntAB with anthranilate	23±4	24±2	n.d.[f]	14	-	-

[a]Assay conditions: 100 μM NADH, 0.25 mM O_2, 0.5 mM aromatic carboxylate, 0.5 μM AntAB, 0.18 μM AntC, and in 50 mM MES, 100 mM KCl (pH 6.3) at room temperature (23 ºC). Values listed are after 5 min.

[b]Relative activities are defined as the percentage of NADH or O_2 consumed after 5 min relative to AntDO activity with anthranilate. Since AntDO activity with anthranilate consumed 100 μM NADH in 5 min, the amount of NADH consumed with other substrates also reflects the relative activity (%).

[c]+, substrate consumption was detected by HPLC but could not be quantified accurately; ND, not determined.

[d]Detected by the increase at 340 nm due to formation of NADH upon addition of BenD (5 μM) and NAD^+ (0.2 mM). BenD was added to reactions after 5 min. of NADH consumption. +, indicates generation of NADH; -, no generation of NADH was observed.

[e]Gibbs' reagent (15 μL of a 2 % (w/v) solution in ethanol) was added to AntDO reactions (200 μL) and judged to be positive (+) by formation of a blue to purple color; -, no color change occurred. These analyses were conducted without BenD.

[f]None detected.

[g]Product was detected and identified as catechol and quantified by HPLC.

[h]Benzoate diol was identified as the product using HPLC as described in Materials and Methods; the amount of benzoate diol formed was determined by the amount of NADH generated upon addition of BenD (5 μM) and NAD^+ (0.2

mM) to activity assays (described in Materials and Methods except with 0.1 mM benzoate) after 5 min.

[/]Product was detected using HPLC but could not be detected using Gibbs' reagent or BenD.

Table 2.5. Activities, reaction stoichiometries and product formation for recombinant *Acinetobacter* sp. ADP1 BenDO with various benzoate derivatives.[a]

Substrate	NADH (μM/5 min) (Rel. act., %)[b]	O_2 (μM/ 5 min)	H_2O_2 (μM/ 5 min)	Substrate consumed (μM/5 min)[c]	Diol product[d]	Catechol Product[e]
benzoate	67±3 (100)	68±4	-	61±2	+	-
o-aminobenzoate	45±4 (67)	42±2	-	36±2	-	+, 13±1[g]
m-aminobenzoate	55±3 (82)	50±3	10	+[f]	-	+
p-aminobenzoate	36±5 (53)	31±7	-	2±1	-	+
o-fluorobenzoate	38±7 (57)	32±6	-	10±5	+	-
m-fluorobenzoate	50±8 (74)	48±9	-	41±4	+	-
p-fluorobenzoate	53±2 (79)	40±5	7	7±2	+	-
o-chlorobenzoate	26±4 (38)	24±2	5	2±1	-	-
m-chlorobenzoate	49±7 (73)	42±9	3	37±9	+	-
p-chlorobenzoate	21±3 (31)	18±5	5	None	-	-
o-methylbenzoate	30±2 (44)	21±6	7	17±4	-	-
m- methylbenzoate	65±9 (97)	62±2	3	41±19	+	-
p-methylbenzoate	25±6 (37)	21±4	20	None	-	-
o- methoxybenzoate	18±5 (26)	18±2	17	None	-	-
m-methoxybenzoate	21±3 (31)	19±4	3	8±1	-	-
p-methoxybenzoate	23±2 (34)	12±3	3	9±7	-	-
o-hydroxybenzoate	30±4 (44)	23±7	10	13±4	-	-
m-hydroxybenzoate	24±5 (35)	18±2	8	+[f]	-	+
p-hydroxybenzoate	20±1 (30)	14±3	5	10±2	-	+

[a]Assay conditions: 100 μM NADH, 0.25 mM O_2, 0.5 mM aromatic carboxylate, 50 μM ferrous ammonium sulfate, 0.8 μM BenAB ($\alpha_3\beta_3$), 0.5 μM BenC, and in

50 mM HEPES, 100 mM KCl (pH 7.5) at room temperature (23 ºC). NADH and O_2 consumption values listed are after 5 min.

[b]Relative activities are defined as the percentage of NADH consumed after 5 min relative to BenDO activity with benzoate.

[c]Substrate consumption was monitored by HPLC as described in the Materials and Methods.

[d]Detected by the increase at 340 nm due to formation of NADH upon addition of BenD (5 μM) and NAD^+ (0.2 mM). BenD was added to reactions after 5 min. of NADH consumption. +, indicates generation of NADH; -, no generation of NADH was observed.

[e]Gibbs' reagent (15 μL of a 2% (w/v) solution in ethanol) was added to reactions (200 μL) monitoring NADH consumption after 5 min and determined to be positive (+) by formation of a blue to purple color; -, no color change occurred. These analyses were conducted without addition of BenD.

[f]+, substrate consumption was detected but could not be quantified accurately.

[g]Catechol was identified and quantified as the product by HPLC as described in the Materials and Methods section.

Figure 2.1. Degradation of anthranilate and benzoate in *Acinetobacter* sp. ADP1 via the β-ketoadipate pathway (72)**.** Relevant compounds and roles of the component AntDO (AntAB and AntC) proteins are indicated. The corresponding BenDO (Ben) components and reactions are enclosed within dashed boxes.

Acinetobacter sp. ADP1 ring-hydroxylating dioxygenases

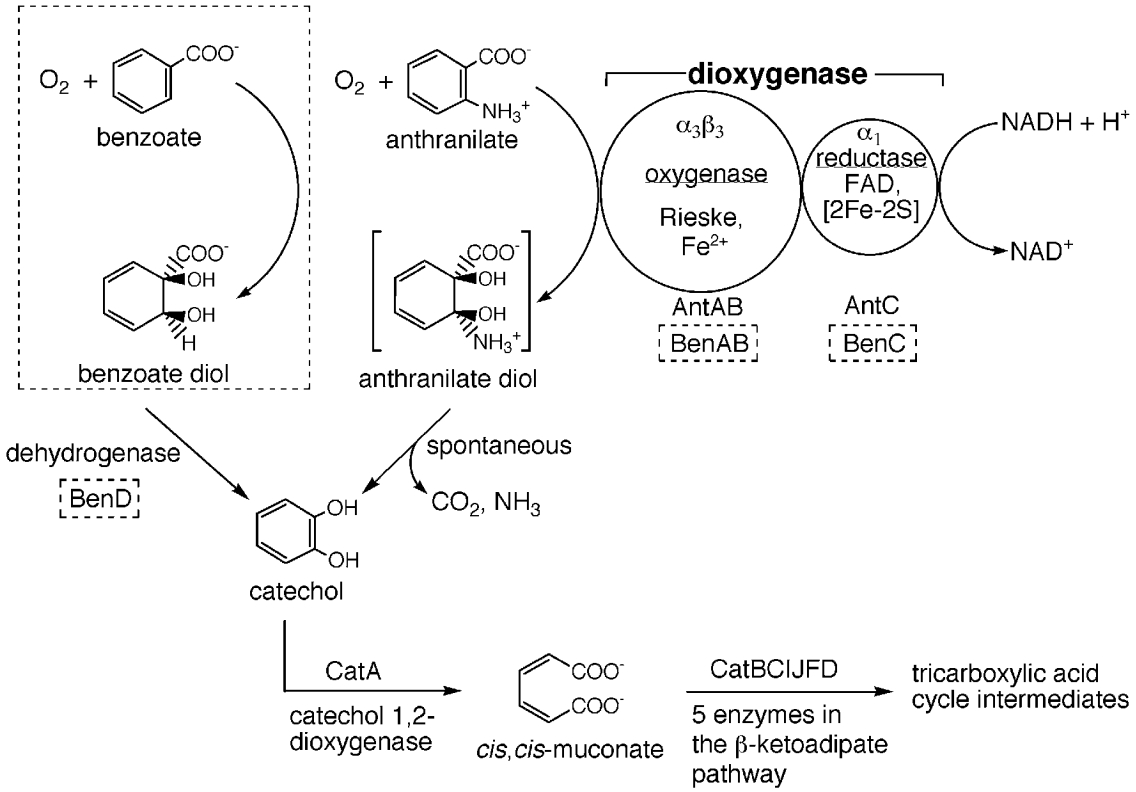

Figure 2.2. SDS-PAGE of AntAB, AntC, and the M43K AntAB variant. Lane 1, total protein of non-induced TOP10F' (pBAC209); Lane 2, total protein of TOP10F'(pBAC209) with AntAB induced; Lane 3, purified AntAB; Lane 4 total protein of non-induced DH5α (pBAC208); Lane 5, total protein of DH5α (pBAC208) with AntC induced; Lane 6 purified AntC ; Lane 7, total protein of non-induced TOP10F'(pDMK3). Lanes 8 and 9 are the cell-free extract and pellet, respectively, following sonication and centrifugation of TOP10F'(pDMK3) with M43K AntAB induced. Numbers at left correspond to the sizes (in kDa) corresponding to adjacent molecular weight markers (lane MW).

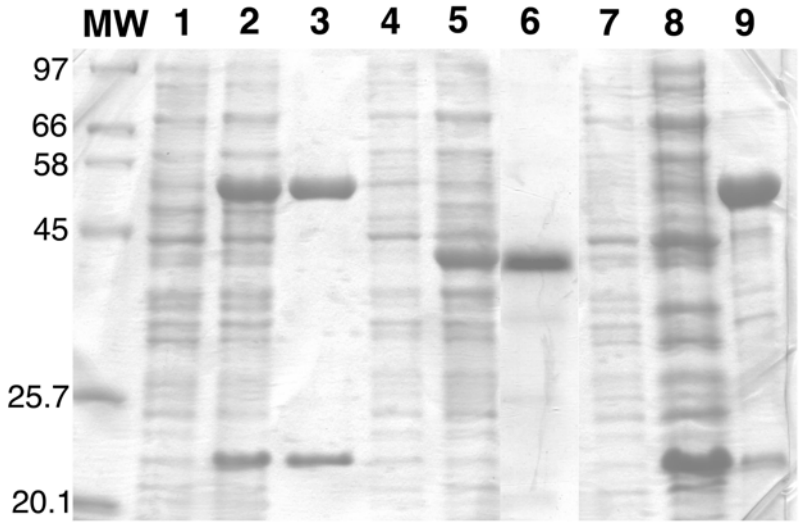
MW
1
2
3
4
5
6
7
8
9
97
66
58
45
25.7
20.1

Figure 2.3. Ultraviolet-visible absorption spectra of **A.** oxidized (solid) and reduced (dashed) AntAB (12 μM $\alpha_3\beta_3$) and oxidized M43K AntAB (15 μM $\alpha_3\beta_3$) (inset) and **B.** oxidized (solid) and FAD-depleted AntC (dashed).

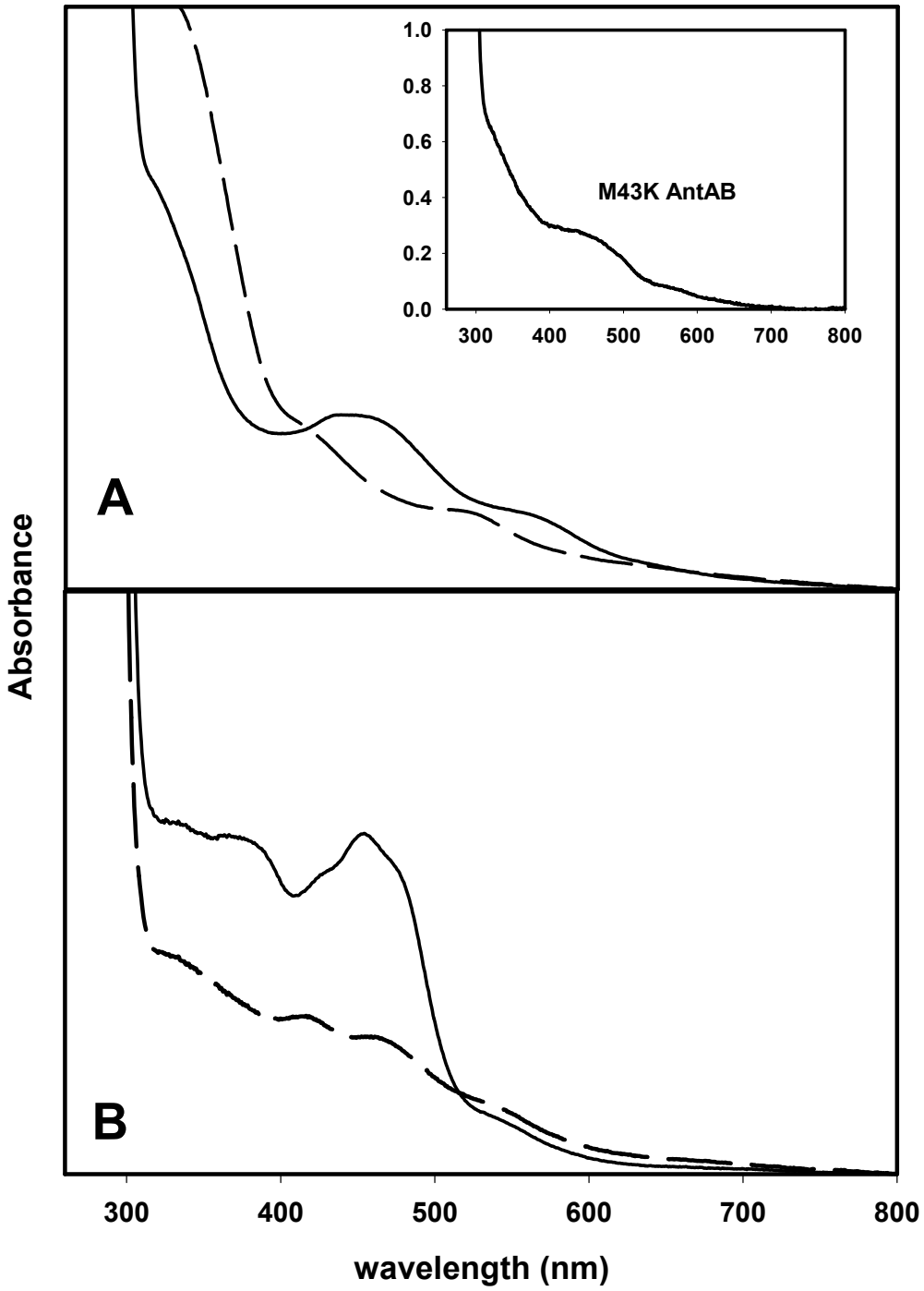
A
B
M43K AntAB
1.0
0.8
0.6
0.4
0.2
0.0
300
400
500
600
700
800
Absorbance
wavelength (nm)

Figure 2.4. EPR spectra of reduced AntAB (A) and AntC (B). Purified samples of protein (250 μM) were reduced anaerobically with excess sodium dithionite (0.5M). Spectra were recorded under the following conditions: temperature,10K; microwave frequency, 9.59 GHz; modulation amplitude, 6.366 G; microwave power 4 mW.

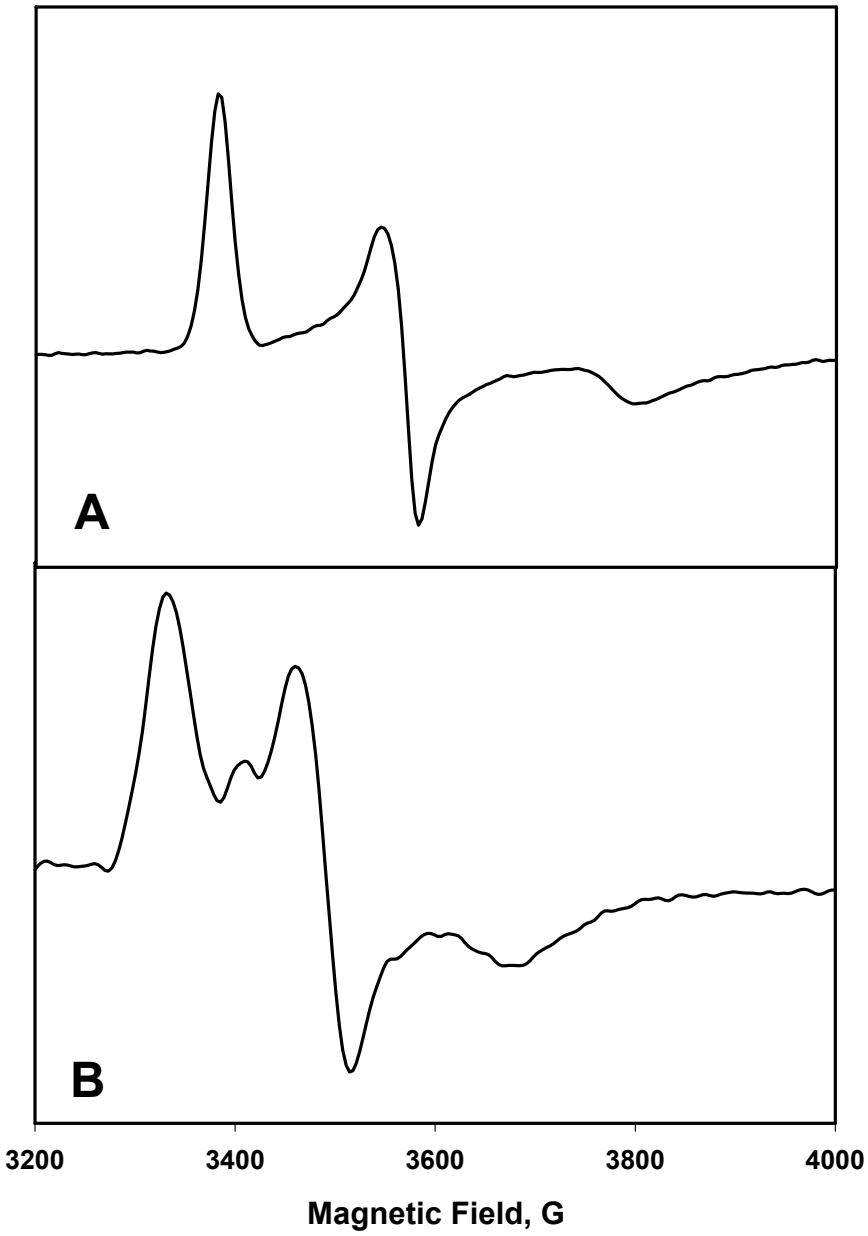
A
B
3200
3400
3600
3800
4000
Magnetic Field, G

Figure 2.5 Phylogenetic trees of the α-subunits (a), β-subunits (b), and reductases (c) of known and putative class IB dioxygenases. Also included were two α-subunit components from different ARHDO classes (Table 2.1), NDO (NdoB, class III; M23914; (102)) and phthalate dioxygenase (Pht3, class IA; D13229; (120)). An outgroup (Pht3) was used only in (a). Nomenclature: Abs, 2-aminobenzenesulfonate dioxygenase of *Alcaligenes* sp. (AF109074; (107)); Ant, AntDO of *Acinetobacter* ADP1 [6] or Ant(Pa), putative sequence of *P. aeruginosa* PAO1; Ben, BenDO of *Acinetobacter* ADP1 [32] or Ben(Pa), putative sequence of *P. aeruginosa* PAO1, or Ben(Pp), sequence of *P. putida* PRS2000 (34); Cbd, 2-halobenzoate 1,2-dioxygenase of *Burkholderia cepacia* (X79076; (64)); Tft, 2,4,5-trichlorophenoxyacetic acid oxygenase of *B. cepacia* (U11420; (38)); Xyl, toluate 1,2-dioxygenase of *P. putida* (PIR A41659; (67)). The numbers at branch points indicate the confidence (in percent) as determined by bootstrap analysis with 100 replicates. The scale bar indicates the relative phylogenetic distances measured as number of amino acid substitutions per site.

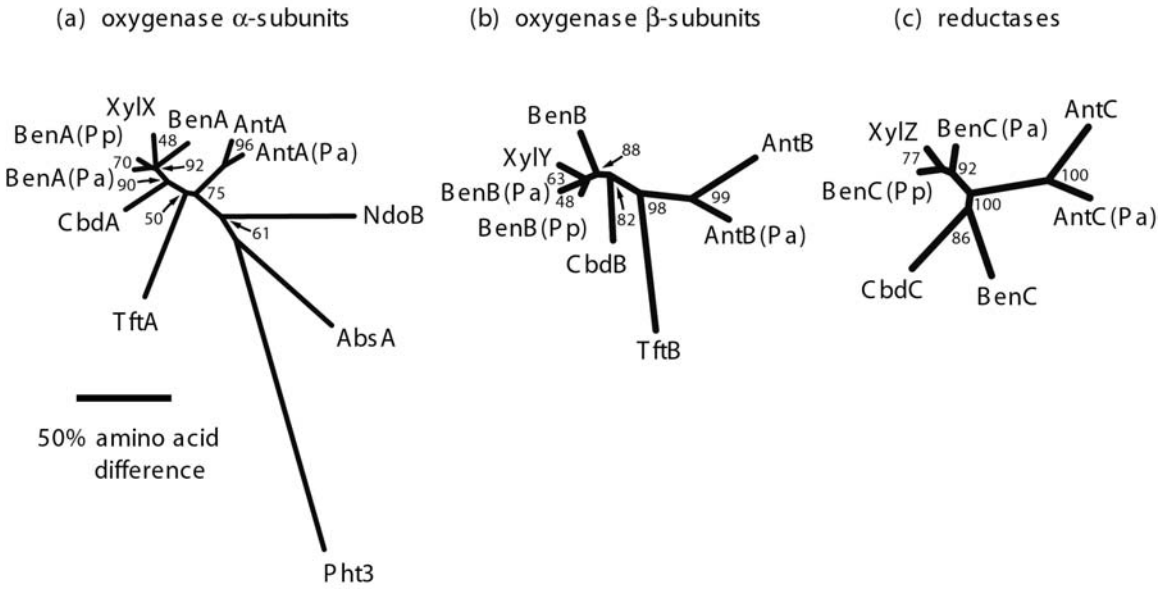
(a) oxygenase α-subunits
(b) oxygenase β-subunits
(c) reductases
XylX
BenA
AntA
BenA(Pp)
AntA(Pa)
BenA(Pa)
CbdA
NdoB
TftA
AbsA
Pht3
50% amino acid difference
BenB
XylY
AntB
BenB(Pa)
BenB(Pp)
AntB(Pa)
CbdB
TftB
XylZ
BenC(Pa)
AntC
BenC(Pp)
AntC(Pa)
CbdC
BenC
48
70
92
90
75
50
61
88
63
48
82
98
99
77
92
100
100
86

Figure 2.6. Sequence of ADP1 AntA and a consensus sequence derived from an alignment of the α-subunits from nine class IB ARHDOs and the class III NDO (Table 2.1 and Fig. 2.5). The consensus sequence indicates residues that are identical in the nine class IB sequences. Bold residues are also identical in NdoB of NDO. Residues known to furnish ligands to the Rieske and mononuclear iron sites in NdoB are boxed. The italicized asparagine at position 213 is a possible ligand to the mononuclear iron site [24] and is conserved in nine of the sequences but not in AbsA.

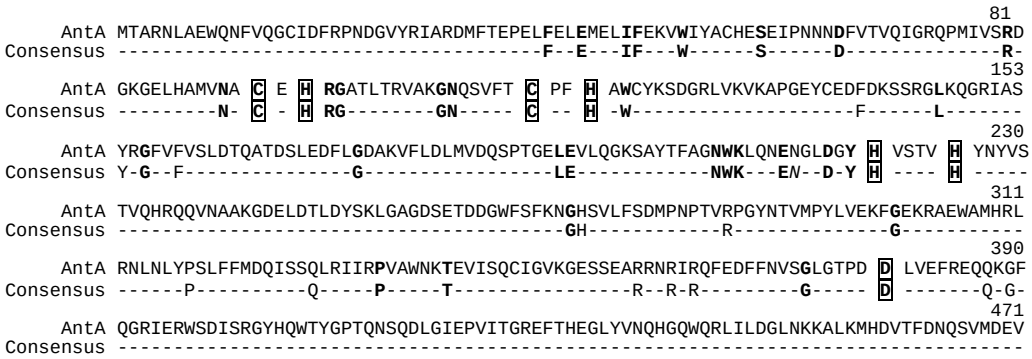
81
AntA MTARNLAEWQNFVQGCIDFRPNDGVYRIARDMFTEPELFELEMELIFEKVWIYACHESEIPNNNDFVTVQIGRQPMIVSRD
Consensus ----------F--E---IF---W------S------D----------R-
153
AntA GKGELHAMVNA C E H RGATLTRVAKGNQSVFT C PF H AWCYKSDGRLVKVKAPGEYCEDFDKSSRGLKQGRIAS
Consensus ---------N- C - H RG--------GN----- C -- H -W--------------------F------L-------
230
AntA YRGFVFVSLDTQATDSLEDFLGDAKVFLDLMVDQSPTGELEVLQGKSAYTFAGNWKLQNENGLDGY H VSTV H YNYVS
Consensus Y-G--F---------------G----------LE----------NWK---EN--D-Y H ---- H -----
311
AntA TVQHRQQVNAAKGDELDTLDYSKLGAGDSETDDGWFSFKNGHSVLFSDMPNPTVRPGYNTVMPYLVEKFGEKRAEWAMHRL
Consensus ----------GH----------R----------G----------
390
AntA RNLNLYPSLFFMDQISSQLRIIRPVAWNKTEVISQCIGVKGESSEARRNRIRQFEDFFNVSGLGTPD D LVEFREQQKGF
Consensus ------P----------Q-----P-----T----------R--R-R---------G----- D -------Q-G-
471
AntA QGRIERWSDISRGYHQWTYGPTQNSQDLGIEPVITGREFTHEGLYVNQHGQWQRLILDGLNKKALKMHDVTFDNQSVMDEV
Consensus ----------

CHAPTER 3

MEASURING THE EFFICIENCY OF RANDOMLY GENERATED MUTATIONS IN THE *ACINETOBACTER* SP. STRAIN ADP1 *CATA* GENE[1]

---

[1]Eby, D.M., S. Haddad and E.L. Neidle. To be submitted to *Applied and Environmental Microbiology.*

Abstract

The *catA* gene of *Acinetobacter* sp. strain ADP1, which encodes catechol 1,2-dioxygenase (CatDO), was mutated in an attempt to identify variant enzymes with altered substrate specificity. The *catA* gene was PCR-amplified under a variety of conditions aimed at reducing the fidelity of DNA replication, thereby incorporating random mutations into the gene. In order to estimate the efficiency of PCR mutagenesis, the PCR-amplified DNA was used in an *in vivo* assay determining the frequency at which randomly mutated DNA created loss-of-function CatDO mutants. Mutant strains with significantly reduced CatDO activity were selected by their failure to convert catechol to a toxic intermediate. This selection of loss-of-function mutations provides a powerful method for optimizing a mutagenesis procedure to alter the substrate specificity of CatDO.

Introduction

Random mutagenesis of genes to introduce amino acid changes into proteins has become a useful approach in elucidating residues of catalytic or functional importance. This type of mutagenesis is also important for directed evolution and designing enzymes with improved activities. Error-prone PCR is one method that can generate a large number of gene copies containing random nucleotide changes. Specific reaction conditions can be used to control the extent of mutagenesis. Optimizing the mutational frequency is important to achieve a sufficient number of mutations to create the desired enzymes without generating additional deleterious mutations.

A procedure for efficient random mutagenesis of specific genes in the chromsome of ADP1 has been described by Kok et al. (98, 99). PCR-generated, random mutations were introduced into the *pobR* gene encoding the transcriptional activator of *pobA*, the gene responsible for the initial catalytic step in degradation of *p*-hydroxybenzoate (98). Deleterious mutations in *pobR* will inhibit toxic accumulation of a catabolic intermediate in an ADP1 mutant. PCR-amplified *pobR* was transformed into this particular strain. Transformants were selected for growth in the presence of a compound that produces a lethal phenotype if PobR is functional. Relative polymerase fidelity was examined by quantifying the rate at which the incorporation of errors by PCR caused a gene to encode a non-functional protein.

A similar approach can be used in studies of the *catA* gene, which encodes conversion of catechol to *cis,cis*-muconate. When *catB* is deleted from the chromosome of ADP1, growth in the presence of a compound degraded through the catechol branch of the β-ketoadipate pathway will cause the toxic accumulation of *cis,cis*-muconate (Fig. 3.1). Selection for growth under these conditions can yield mutants that are unable to form *cis,cis*-muconate. For example, genes encoding anthranilate 1,2-dioxygenase (*antABC*) were discovered by isolating a spontaneous mutant that allowed a Δ*catB* strain to grow on another carbon source in the presence of anthranilate (19). The mutation severely impaired the ability of AntABC to convert anthranilate to catechol, thereby inhibiting the subsequent production of *cis,cis*-muconate. These assay

conditions also produced spontaneous mutations in the *catA* gene, but the specific mutations were not characterized in this study.

Strain ISA25 will accumulate *cis,cis*-muconate in the presence of benzoate, due to deletion of the *catBCDIJF* genes (Fig. 3.1, (54)). Analogous to the studies completed by Kok et al., ISA25 can be used as a host strain to assay mutations blocking toxic production of the metabolic intermediate *cis,cis*-muconate. Following transformation of ISA25 with PCR-amplified *catA* DNA, mutations in *catA* that prevent the conversion of catechol to *cis,cis*-muconate will allow ISA25 to grow in the presence of benzoate. The frequency at which resistance to benzoate is acquired can be quantified by enumerating the transformed cells growing in the presence of benzoate. This frequency can be correlated with specific error-prone PCR conditions to provide an accurate assessment of how each random mutagenesis condition alters *catA*. In this way, a measure of mutagenesis efficiency can be determined for various error-prone PCR conditions.

Materials and Methods

General reagents, strains, and procedures.

Minimal medium (MM) and *Acinetobacter* sp. strain ADP1 have been previously described (90, 145). Plasmid DNA was purified from *E. coli* strain DH5α using previously described techniques (139). Strain ISA25, containing a chromosomal deletion of *catBCDIJF*, was previously described (54). DNA gel

electrophoresis was conducted using common procedures (139). Products of PCR were purified using the QIAquick DNA Gel-Purification Kit (Qiagen, Inc.) and quantitated by UV absorbance at 260 nm (139). All DNA sequences were confirmed at the Molecular Generics Instrumentation Facility (University of Georgia, Athens, GA).

catA DNA used to transform ISA25.

A DNA fragment beginning 411 bp upstream and continuing 1542 bp downstream of the *catA* coding sequence was isolated by digesting a plasmid, pIB1362, with *Eco*RV and *Hin*dIII restriction enzymes (118). Using *Eco*ICR and *Hin*dIII restriction enzymes, pUC18 was digested at restriction sites within the multiple cloning site (158). The fragments containing *catA* DNA and pUC18 were ligated at the *Hin*dIII restriction site and at the *Eco*ICR- and *Eco*RV-generated blunt ends to create pBAC201. All subsequent *catA* DNA used in this study originated from pBAC201.

To obtain a disruption in *catA*, an omega cartridge conferring resistance to spectinomycin and streptomycin (ΩS) was excised from pUI1638 and inserted into the *catA* gene (48). Transcriptional and translational stop signals are located on ΩS. Plasmids were digested with the *Sph*I restriction enzyme to remove the ΩS from pUI1638 and also to linearize pBAC201 at a unique restriction site in the middle of *catA*. The two fragments were then ligated to form pBAC390.

The plasmid pBAC390 was manipulated to create a deletion in *catA*. Digestion with the *Sal*I restriction enzyme removed a 2 kbp fragment from

pBAC390, which contained the majority of the ΩS and the 5' end of *catA*. This fragment was discarded, and the remaining portion of pBAC390 was ligated together at the *Sal*I restriction sites to form pBAC392, resulting in a 512 bp deletion of *catA* on the plasmid. pBAC392 was linearized with the *Eco*RI restriction enzyme before being used to transform ISA25 cultures.

The primers CATA[FOR] (5'-ggaaggtatagaaacgactatcga-3') and CATA[REV] (5'-tgatcttgtttatgttcggccagt-3') anneal approximately 177 bp upstream and 319 bp downstream of the *catA* coding sequence. These primers were used to PCR amplify the Δ*catA* allele from pBAC392 using the FastStart Taq polymerase (*Taq*-PCR, Hoffmann-La Roche, Inc). Amplification using pBAC392 as a template provided a stock of PCR-generated Δ*catA* DNA for transforming ISA25. Wild-type *catA* DNA for transformation experiments was similarly generated by PCR amplification with the same primers, using pBAC201 as the template.

Random mutagenesis of catA using error-prone PCR.

Random mutations were introduced into *catA* by two different PCR amplification methods: the addition of $MnCl_2$ to *Taq* polymerase-mediated PCR and the use of an error-prone polymerase. The polymerase and reaction buffer used in PCR amplifications containing $MnCl_2$ were from the FastStart *Taq* polymerase kit (Roche). The following reaction conditions were adapted from recommendations from the vendor. Each reaction contained 500 mM Tris/HCl

(pH 8.3 at 25°C), 500 mM KCl, 20 mM $MgCl_2$, 500 mM $(NH_4)_2SO_4$, 0.1 mM of each dNTP, 0.4 μM of each primer (CATA[FOR] and CATA[REV]), 1 ng template (pBAC201), and 5 U FastStart *Taq* DNA polymerase. Different frequencies of polymerase errors per gene were achieved by adding $MnCl_2$ to the reaction buffer with a final concentration varying between 0 and 1 mM.

Random mutagenesis of *catA* was also accomplished with the GeneMorph PCR Mutagenesis kit (Stratagene). The kit contains a thermal-stable polymerase engineered to have a higher intrinsic error rate than *Taq* polymerase. The following conditions were used as recommended by the manufacturer: 1 X Mutazyme reaction buffer, 0.1 mM of each dNTP, 0.4 mM of each primer (CATA[FOR] and CATA[REV]), and 2.5 U Mutazyme DNA polymerase. Different mutational frequencies were generated in *catA* by varying the final concentration of the initial template (pBAC201), between 10 pg and 10 ng. The total volume of all PCR amplifications was 50 μl. Amplicons from error-prone PCR were used as templates for subsequent PCR to further increase the number of mutations per gene.

Transformation assay conditions.

ISA25 was grown in 5 ml MM with 10 mM succinate in liquid culture overnight. The next day, ISA25 was diluted (1:25) into the same medium and grown for approximately 2 hours to obtain an OD_{600} of approximately 0.2. The culture was then divided into either 1 ml aliquots in 12 ml test tubes or into 200 μl aliquots in 2 ml capacity microfuge tubes. Donor DNA was added to transform

the recipient cultures, and the aliquots were incubated for approximately 3 hours. Turbidity of the cultures was measured spectrophotometrically. Serial dilutions were plated to MM solid agar containing 10 mM succinate as the carbon source with and without 2.5 mM benzoate.

Results

Assessment of transformation efficiency by enumerating colonies selected from cultures grown in the presence of the ∆catA allele.

The frequency of successful transformation and allelic replacement with defective *catA* genes was determined by selecting transformants that could grow on succinate in the presence of benzoate (ben-resistant cells). The number of ben-resistant colony forming units (CFUs) per viable cell in ISA25 cultures transformed with ∆*catA* DNA were counted. Viable cell counts for ISA25 cultures were determined by enumerating colonies grown on MM agar plates containing only succinate. Cells successfully transformed with ∆*catA* DNA and, therefore, unable to convert benzoate to the toxic intermediate *cis,cis*-muconate, were enumerated as colony forming units (CFUs) on the MM agar plates containing succinate and benzoate. Various quantities of ∆*catA* DNA, from two different sources, were added to cultures, and transformation efficiency was assessed in each case by the increased frequency of successful transformation and allelic replacement.

The number of ben-resistant CFUs per viable cell, selected from cultures grown in the presence of linearized pBAC392 or PCR-amplified Δ*catA* is represented in Figure 3.2A. There was no significant difference in the number of ben-resistant CFUs selected when plasmid-borne or PCR-generated Δ*catA* was used as donor DNA at any concentration. As shown by these results, transformation efficiency is not dependent on the source of the donor DNA. Mutated gene stocks originating from PCR amplifications do not need to be cloned before transformation. The efficient chromosomal integration of randomly mutated DNA, directly from the thermocycler, is important to high-throughput assays that rapidly screen for randomly mutated DNA encoding desirable enzyme phenotypes.

Equally important is determining the optimal amount of donor DNA needed in cultures to maximize transformation efficiency. Donor DNA at concentrations of greater than 1 μg per ml of recipient culture did not significantly increase the number of ben-resistant CFUs. After these measurements were completed, all remaining transformation assays used approximately 1 μg of donor DNA per ml of recipient culture to ensure the most efficient transformation conditions.

When un-transformed cultures of ISA25 were plated to solid medium containing succinate and benzoate, approximately 1 CFU emerged for every 10^6 viable cells plated (Fig. 3.2B). These ben-resistant colonies are presumed to arise after spontaneous mutations in either *catA* or the *ben* genes inhibit the conversion of benzoate to *cis,cis*-muconate. *Taq*-PCR of wild-type *catA*, when

added to ISA25 cultures at a final concentration of 1 μg/ml culture, produced 45 ben-resistant CFUs per 10^6 viable cells. Using the same concentrations of donor DNA in cultures, the Δ*catA* amplicon confers benzoate resistance to ISA25 at a frequency of 3200 CFUs per 10^6 viable cells.

Exposure of PCR-amplified Δ*catA* DNA to ISA25 cultures caused an over 70-fold increase in the frequency of ben-resistant CFUs over the same frequency in cultures grown in the presence of wild-type *catA* PCR amplified by *Taq* polymerase. These two transformation frequencies represent the upper and lower limits in the scale of measuring the degree to which different *Taq*-mediated, random mutagenesis procedures will incorporate mutations in *catA*, that result in a non-functional enzyme. Any mutated *Taq*-PCR *catA* DNA, transformed into ISA25, will result in a frequency of ben-resistant CFUs between that produced by *Taq*-PCR amplification of wild-type *catA* under non-mutagenic conditions and similar amplification of the Δ*catA* allele used as donor DNA.

Enumerating benzoate resistant CFUs arising after ISA25 cultures were transformed by catA amplicon from Taq-PCR with $MnCl_2$.

The addition of $MnCl_2$ in PCR diminishes template specificity of the polymerase, presumably by the incorporation of Mn ions instead of Mg ions in the polymerase. Reduction of polymerase fidelity is increased by the increase of Mn ions in the reaction buffer. In one series of PCR amplification of *catA*, the final concentration of $MnCl_2$ was varied between 0 and 1 mM. Each PCR product was

added to separate ISA25 cultures and the number of ben-resistant CFUs isolated per viable cell was calculated (Fig 3.3A).

The products of wild-type *catA* PCR amplifications containing 0.1 mM $MnCl_2$ were also used as the starting template in a series of PCR amplifications. These reactions contained final concentrations from 0 to 0.7 mM $MnCl_2$, and they were used as donor DNA for transformation of ISA25 (dark green line, Fig. 3.3A). In this second round of PCR, reactions having between 0.5 and 0.7 mM $MnCl_2$ were not used to transform ISA25, because amplicons were not detected by UV absorbance at 260 nm. The products of all PCR amplifications containing $MnCl_2$ were visualized in agarose gels containing ethidium bromide (Fig. 3.3B).

When $MnCl_2$ was added to wild-type *catA* PCR at concentrations greater than 0.7 mM, a decrease in the number of ben-resistant transformants was measured. The decline may be due to amplicons mutated to such a large degree that it reduces the probability of homologous recombination and allelic replacement in the chromosome of ISA25. When these PCR amplifications were separated in gel electrophoresis, there was a noticeable decrease in the amount of product that could be visualized (Fig. 3.3B). Highly mutated DNA should not anneal properly during successive cycles of PCR, resulting in lower amplicon yields. Even though less amplicon was generated when higher $MnCl_2$ concentrations were used in PCR, the amount of DNA added to each culture was normalized to 1 μg per ml culture. Therefore, the decrease in ben-resistant CFUs is not reflective of a smaller amount of donor DNA added.

Enumerating benzoate resistant CFUs arising after ISA25 cultures were transformed by catA amplicon from PCR with Mutazyme.

As reported by the manufacturer of the Mutazyme polymerase, smaller initial template quantity in PCR amplifications will allow for increased mutation frequency. Lower amounts of initial template DNA undergo more rounds of duplications in PCR, so more mutations are incorporated by the error-prone polymerase. Performing successive PCR amplifications, using products of one PCR as the starting template in another PCR, further increases the mutation frequency. The mutation rate of Mutazyme is reflected in the transformation assays, where donor DNA originating from Mutazyme-mediated PCR with lower template concentrations resulted in increased numbers of ben-resistant CFUs.

The number of ben-resistant CFUs arising after transformation with *catA* amplicons made by the error-prone polymerase Mutazyme is shown in Figure 3.4. Three initial PCR amplifications were performed on wild-type *catA*, using 1 ng, 100 pg, and 10 pg of template per 50 μl reaction. The PCR products were added to ISA25 cultures and the number of ben-resistant colonies per viable cell was counted (light blue line, Fig. 3.4). Aliquots of completed PCR with the wild-type *catA* template were mixed and used as the initial template for another series of reactions with 1 ng, 100 pg, and 10 pg as starting DNA concentrations per 50 μl reaction. Successive PCR amplifications incorporate more mutations into *catA*. ISA25 cultures were exposed to the second set of PCR products and frequency of transformation and allelic replacement was enumerated (dark blue line 1, Fig. 3.4). PCR was repeated one more time to produce a third set of

amplifications, using the second set of PCR products as starting template. Ben-resistant colonies were counted after these PCR products were added to cultures (dark blue line 2, Fig. 3.4).

Discussion

Measuring the efficiency of random mutagenesis methods to be used in altering the substrate specificity of CatA.

Error-prone PCR random mutagenesis offers a powerful tool for elucidating substrate-specific sequence elements in catalytic enzymes. The success rate of such studies is dependent upon the probability at which a phenotype encoded by altered DNA can be identified. The convenient genetic system of ADP1 allows for easy in vivo selection of altered genes introduced by natural transformation. For example, the *catA* gene could be randomly mutated, integrated into the ADP1 chromosome by allelic exchange, and then variant CatDO enzymes acting on catechol analogs can be selected by growth on a medium containing the analog as a sole source of carbon.

Use of randomly mutated catA DNA in increasing catalytic activity of catechol 1,2-dioxygenase on protocatechuate

Randomly mutated *catA* DNA, from this study, was transformed into an ADP1 strain unable to utilize the catechol analog, protocatechuate as a carbon source. Any mutant *catA* in the chromosome, that would encode an enzyme with

sufficient activity on protocatechuate to support growth, would then grow in medium containing the aromatic compound as the sole carbon source (ADP1 strains used in this assay are described in Appendix A). The success of generating CatA enzymes with altered substrate specificity, in an in vivo assay, is dependent upon transformation efficiency and the appropriate degree of random mutagenesis.

To date, CatA enzymes with increased catalytic activity towards protocatechuate have not been isolated from *catA* DNA mutated by error prone PCR. The ISA25 transformation assays in this study demonstrate that randomly mutated *catA* DNA was successfully transformed into ADP1 strains. The mutational frequency was not at a level that produced a majority of mutated genes encoding inactive enzymes. This suggests that other factors than transformation efficiency and mutation frequency are inhibiting attempts to allow the ADP1 mutant to grow on protocatechuate through the activity of a mutant CatA. Optimizing features such as the regulation of gene expression or substrate transport could play a role in successfully assaying for mutant CatA enzymes in vivo. Current analysis is underway to address these concerns. Furthermore, a combination of site-directed and random-mutagenesis procedures may facilitate the isolation of enzymes with altered substrate specificity.

Figure 3.1. Degradation of aromatic compounds by ADP1 through the β-ketoadipate pathway. Deletion of the *catB* gene inhibits conversion of catechol to *cis,cis*-muconate. A Δ*catB Acinetobacter* strain is unable to grow in the presence of any compound metabolized through the catechol branch, due to the toxic accumulation of *cis,cis*-muconate in the cell. ISA25, the ADP1-derived strain used in this study, has a deletion in the *catBCDIJF* genes.

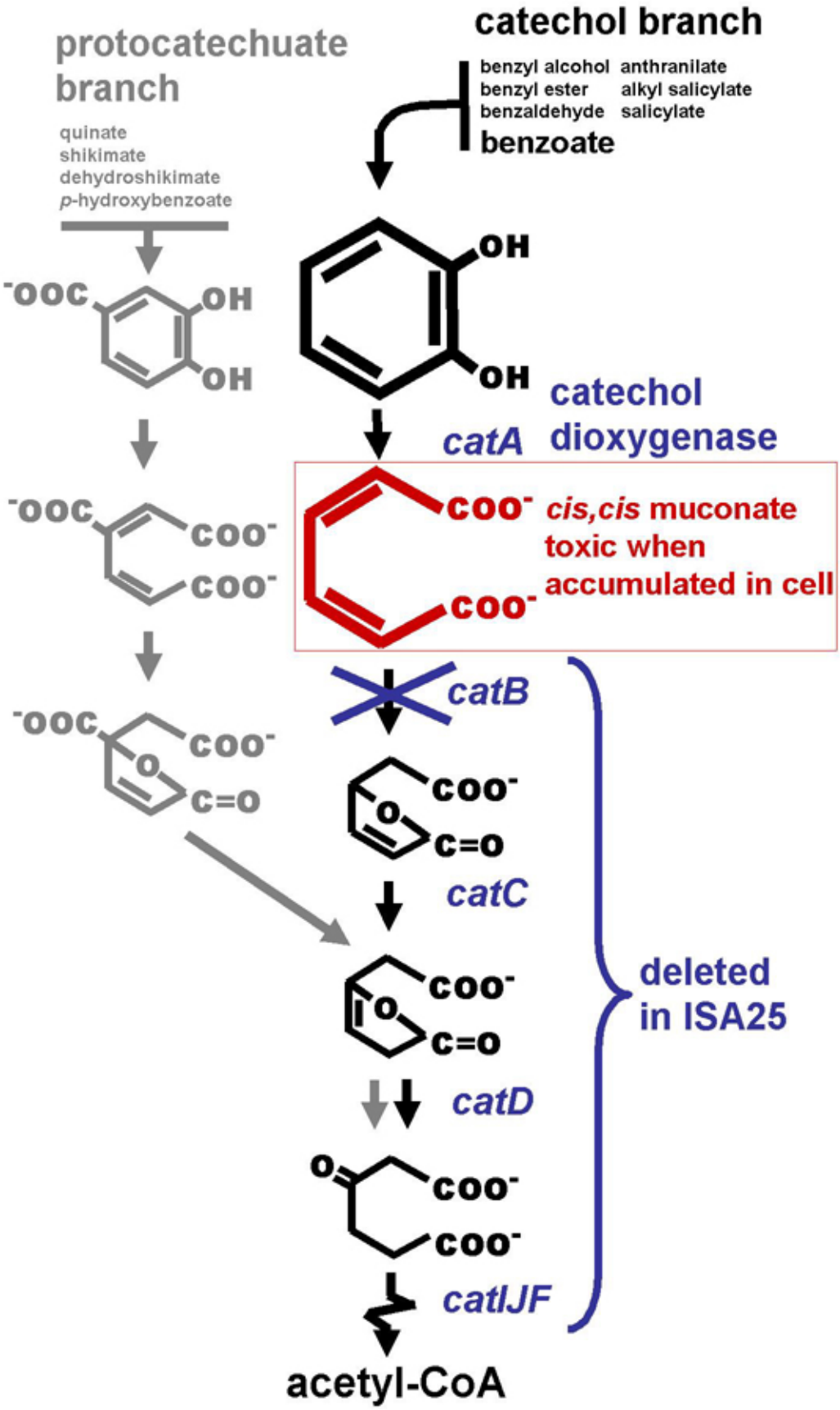
protocatechuate branch
quinate
shikimate
dehydroshikimate
p-hydroxybenzoate
catechol branch
benzyl alcohol
benzyl ester
benzaldehyde
benzoate
anthranilate
alkyl salicylate
salicylate
catechol dioxygenase
catA
cis,cis muconate toxic when accumulated in cell
catB
catC
catD
catIJF
deleted in ISA25
acetyl-CoA

Figure 3.2. Enumeration of ISA25 cells able to grow in the presence of benzoate after transformation by PCR-amplified wild-type and deleted *catA* DNA. Regression plot of the number of ben-resistant CFUs per 10^6 viable cells versus concentration of plasmid-encoded or PCR-amplified Δ*catA* donor DNA is shown in A. Average frequency of ben-resistant CFUs selected from cultures exposed to no DNA, *Taq*-PCR wild-type and deleted *catA* DNA is shown in B.

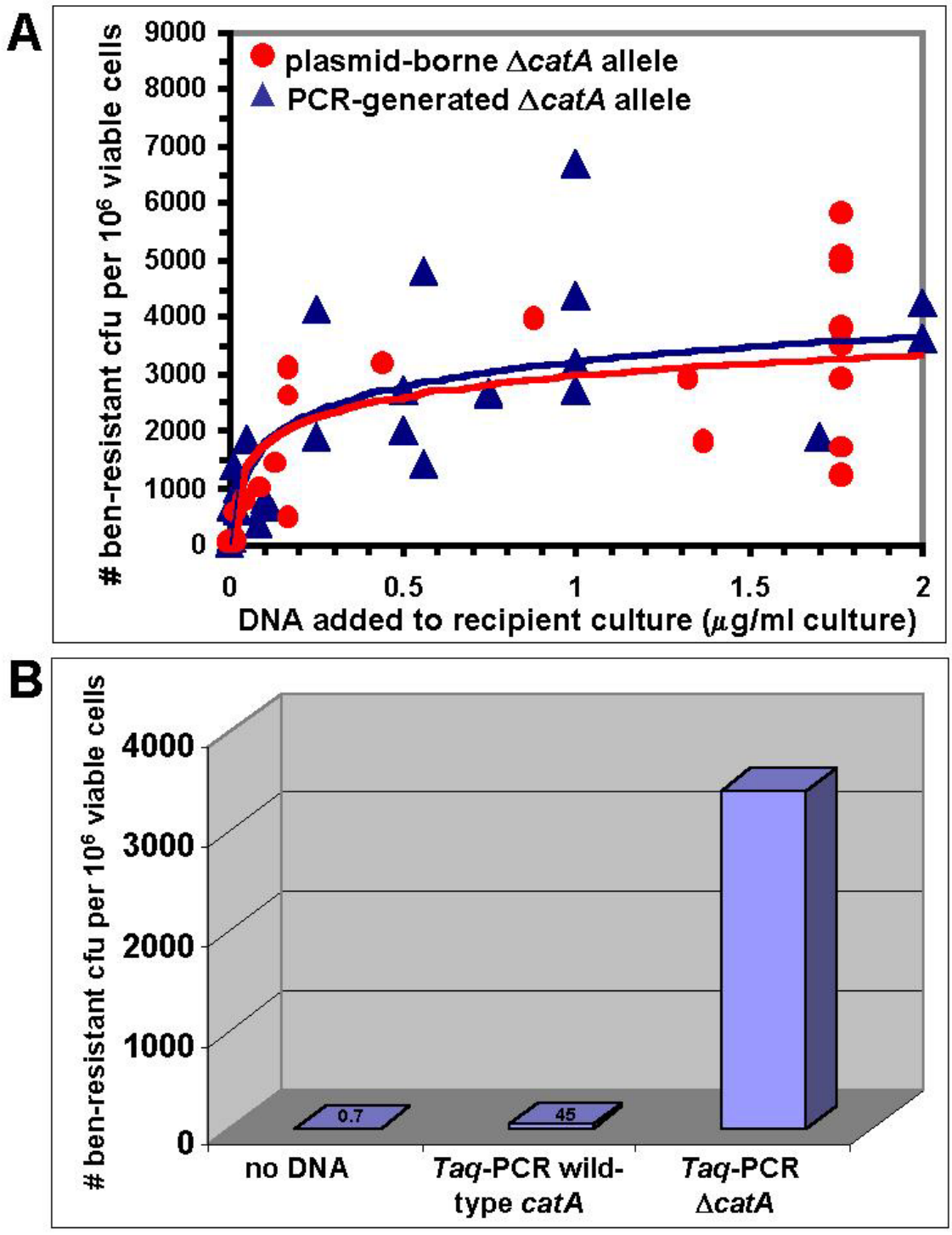
A
plasmid-borne ΔcatA allele
PCR-generated ΔcatA allele
ben-resistant cfu per 10^6 viable cells
9000
8000
7000
6000
5000
4000
3000
2000
1000
0
0
0.5
1
1.5
2
DNA added to recipient culture (μg/ml culture)
B
ben-resistant cfu per 10^6 viable cells
4000
3000
2000
1000
0
0.7
45
no DNA
Taq-PCR wild-type catA
Taq-PCR ΔcatA

Figure 3.3. Enumeration of ben-resistant CFUs arising from cultures transformed with *catA* DNA that was PCR amplified with $MnCl_2$. In graph A, the light green line represents a first round of PCR with wild-type *catA* template. The dark green line represents a second round of PCR with template DNA originating from the product of previous *catA* PCR amplifications containing 0.1 mM $MnCl_2$ in the reaction (represented by the orange data point). Saturating concentrations of DNA (approximately 1 μg) were added to transform the recipient cultures. Agarose gels showing *catA* products of PCR amplified with varying concentrations of $MnCl_2$ (B). The left gel shows amplicons of wild-type *catA* when concentrations, ranging between 0 to 1 mM $MnCl_2$, were added to PCR (lanes 0 to 1, respectively). In the right gel, PCR amplifications from template DNA originating from the product of PCR containing 0.1 mM $MnCl_2$ and wild-type *catA* template are shown (0.1 lane in left gel). $MnCl_2$ was added to these reactions at a range of concentrations between 0 and 0.7 mM (lanes 0 to 0.7, respectively). Lane S1 contains DNA size standards.

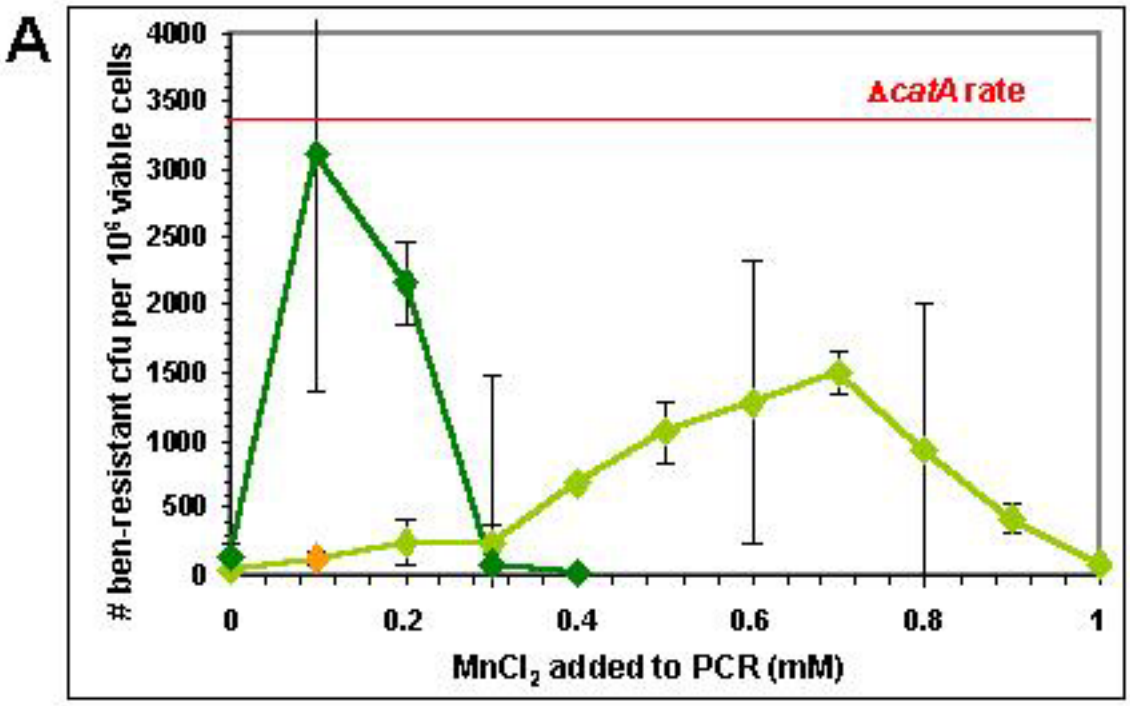
A
ben-resistant cfu per 10^6 viable cells
4000
3500
3000
2500
2000
1500
1000
500
0
ΔcatA rate
0
0.2
0.4
0.6
0.8
1
$MnCl_2$ added to PCR (mM)

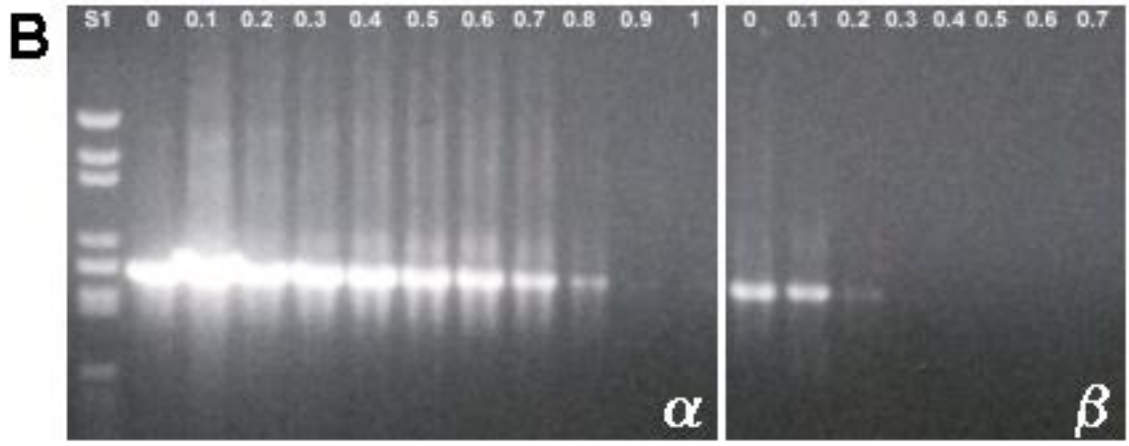
B
S1 0 0.1 0.2 0.3 0.4 0.5 0.6 0.7 0.8 0.9 1
α
0 0.1 0.2 0.3 0.4 0.5 0.6 0.7
β

Figure 3.4. Enumeration of ben-resistant CFUs arising from cultures transformed with *catA* DNA that were PCR amplified using Mutazyme polymerase. The light blue line represents error-prone PCR with wild-type *catA* as the template. The numbered dark blue lines represent successive PCR with template DNA originating from a mixture of the previous *catA* PCR amplicons (see Results section for further explanation). Saturating concentrations of DNA (approximately 1 μg) were added to transforming cultures.

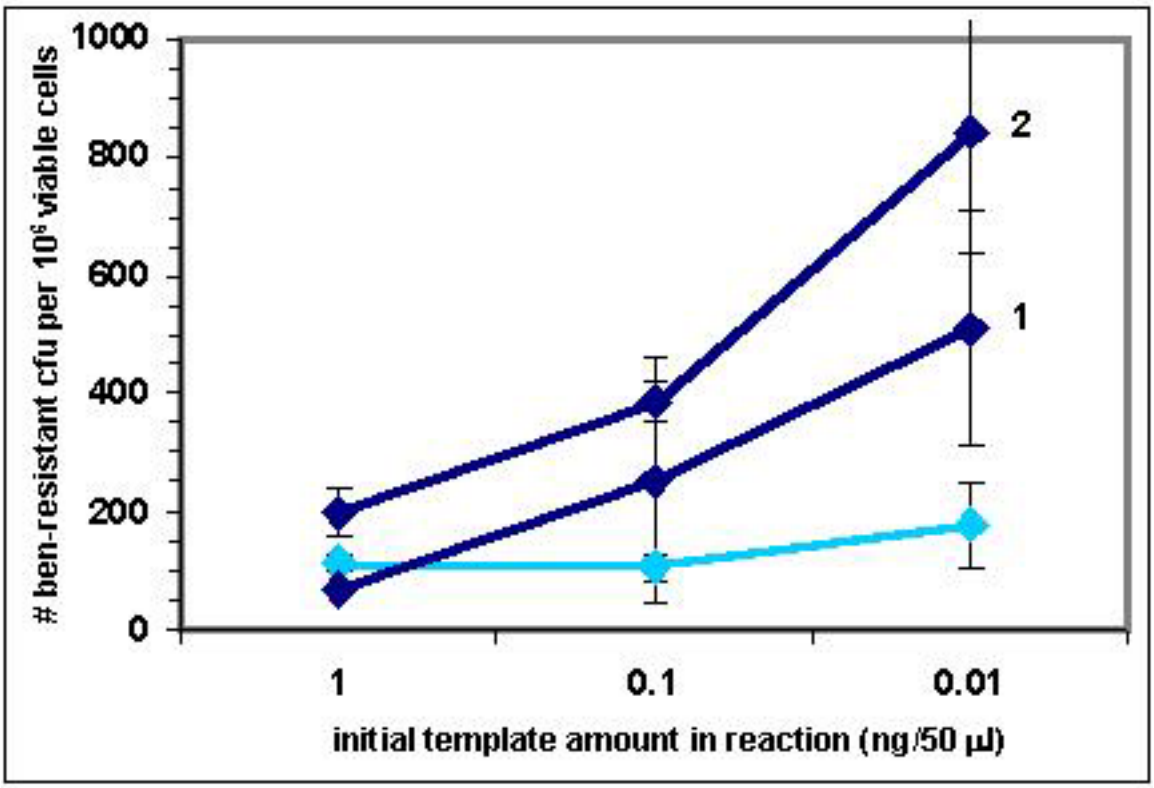
1000
800
600
400
200
0
ben-resistant cfu per 10^6 viable cells
2
1
1
0.1
0.01
initial template amount in reaction (ng/50 µl)

CHAPTER 4

EXPRESSION OF GENES ENCODING THE PROTOCATECHUATE 3,4-DIOXYGENASE FROM AN ENGINEERED PROMOTER: CONSEQUENCES OF EXTRACHROMOSOMAL GENE EXPRESSION IN *ACINETOBACTER* SP. STRAIN ADP1[1]

[1]Eby, D.M., A. Buchan, M.A. Moran, and E.L. Neidle. To be submitted to *Applied and Environmental Microbiology*.

Abstract

An expression vector was constructed to express genes in *Acinetobacter* sp. strain ADP1 independently from their chromosomal positions. This vector carries an *Acinetobacter* promoter sequence, originating from the chromosomal *catB* gene in ADP1. The plasmid-borne *catB* promoter differs from the wild-type copy due to a single bp mutation near the –10 promoter region. This engineered mutation allowed relatively high-level expression, independent of transcriptional activators that normally are needed to induce expression at this promoter. The *pcaHG* genes, encoding the protocatechuate 3,4-dioxygenase (PcaDO) from ADP1 were expressed, in trans, in an ADP1-derived mutant (ACN462) that carries a deletion of the *pcaHG* genes on the chromosome. Growth measurements and PcaDO activity assays confirmed that expression of the *pcaHG* genes from the *Acinetobacter* vector enabled ACN462 to grow on the carbon sources protocatechuate and *p*-hydroxybenzoate. Furthermore, extrachromosomal expression of *pcaHG* genes from the marine estuary isolate *Roseobacter* sp. strain ISM also allowed ACN462 to utilize protocatechuate and *p*-hydroxybenzoate as sole carbon sources, albeit at 25^{o}C and not at 37^{o}C. PcaDO activity was also assayed in ACN462 expressing plasmid-borne *pcaHG* genes during growth on different carbon sources. The specific activity of PcaDO in these strains was reduced when cells were grown on succinate, pyruvate, acetate, and LB, compared to higher activity from cells grown on citrate. Specific activity of PcaDO in cells grown on citrate was comparable to wild-type PcaDO specific activity grown on protocatechuate. This study presents an expression

system in *Acinetobacter* that can successfully express functional, recombinant dioxygenases. Furthermore, this *Acinetobacter* vector can be useful in expressing genes and allowing native and foreign dioxygenases to be assayed. The *Acinetobacter* expression system, presented in this report, will facilitate continued dioxygenase analysis and bioremediation research.

Introduction

Numerous genetic approaches are being developed to engineer the organisms, metabolic pathways and enzymes relevant for biodegradation. Microorganisms that degrade aromatic compounds are one focus of bioremediation research, because aromatic hydrocarbons are common contaminants of soils and groundwater (131). Furthermore, the studies on dioxygenase enzymes that oxidize aromatic compounds are of importance for the development of bioremediation technology (52, 60). Because dioxygenases are crucial to aromatic compound degradative pathways, they are the focus in directed evolution experiments to alter their substrate specificity. For purposes of developing microbes to acquire novel degradative capabilities, an understanding of the physiological significance of native gene expression, regulation and organization can lay the foundation for successful genetic manipulation and heterologous gene expression.

Many different naturally-occurring aromatic compounds are degraded through the protocatechuate branch of the β-ketoadipate pathway. Protocatechuate 3,4-dioxygenase (PcaDO) is a key enzyme in the β-ketoadipate

pathway, because it cleaves the stable, benzene nucleus of protocatechuate (72, 75, 122). In all microbes that produce this dioxygenase, the genes (*pcaHG*) encoding its two non-identical enzymatic subunits are located immediately adjacent to each other. The apparent operon containing these *pcaH* and *pcaG* genes almost always also includes *pcaC*, a gene needed for the subsequent step in the β-ketoadipate pathway (Fig. 4.1). In the soil bacterium *Acinetobacter* sp. strain ADP1, these three genes are co-transcribed with additional upstream genes involved in protocatechuate degradation.

The *pcaHG* genes are members of an operon responsible for conversion of protocatechuate and other hydrocarbons to tricarboxylic acid cycle intermediates and transport of protocatechuate and other aromatic compounds into the cytoplasm (43, 47, 70, 119). A regulator gene, *pcaU,* encodes the transcriptional activator that induces expression of the *pca* operon (Fig 4.1) (59). Several studies have shown that expression of this multifaceted operon is complex and controlled by many different regulatory mechanisms (14, 20, 37, 39, 134, 151, 160). In this study, *pcaHG* was expressed independently from the remaining *pca* genes in order to test the physiological significance of disrupting the operon, while developing an ADP1-based heterologous gene expression system for dioxygenases.

In some previous studies of microbial PcaDO enzymes, difficulties were encountered with attempts to produce large amounts of the protein in an active state in *Escherichia coli* (15, 130). This bacterium does not carry *pcaHG* in its genome nor does it degrade aromatic compounds via the β-ketoadipate pathway

(10, 74). In comparison to *E. coli*, *Acinetobacter* strains have some potential advantages as hosts for the expression of foreign genes. In the appropriate ADP1-derived mutant strains, foreign genes involved in aromatic compound degradation could be selected directly by functional complementation. Furthermore, bacterial strains such as *Acinetobacters* that normally produce enzymes for aromatic compound catabolism might be better suited than *E. coli* for synthesizing and maintaining active enzymes. However, despite these possibilities, ADP1 remains to be effectively developed as a host for foreign enzyme production.

The current studies were designed to improve the utility of *Acinetobacter* strains for bioengineering and also to improve our understanding of how gene organization and transcriptional regulation affect aromatic compound catabolism. Initial studies determined whether deleterious effects would result during growth on aromatic substrates when the ADP1 *pcaHG* genes were expressed independently of the other *pca* genes. Following the chromosomal deletion of the PcaDO-encoding genes, they were expressed in trans from a shuttle vector that was specifically generated for this purpose. This novel vector employed a promoter that was designed by site-specific mutation to allow relatively high gene expression without the need for a transcriptional activator and co-effector metabolite. These studies confirmed predictions about the significance of promoter sequences in ADP1. The resulting vector should be useful for broad applications in *Acinetobacter*, a bacterium for which few vectors have previously been constructed.

To test the efficacy of this vector, it was used in *Acinetobacter* to express the *pcaHG* genes of an isolate from the *Roseobacter* lineage of marine bacteria (16, 17). This lineage of the α-proteobacteria may form the dominant clade of aromatic compound-degrading bacteria in southeastern United States salt marshes and coastal environments. However, despite the ecological importance of these bacteria, the *Roseobacter* proteins involved in aromatic compound catabolism have yet to be biochemically characterized. Moreover, genetic systems for manipulating these marine bacteria remain to be developed. As described in this report, ADP1-derived strains may serve as convenient hosts for comparative studies of aromatic compound catabolism in diverse bacteria. Furthermore, carbon-source dependent gene expression was explored by testing enzyme activities under different growth conditions. A PCR-based method to easily introduce point mutations and precise deletions into the chromosome is presented, which support the continued development of ADP1-derived strains for biotechnology.

Materials and Methods

Reagents, bacterial strains, general growth conditions and DNA manipulations.

Substrates and antibiotics were purchased from Sigma. Bacterial strains and plasmids are described in Table 4.1. *Acinetobacter* sp. strain ADP1 has been previously described (90). Cells were grown in Luria-Bertani (LB) broth and minimal medium (MM) according to published methods (139, 145). Carbon

sources added to MM were in the final concentrations: 3 mM protocatechuate, 3 mM *p*-hydroxybenzoate, 10 mM succinate, 30 mM acetate, 30 mM citrate, and 30 mM pyruvate. Cultures were grown at either 25^{o}C or 37^{o}C for 48 to 96 h, with shaking to increase aeration and in the dark. Ampicillin was added, at a final concentration of 300 mg/L for *Acinetobacter* and 150 mg/L for *E. coli*, to maintain plasmids in cultures. *E. coli* strain TOP10F' (Gibco BRL) was used as the host for general plasmid manipulations and when recombinant expression of PcaDO was from *E. coli*. Expression was induced with 0.3 mM isopropyl-α-D-thiogalactopyranoside (IPTG) when cultures were in exponential growth phase, where necessary. All cultures used for enzyme assays were grown in triplicate.

Standard methods were used for chromosomal and plasmid DNA purifications, restriction enzyme digestions, ligations, electrophoresis, and plasmid transformations by electroporation (139). FastStart *Taq* polymerase kit (Roche) was used in all polymerase chain reactions (PCR) using amplification conditions recommended by the manufacturer (139).

PCR generated deletion of the pcaHG genes in Acinetobacter strain ACN462, the host for expression of pcaHG in trans.

The *Acinetobacter* host used for vector-based production of PcaDO was an ADP1-derived mutant with *pcaHG* removed from the chromosome, designated ACN462. DNA containing a *pcaHG* deletion was generated using three successive PCR amplifications. The resulting amplicon, when integrated into the chromosome of ADP1 by homologous recombination, deleted *pcaHG* by

allelic replacement (Fig. 4.2, description of PCR-generated *pcaHG* deletion follows in text).

Two primers, complementary to each other, were synthesized containing sequence directly upstream and downstream of the *pcaHG* coding DNA: Pcadel1 (5'-AATGTCTCAAATTATTTggccgccTATTTTTCGATATCTAA-3') and pcadel2 (5'-TTTAGATATCGAAAAATAGCggccgccAAATAATTTGAGACATT-3') Sequences annealing to template are capitalized, with a *Not*I restriction enzyme site in the middle. Two more primers were created, which anneal to regions approximately 1.1 kbp upstream of *pcaH* and 1.3 kbp downstream of *pcaG*: pcaHup (5'-GGCGTGACCGAGTTTCATGTTCCAG-3') and pcaGdown (5'-CCAAACCTGGTAAAGTCATGGTACGAAC-3'), respectively. In the first two PCR amplifications, primers pcaHup and Pcadel2 were combined in one reaction and pcaGdown and Pcadel1 were combined in another reaction. The plasmid pZR1 was used as the template in both reactions. The resulting amplicons were a 1.1 kbp fragment containing sequence upstream of *pcaH* and a 1.3 kbp fragment containing sequence downstream of *pcaG* (PCR 1 and 2 in Fig. 4.2). These two amplification reactions were diluted approximately 1:1000 and added to the third PCR amplification containing the primers pcaHup and pcaGdown (PCR 3 in Fig. 4.2). The two amplicons from the first two PCR amplifications annealed to the complementary primers, Pcadel1 and Pcadel2, forming a substrate for polymerization. The third PCR generated a 2.4 kbp product, containing sequence upstream and downstream of *pcaHG*, but not *pcaHG* itself (Δ*pcaHG*).

The ∆*pcaHG* amplicon was then introduced into the chromosome of ADP1 to delete the *pcaHG* genes by allelic replacement. The ∆*pcaHG* amplicon was added to growing cultures of ADP1. Transformants were screened to identify cells in which *pcaHG* were deleted from the chromosome, by testing for growth on solid MM agar plates containing 2.5 mM protocatechuate as the sole carbon source. Cells that were unable to grow on protocatechuate were examined to characterize the chromosome *pca* gene region. Chromosomal DNA from lysed cells was used as template in PCR to amplify the region surrounding *pcaHG*, using primers pcaHup and pcaGdown. A deletion in *pcaHG* was confirmed by the size of the amplicon, which was estimated electrophoretically when compared to known standards. The PCR product was also sequence to confirm the deletion.

Construction of the Acinetobacter expression base vector, pBAC512.

A schematic of the *Acinetobacter/E. coli* expression/shuttle vector pBAC512 is represented in Figure 4.3. This vector, derived from the *E. coli* plasmid pKK223-3 (Stratagene, Inc.), carries an *Acinetobacter* origin of replication (*Acinetobacter* ori) and a mutated promoter, derived from the *catB* gene in ADP1. The mutation in the *catB* promoter was generated by a series of PCR amplifications. Construction of pBAC512 and the PCR method of engineering the mutation in the *catB* promoter are detailed in the following sections.

A 2.8 kbp fragment containing the *Acinetobacter* plasmid origin of replication from pWH845 (78, 142) was PCR amplified using the primer combination: ACORI5 (5'-atatcagctgCTTTCGTCTTCACCTC-3') and ACORI3 (5'-cgcgcagctgTTTTTTATGATTTCTCGA-3'). Sequences annealing to the 5' and 3' ends of the fragment, respectively, are capitalized; added *Pvu*II sites are underlined. After both linearizing the *E. coli* expression vector pKK223-3 (Stratagene Inc.) and digesting the amplicon with *Pvu*II restriction enzyme, the fragments were ligated together to generate pBAC417. The P_{taq} promoter on pBAC417 was then replaced with the *Acinetobacter* mutated *catB* promoter to generate pBAC512 (detailed in the next sections).

Engineering of the mutation in the catB promoter using PCR.

A series of three successive PCR amplifications was performed to generate a 1.5 kbp DNA amplicon of the *catB* promoter region containing a G to A transition, 8 bp upstream from the transcriptional start site of *catB* (Fig. 4.4). Two primers were created, one annealing to the sense DNA strand and the other to the antisense DNA strand, in the region surrounding the –10 promoter region of *catB*. Each primer contains the single base mutation, relative to the wild-type sequence. This mutation is underlined in the following primer sequences: catBO/Pfor (5'-ATTATTACATTAATTTAAGATATG-3') and catBO/Prev (5'-ACTATTTACATATCTTAAATTAAT-3'). Two more primers, which anneal to regions approximately 1.0 kb upstream and 0.5 kb downstream, respectively, from the -10 promoter region of *catB*, were as follows: catMfor (5'-

TAAATTTTTCAGACATATTTTATT-3') and catB-MIDrev (5'-ATTTGAACCAATTTTTAATTTAAA-3'). The sequence upstream and downstream of the *catB* O/P region was amplified by pairing catMfor with catBO/Prev and catBO/Pfor with catB-MIDrev primers together in two separate PCR amplifications using pIB1352 (115) as the template (first and second PCR amplifications in Figure 4.4). Primers, individual nucleotides, and other reaction components were removed from the amplicons using a PCR clean-up kit (Qiagen, Inc.). Both PCR products were then added to a third PCR with primers catMfor and catB-MIDrev (third PCR in Figure 4.4). The products from the previous two PCR amplifications annealed at the sequence of the complementary primers, catBO/Pfor and catBO/Prev and formed a substrate to allow polymerization of an approximately 1.5 kbp product. This final amplicon contained sequence upstream and downstream from the *catB* O/P and the single bp mutation.

The mutated *catB* PCR product, became the template for PCR using the primers: catMnobind2 (5'-tacgg<u>catgca</u>TACCAAATTGTTTTATCTTTT-3') and catBlowp (5'-gcgc<u>gaaTtC</u>ATCTTCTTTTCAATAAATACT-3'). Sequences annealing to the 5' and 3' ends of the fragment, respectively, are capitalized; added restriction enzyme sites are underlined, so as to add *Sph*I and *Eco*RI restriction enzyme sites at the 5' and 3' ends, respectively. The new amplicon was digested with *Sph*I and *Eco*RI restriction enzymes. Using the same restriction enzymes, pBAC417 was digested to remove the P_{tac} region, originally from pKK223-3. The mutated *catB* promoter was ligated so that the promoter

was directly upstream of the multiple cloning site (MCS) in pBAC417, generating the plasmid pBAC512.

Construction of the vector for recombinant expression of the pcaHG genes from ISM in E. coli (pNB6).

The plasmid pNB6 was made by first PCR amplifying *pcaHG* from *Roseobacter* sp. strain ISM (ISM) chromosomal DNA using the following primers: ISMNdeI.for (5'-tcaactcatATGAAAACGCCCGCC-3') and ISMBam.rev (5'-aattgaggattcTGGGCCTAGATGTCG-3'). Sequences annealing to the 5' and 3' ends of the fragment, respectively, are capitalized; added restriction enzyme sites are underlined. After digestion of the amplicon and the vector pCYB1 (NEB labs) with *Nde*I and *Bam*HI restriction enzymes, the amplicon was ligated to pCYB1, yielding pNB6.

Construction of the Acinetobacter expression vectors containing the pcaHG genes.

The expression vector containing *pcaHG* from ISM was constructed by first PCR amplifying the *pcaHG* genes from pNB6 and using the primers: ISMEcorI.for (5'-tcaattgaattcATGAAAACGCCCGCC-3') (sequences annealing to the 5' and 3' ends of the fragment, respectively, are capitalized; added *Eco*RI restriction enzyme site is underlined) and ISMBam.rev (described above). After digesting both the amplicon and pBAC512 using restriction enzymes *Eco*RI and *Bam*HI, the fragments were ligated to form pBAC538.

The vector expressing *pcaHG* from ADP1 was constructed by first PCR amplifying the *pcaHG* genes using pZR1 (43) as template and the following primers: pcaHEcoRI (5'-tgccgaattcATGTCTCAAATTATTTGG-3') and pcaGPst1NEW (5'-tgcactgcagTTAGATATCGAAAAATAC-3') (sequences annealing to the 5' and 3' ends of the fragment, respectively, are capitalized; added *Eco*RI and *Pst*I restriction enzyme sites are underlined). The resulting amplicon was then ligated into pBAC512 after both were digested with restriction enzymes *Eco*RI and *Pst*I to form pBAC547.

Transformation of plasmids in ACN426

Plasmids were transformed into the *Acinetobacter* mutant lacking *pcaHG*, strain ACN426, by electroporation. ADP1 strains are naturally transformable by plasmid DNA, but higher transformation efficiencies were accomplished with electroporation. Electrocompetent ACN462 cells were made following established methods used to prepare electrocompetent *E. coli* cells (139). Plasmid-containing transformants were selected by appropriate antibiotic resistance.

DNA sequencing analysis.

DNA sequencing was performed at the University of Georgia, Molecular Genetics Instrumentation Facility using an automated DNA sequencer (ABI373A; Applied Biosystems, Inc.). Plasmid templates were isolated from *E. coli* using the Qiaprep plasmid purification kit (Qiagen, Inc.). Chromosomal regions of

Acinetobacter strains to be sequenced were first PCR amplified using a cell lysate as the template DNA (89). The resulting amplicon was used as the template for sequencing reactions.

The *catB* promoter from the chromosome of wild-type *Acinetobacter* and the mutated *catB* promoter DNA were sequenced using the primers catMnobind2 and catBlowp (sequences indicated above). The entire *Acinetobacter ori* regions of pBAC417, pBAC512, pBAC538, and pBAC547 were sequenced using the following primers: ACORI-1 (5'-GATCGTAGAAATATCTATGAT-3'), ACORI-2 (5'-GGATTTTAACATTTTGCGTTG-3'), ACORI-3 (5'-GGACGCAATGAGTAGTCA-3'), and ACORI-4 (5'-CCCATTCGATGTACCGTC-3'). Cloned *pcaHG* genes in the *Acinetobacter* vectors were sequenced using catMnobind2 and primers corresponding to their respective *pcaHG* genes, whose sequences are stated above. DNA sequences were analyzed using DNA analysis software AssemblyLign (Accelrys, Inc.).

Removing plasmids from Acinetobacter cells by treatment with sodium dodecyl sulfate (SDS).

A logarithmically growing culture of ACN462, harboring either pBAC538 or pBAC547, was diluted 1:25 into LB medium containing varying concentrations of SDS, ranging from 1% to 0.001% (w/v). The cultures were incubated overnight at 37^{o}C. The cultures, that showed a slight detectable increase in turbidity, were selected and dilutions were plated to LB solid medium to isolate individual colonies. These colonies were then screened for growth when patched to LB

agar media plates containing 300 mg/L ampicillin and MM agar plates containing 2.5 mM protocatechuate. Cells that had become sensitive to the antibiotic were likely to have lost their plasmids and were tested further.

Preparation of PcaDO assays

Acinetobacter or *E. coli* cultures were grown in 100 ml of MM with a carbon source or in LB liquid medium, respectively. The cells were harvested by centrifugation (5,000 x g, 9 min.), washed once with sterile deionized water, and stored at –20^{o}C. Cell pellets were resuspended in 100 to 200 μl of breaking buffer (50 mM Tris-HCl, 10% glycerol, 5 mM $(NH_4)_2SO_4$, 2.5 mM EDTA, 1 mM dithiothreitol, pH 7.5). Cell extracts were prepared as previously described (145), and PcaDO activity was determined spectrophotometrically by measuring the decrease in absorbance at 290 nm (ε = 2280 M^{-1} cm^{-1})(146). Protein concentrations were determined by the method of Bradford (12).

Results

Construction of an Acinetobacter mutant with a precise chromosomal deletion of the coding regions of pcaHG.

An examination of gene organization in well-characterized and recently-sequenced genomes suggested that the microbial *pcaHG* genes encoding PcaDO are almost always co-transcribed with other genes needed for protocatechuate catabolism. This observation raised the question of whether or

not these genes would allow growth on aromatic substrates via the protocatechuate branch of the β-ketoadipate pathway if they were expressed independently of their neighboring *pca* genes. As a first step in addressing this question, a mutant strain was generated in which the *pcaHG* coding regions were deleted from the wild-type *Acinetobacter* sp. strain ADP1 chromosome.

To generate this mutant, linear DNA with the *pcaHG* deletion was first obtained by PCR methods as described in the Materials and Methods section (depicted in Fig. 4.3). After transformation of the wild-type strain by the PCR-generated fragment, transformants were screened to identify cells in which *pcaHG* had been removed from the chromosome by homologous recombination. Chromosomal acquisition of the engineered deletion should prevent growth with protocatechuate as the sole carbon source. Therefore, this phenotype was used as a screen to identify transformants warranting further examination. As described in the Materials and Methods section, one strain in which it was confirmed that the engineered deletion had replaced the corresponding chromosomal region was designated ACN462. As expected, ACN462 was unable to grow on *p*-hydroxybenzoate or other aromatics degraded via the protocatechuate branch of the β-ketoadipate pathway.

Construction of Acinetobacter vectors to test complementation of the mutant with plasmid-borne pcaHG genes.

One goal of the current studies was to determine whether *pcaHG* could be expressed independently of the chromosomal *pca* region to correct for the

inability of the Δ*pcaHG* mutant (ACN462) to grow on protocatechuate or *p*-hydroxybenzoate as the sole carbon source. For this purpose, the wild-type *pcaHG* genes could be inserted into a vector and used in standard complementation procedures. However, few cloning vectors have previously been developed for use in *Acinetobacter*. Previously, *E. coli-Acinetobacter* shuttle vectors were made in the laboratory of Dr. Wolfgang Hillen after cloning the region of the origin of plasmid replication (ori) from a cryptic plasmid, pWH1277, isolated from *A. calcoaceticus lwoffi* (78, 142). As previously published, pWH1277 was linearized by restriction digest and ligated to linearized pBR332, to create a plasmid (designated pWH1266) containing both an *Acinetobacter* and pBR322 ori. The *Acinetobacter* ori from pWH1266 was then removed by restriction digest and ligated to the linearized plasmid pQE9 (Table 4.1) to form pWH845, also containing both an *Acinetobacter* and pBR322 ori. Normally, plasmids with *colE*1 replicons such as pBR322 are not well maintained in ADP1 and cannot be used as cloning vectors, although the underlying reasons are not understood. However, the shuttle vector pWH1266 and the similarly constructed pWH845 were shown to function well as cloning vectors in both ADP1 and *E. coli*.

To express *pcaHG* in ADP1-derived strains, the previously constructed vectors were not ideal because they did not use promoter regions that were designed for, or characterized in, *Acinetobacter* hosts. Therefore, to generate a cloning vector for these studies, the approach taken was to make a new shuttle vector that contained a relatively strong promoter from ADP1. As a first step in

this construction process, a new vector, pBAC417, was made with the approach described above. This approach was based on combining an *E. coli* (*colE*1 replicon) cloning plasmid pKK223-3 (from Stratagene) with the *Acinetobacter* ori that had been characterized by the Hillen lab (see Materials and Methods for details of pBAC417 construction). Plasmid pBAC417 was able to transform ADP1, ACN462 and other ADP1-derived strains. Transformants were selected on LB plates containing 300 mg/L ampicillin, and the plasmid could be successfully isolated from drug-resistant transformants (data not shown). Similarly, pBAC417 transformed *E. coli* and was stably maintained in this bacterium (data not shown). The next step in constructing a desirable expression vector was to replace the P_{tac} promoter region of pBAC417 with an appropriate promoter region for use in *Acinetobacter*.

Design of a promoter region for an Acinetobacter expression vector.

To date, the well-characterized promoters of strain ADP1 require a transcriptional activator together with a co-effector metabolite to regulate high-level gene expression. Since this type of transcriptional activation might not be useful for some intended purposes of the expression vector, the decision was made to use a site-specific mutation to increase the promoter strength of the wild-type promoter of the *catB* gene. Normally, high-level expression of *catB* requires a transcriptional activator, CatM, or in some cases BenM, together with the co-effector *cis,cis*-muconate. However, by comparison with the *benA* promoter region, it appeared that introduction of a G to A mutation at position -8

relative to the transcriptional start site might alleviate the need for a transcriptional activator (Fig. 4.5). The corresponding mutation in the *benA* promoter increases promoter strength and allows the *benABCDE* operon to be expressed in the absence of the BenM or CatM activator proteins (20, 27).

The decision was made to introduce the single point mutation in the *catB* promoter and to use this engineered promoter in the expression vector. A different option for the expression vector would have been to use the previously characterized *benA* promoter (allele *benA5147*) that already contained a relatively strong promoter. The former option was chosen for two reasons. Making the site-specific mutation in *catB* would provide an opportunity to test our prediction about promoter strength in ADP1. Furthermore, the mutated *catB* region could be introduced into the chromosome to generate a mutant strain that would be useful for continuing studies of the BenM-CatM regulon.

Construction of the mutated catB promoter DNA fragment.

A three-step, PCR-based method was used to generate a DNA fragment that carried the desired mutation in the *catB* promoter region (Fig. 4.4, see Materials and Methods). The complementary primers, catBO/Pfor and catBO/Prev harbor the single base mutation. Even though the sequence of the primers is not identical to the wild-type *catB* promoter template, sufficient sequence homology allowed annealing of these primers to the appropriate location to the wild-type *catB* template, permitting polymerization of a product in the first two PCR amplifications. The PCR amplicons, each containing the

promoter mutation, were isolated from wild-type *catB* template DNA, so that when these products were added to the third PCR, the only template present would be *catB* promoter DNA carrying the mutation.

The mutated catB promoter allowed expression of the catBCDIJF genes in the absence of a transcriptional activator.

In wild-type ADP1, the transcriptional activator, CatM, along with the effector molecule *cis, cis*-muconate, is needed to induce expression of the *catBCDIJF* genes (114). Under certain conditions, BenM, the transcriptional activator of the *ben* genes, can induce expression of the *cat* genes (20, 27). ADP1 strains lacking a functional CatM and BenM cannot grow on the carbon source *cis,cis*-muconate, because the expression of the *cat* genes cannot be induced. If the mutated *catB* promoter can allow expression of *catBCDIJF* in the absence of transcriptional regulators, then a *catM*- and *benM*-deleted ADP1 strain should be able to grow on *cis,cis*-muconate, if it is carrying the mutated *catB* promoter on the chromosome. This hypothesis was tested in order to confirm that the mutated *catB* promoter could allow expression in the absence of transcriptional activators.

In the ADP1-derived strain, ACN293, *catM* and *benM* have been knocked out on the chromosome. Because of these mutations, CatM and BenM are not present to induce expression of *catBCIJFD* to permit growth of ACN293 on *cis, cis*-muconate. Mutated *catB* promoter DNA was added to cultures of ACN293 to replace the wild-type *catB* promoter in ACN293 by allelic exchange. The

transformed cultures were plated to solid MM containing *cis,cis*-muconate as the sole carbon source. Cells growing on *cis,cis*-muconate were lysed and added to PCR, which included primers to amplify the *catB* promoter region on the chromosome. The resulting amplicon was sequenced to confirm that the *catB* promoter from the chromosome of cells, growing on *cis,cis*-muconate, contained the mutation 8 bp upstream from the transcriptional start site of *catB* and that no other mutation existed between the coding regions of *catM* and *catB*. The new strain, in which the mutated *catB* promoter permitted expression of *catBCDIJF* in the absence of transcriptional activators, was designated ACN275.

Introduction of the mutated catB promoter into the shuttle vector pBAC417 to generate an Acinetobacter expression plasmid (pBAC512).

After confirming the inducer-independent expression of the mutated *catB* promoter in vivo, the P_{tac} region on pBAC417 was excised and replaced with the mutated *catB* promoter to form the new base vector pBAC512. The mutant *catB* promoter was placed within pBAC512 so that when a gene is integrated into the MCS at the *Eco*RI restriction site (i. e. the gene is cloned into the vector using *Eco*RI restriction site and has the ATG of the gene begin directly after the *Eco*RI restriction site), the bp spacing between the mutant *catB* promoter elements (e. g. ribosome binding site and -10 and -35 regions) and coding region of the gene would be identical to the same spacing of promoter elements and the wild-type *catB* gene in the chromosome.

Integration of pcaHG genes into pBAC512 and confirmation of plasmid stability in ACN462.

As stated in the Materials and Methods, the *pcaHG* genes from ADP1 and ISM were cloned into pBAC512 using the *Eco*RI restriction site in the MCS to ligate the 5' end of the *pcaH* coding region to the plasmid. The pBAC417-based plasmids (pBAC512, pBAC538, and pBAC547) were selected and stably maintained in ACN462 when grown in the presence of 300 mg/L ampicillin. These plasmids are also maintained in *E. coli* growing in medium containing ampicillin concentrations of 150 mg/L.

It was necessary to periodically sequence certain areas of the plasmids and the ACN462 chromosome to determine if any genetic rearrangements occurred when plasmids were maintained in ACN462, or if homologous plasmid sequence would recombine into the chromosome of ADP1. We needed to confirm that the measured growth phenotypes and enzyme activities were not attributed to spontaneous mutations in the *Acinetobacter* ori, the *catB* promoter, or the *pcaHG* genes itself. For example, ACN462 with plasmid-borne *pcaHG* genes from ISM grew very slowly on *p*-hydroxybenzoate. Because of this, there may have existed selective pressure to increase copy number of the plasmid, increase expression of *pcaHG* from the mutated *catB* promoter, or mutate the *pcaHG* genes to generate a PcaDO with increased activity, which would permit faster growth on *p*-hydroxybenzoate. This is why the *Acinetobacter* ori, the mutated *catB* promoter, and the *pcaHG* genes were sequenced in plasmids that were maintained in ACN462 after many generations.

Populations of ACN462, containing either pBAC512, pBAC538, or pBAC547, were grown on MM containing either protocatechuate or *p*-hydroxybenzoate as carbon sources. After several weeks, the plasmids were cured from the host cells. The isolated plasmids were used as templates for separate PCRs amplifying the *catB* promoter region, the *Acinetobacter* ori, and the *pcaHG* genes. The sequences of these plasmid elements were found to be unchanged. Plasmid-cured cells were lysed and used as template in PCR amplifications of the *catB* promoter region and the ∆*pcaHG* allele on the chromosome. Sequencing the PCR amplicons confirmed that the *catB* promoter region was wild-type and did not contain the single bp mutation, originating from the pBAC512-based plasmids. Also, complete *pcaHG* genes failed to be amplified from the chromosome of these lysed cells. Therefore, no detectable allelic exchange occurred between the mutant *catB* promoter on the plasmid and the wild-type *catB* promoter on the chromosome, nor at the *pcaHG* loci on the chromosome, after maintaining these plasmids in ACN462 for many generations.

Extrachromosomal expression of pcaHG in ACN462 and growth of the strains on protocatechuate and p-hydroxybenzoate.

As constructed, ACN462 contains only 18 bp of the 5' end of *pcaH* and 17 bp of the 3' end of *pcaG*. Because of the *pcaHG* deletion, this strain is unable to grow on *p*-hydroxybenzoate or protocatechuate as a sole carbon source. When transformed with plasmid-borne *pcaHG* genes for ADP1 (ACN462(pBAC547)), the strain is able to grow on both *p*-hydroxybenzoate and protocatechuate, but

only after the cells have been exposed to these carbon sources for 3 to 4 days (data not shown). This is several days longer than ADP1 needs to acclimate to *p*-hydroxybenzoate or protocatechuate when transferred from growth on another carbon source. After maintaining the plasmid in the strain for several weeks, removal of the plasmid from ACN462 cells by SDS treatment is consistent with loss of growth on protocatechuate or *p*-hydroxybenzoate, along with loss of Ap^r. This procedure insured that the ability for ACN462 to utilize protocatechuate and *p*-hydroxybenzoate was dependent upon *pcaHG* expression from the plasmid and further confirmed that a functional copy of the *pcaHG* genes did not recombine into the chromosome by allelic exchange.

When the plasmid containing *pcaHG* genes from ISM (pBAC538) was transformed into ACN462, the strain exhibited a lag in growth, similar to ACN462(pBAC547) when plated to solid MM containing either protocatechuate or *p*-hydroxybenzoate (data not shown). Also, growth on protocatechuate and *p*-hydroxybenzoate was much slower than the growth rate of ACN462(pBAC547). Furthermore, the strain was unable to grow at temperatures >30^oC on these carbon sources. Consistent with ACN462(pBAC547), loss of growth on protocatechuate and *p*-hydroxybenzoate, and loss of Ap^r was observed after the plasmid was cured from the strain by SDS treatment.

The significant lag in growth phase, exhibited by ACN462 with either pBAC538 or pBAC547, growing on either protocatechuate or *p*-hydroxybenzoate may be the result of the inducer-independent expression of *pcaHG* genes. As shown by previous studies, the *pca* genes are induced in the presence of

protocatechuate (59). The short lag in growth when ADP1 cells are removed from a different carbon source and exposed to either protocatechuate or *p*-hydroxybenzoate is most likely is dependent upon, in part, by the time it takes to sufficiently induce expression of the *pca* genes to produce detectable cell growth. Based upon this hypothesis, a longer lag phase measured during initial growth on protocatechuate or *p*-hydroxybenzoate of ACN462 carrying inducer-independent, plasmid-borne *pcaHG* genes may be caused, in part, by a lower level of inducer-independent *pcaHG* expression in comparison to wild-type, transcriptional activator-induced expression of these genes.

Comparison of PcaDO specific activity when expressed in ADP1and ACN462 containing plasmid-borne pcaHG genes from ADP1.

Activity of PcaDO from ADP1 and from ACN462 carrying plasmid-borne *pcaHG* genes, originating from ADP1, is shown in the left half of Figure 4.6. Maximal activity was observed when wild-type ADP1 was grown on protocatechuate at 37^{o}C. ACN462(pBAC547) exhibited 87% activity compared to wild-type under the same conditions. This demonstrates that extrachromosomal, inducer-independent expression of the *pcaHG* genes is comparable to native, induced expression of the genes within the *pca* operon on the chromosome. In contrast, PcaDO activity of ACN462(pBAC547), grown on succinate and at 37^{o}C, exhibited only approximately 5% of wild-type activity grown on protocatechuate. This suggests that growth on succinate may be inhibiting expression of the *pcaHG* genes from the mutated *catB* promoter.

Comparison of PcaDO specific activity when pcaHG genes from ISM are expressed in ACN462 and E. coli.

Activity of PcaDO from recombinant expression of ISM's *pcaHG* genes, in ACN462 and *E. coli*, is shown in the right half of Figure 4.6. When ISM *pcaHG* genes are expressed from p6NB in TOP10F' at 25^{o}C, level of activity was comparable to expression of ISM *pcaHG* genes in *Acinetobacter* under the conditions stated in Materials and Methods. No detectable activity was demonstrated when these strains were grown at 37^{o}C. This particular phenotype could be a product of the heterologous expression system itself, or is inherent to PcaDO of ISM. Marine Roseobacter group members, isolated from coast estuaries in the State of Georgia, have an optimal, mean growth temperature of 30^{o}C and cannot grow at 37^{o}C (15). These differences in PcaDO activity temperature optimum will be better understood with more extensive measurements of PcaDO activity from this prokaryote lineage.

No detectable activity was measured in the following strains: wild-type ADP1 grown on succinate, ACN462(pBAC512) grown on succinate at 25^{o}C or 37^{o}C, ACN462(pBAC538) grown on succinate at 25^{c}C or 37^{o}C, and TOP10F' containing either pCYB1, pBAC512,, and pBAC547 at 37^{o}C (data not shown).

Activity of PcaDO from ACN462(pBAC547) grown on various carbon sources.

To confirm if succinate and other carbon sources repressed expression from the mutated *catB* promoter, ACN462(pBAC547) was grown in 5 different carbon sources and PcaDO activity was measured and reported in Figure 4.7.

The only activity comparable to the construct grown on protocatechuate was measured when the strain was grown on citrate (1.5 versus 1.1 specific activity units/mg protein, respectively under identical assay conditions and similar cell extract preparations). When the strain was grown on either acetate and pyruvate, activity of PcaDO was approximately 3-fold lower in comparison to citrate-grown cells. Specific activity of pcaDO was 4-fold lower when grown on succinate, compared to cells grown on citrate. Cells grown in LB exhibited the lowest activity out of all the carbon sources tested, which was 16-fold lower than citrate-grown cells.

Discussion

Effective expression of PcaDO from the engineered Acinetobacter vector

The primary goal of this study was to gain an understanding of cellular processes that would affect a system to express recombinant and mutant dioxygenases in ADP1. Inherent to ADP1 are several native aromatic ring dioxygenases and, combined with an easy genetic system, genetic manipulation and expression of foreign and mutant dioxygenases could be highly successful in this strain. An *Acinetobacter* expression vector would be useful if recombinantly-expressed dioxygenases would play a functional role in existing catabolic pathways of ADP1, such as allowing ADP1 to utilize novel aromatic compounds as sources of carbon and energy (e. g. halo-substituted benzoates). Before a novel expression vector could be used in such a manner, it would be prudent to

determine the vector's functionality with genes familiar to ADP1. The *pcaHG* genes were the specific focus to elucidate effects of independent expression of the genes from its native loci on the chromosome.

A new *Acinetobacter* expression plasmid was created because existing plasmids, which can be replicated and stability maintained in *Acinetobacter* are very large and do not contain optimal promoters for specific expression in non-*E. coli* strains. The mutant *catB* promoter was chosen because it was presumed to allow high constitutive expression of the *cat* operon, similar to the analogous mutation in the *benA* promoter. Creation of a vector containing the mutant *catB* promoter presented a good method to test expression properties of this new promoter in ADP1.

As shown by this study, the new vector allows sufficient expression of both native and foreign *pcaHG* genes to restore the phenotype of an ADP1 strain caused by deleting these genes from the chromosome. Expression of the ADP1 *pcaHG* genes from the engineered vector in ACN462 produced a phenotype similar to wild-type, in both growth measurements and specific activity assays. Also, enzymatic activity of the PcaDO from ISM and expressed in the ADP1 system, under the conditions established in this study, was comparable to the well-established P_{taq}-based expression system in *E. coli*, under normal recombinant expression conditions for this *E. coli* system. This was the evidence to confirm that an extrachromosomal expression system in ADP1 is functional and a viable alternative to *E. coli*-based expression systems.

The potential of using ADP1 as a host to express mutant dioxygenases for the development of novel strain growth phenotypes.

ADP1 is a model organism to study dioxygenase enzymes and their involvement in aromatic compound catabolic pathways. These catabolic pathways and dioxygenase enzymes that oxidize aromatic compounds are of importance for the development of bioremediation technology. As shown by this study, ADP1 can be easily manipulated to act as a host for analyzing dioxygenases, independent from their native catabolic pathways that they play an essential role in. This study can facilitate the analysis of dioxygenases with enhanced degradation capabilities of xenobiotic compounds and have characteristics that make them attractive synthons for the production of industrially and medically important chiral chemicals.

ADP1 possesses many different aromatic compound catabolic pathways, containing ring-hydroxylating and ring-fission dioxygenases. Removing the dioxygenase genes from the chromosome and placing them on mobile plasmid vectors with independent expression systems facilitates genetic manipulation of these genes. Plasmid-encoded dioxygenase genes can easily undergo in vitro random mutagenesis and other, directed evolution assays to alter their catalytic activity or substrate specificity. Mutant dioxygenases, with the ability to convert novel substrates to products that ADP1 is able to degrade via chromosomal catabolic pathways, could be placed on *Acinetobacter* expression vectors, transformed into ADP1, and assayed in vivo by the strain's ability to utilize the

new aromatic substrate. These steps will be taken in future studies of the *Acinetobacter* expression system presented in this work.

Easy and efficient PCR method to generate precise mutations in the ADP1 chromosome.

An efficient, three-step PCR-based method was used to generate the engineered *pcaHG* deletion and mutation in the *catB* promoter. As designed, this methodology can be used to develop many different types of genetic variations. The simple procedure consist of, (1) synthesizing primers, constructed to contain the desired mutation, (2) another set of primers to allow polymerization of DNA upstream and downstream from the location of the desired mutation in a DNA sequence, and (3) using the primers to perform a series of PCR amplifications to ultimately produce a DNA product containing the desired mutation in the middle of the sequence. The first set of primers, containing the engineered mutation(s), are complementary and are used in two separate PCR amplifications. Two PCR amplifications will produce amplicons, one containing DNA directly upstream, and the other containing DNA directly downstream, of the engineered genetic aberration. The complementary primers, now integrated at the ends of the PCR products, can anneal in a third PCR amplification to provide a template in which the polymerase will form one product combining the two previous amplicons at the location of the mutation. The final product can them be taken directly from the thermocycler and added to growing cultures of ADP1 strains for transformation and allelic exchange in the chromosome. No cloning of the PCR

product is necessary. In this way, precise deletions, insertions, and mutations can be easily constructed and integrated into the ADP1 chromosome.

Acknowledgements

This was completed by a joint effort between myself and Alison Buchan and Mary Ann Moran in the Marine Sciences Department. I would like to thank Todd J. Clark and Andrew B. Reams for their assistance in creating the mutation in the *catB* promoter.

TABLE 4.1. Bacterial strain and plasmids used in this study

Strain or plasmid	Relevant Characteristics	Source or reference
Acinetobacter strains		
ADP1	Wild type (strain BD413, ATCC 33305)	(90)
ACN293	*benM*::AS4036, point mutation (G to A) allowing constitutive expression of *benABCDE*, Δ*catM*	(134)
ACN275	ACN293, *catB* O/P point mutation (G to A)	This study
ACN462	Δ*pcaHG*	This study
E. coli strains		
TOP10F'	F' *mcrA* Δ(*mrr-hsdRMS-mcrBC*) ϕ80 *lacZ*Δ*M15* Δ*lacX74 deoR recA1 araD139* Δ(*ara-leu*)*7679 galU galK rpsL*(Str^r) *endA1 nupG*	Gibco BRL
Plasmids		
pCYB1	Ap^r, *E. coli* expression vector	NEB labs
pKK223-3	Ap^r, *E. coli* expression vector	Stratagene
pNB6	*Roseobacter* sp. st. ISM *pcaHG* in pUC19	This study
pWH1277	cryptic plasmid isolated from *Ac. Lwoffi*	(142)
pWH1266	plasmid containing ori for *Acinetoabcter* from pWH1277	(134)
pWH845	Ap^r, *ori* for *Acinetobacter* from pWH1266, expression vector for *Acinetobacter* derived from pQE9	(142)
pIB1352	*benMABC* from *Acinetobacter* in pUC19	(115)
pZR1	*pcaIJBDKCHG* on 11 kbp *Eco*RI fragment in pUC18	(43)
pBAC417	pKK223-3 with *Acinetobacter ori*	This study
pBAC512	pBAC417 with P*tac* from pKK223-3 removed, replaced with mutant *catB* O/P	This study
pBAC538	pBAC512 with *pcaHG* from *Roseobacter* sp. strain ISM	This study
pBAC547	pBAC512 with *pcaHG* from *Acinetobacter* sp. strain ADP1	This study

Figure 4.1. The protocatechuate branch of the β-ketoadipate pathway encoded by the *pca* operon in ADP1. Gene organization is shown below the reaction pathway. Each gene(s) responsible for catalyzing a reaction is designated by the numbered step in the catabolic pathway. The *qui* genes, responsible for utilization of quinate and shikimate, are transcribed with the *pca* genes (37).

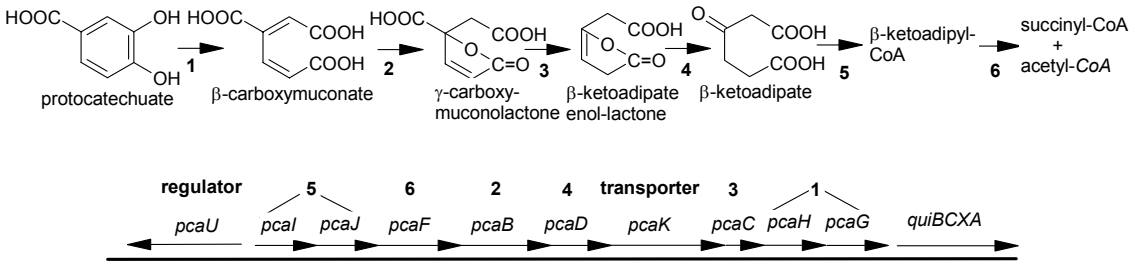
HOOC
OH
OH
protocatechuate
1
HOOC
COOH
COOH
β-carboxymuconate
2
HOOC
COOH
O
C=O
γ-carboxy-
muconolactone
3
COOH
O
C=O
β-ketoadipate
enol-lactone
4
O
COOH
COOH
β-ketoadipate
5
β-ketoadipyl-
CoA
6
succinyl-CoA
+
acetyl-CoA

regulator
5
6
2
4
transporter
3
1
pcaU
pcaI
pcaJ
pcaF
pcaB
pcaD
pcaK
pcaC
pcaH
pcaG
quiBCXA

Figure 4.2. Schematic diagram of the PCR-generated Δ*pcaHG* construct used to delete *pcaHG* in ACN462. Each PCR amplification is numbered. The name of each primer is in parentheses.

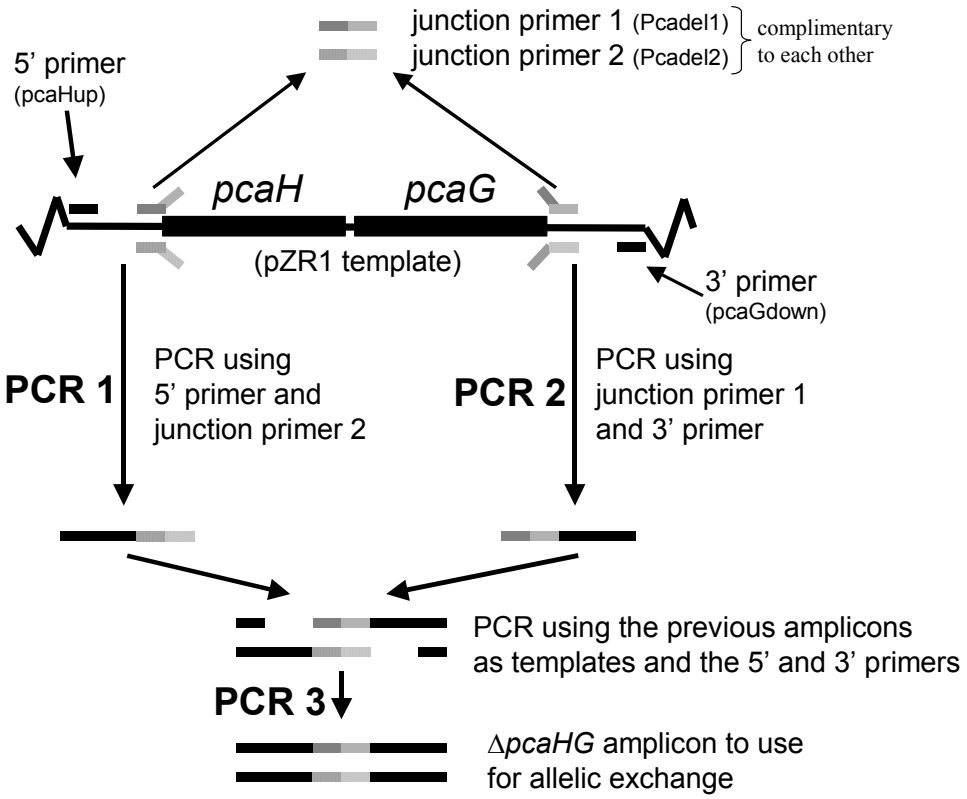
junction primer 1 (Pcadel1)
junction primer 2 (Pcadel2)
complimentary to each other
5' primer
(pcaHup)
pcaH
pcaG
(pZR1 template)
3' primer
(pcaGdown)
PCR 1
PCR using 5' primer and junction primer 2
PCR 2
PCR using junction primer 1 and 3' primer
PCR using the previous amplicons as templates and the 5' and 3' primers
PCR 3
ΔpcaHG amplicon to use for allelic exchange

Figure 4.3. Schematic diagram of the *Acinetobacter* expression/*E. coli* shuttle vector pBAC512. The mutant *catB* promoter sequence and restriction endonuclease sites in the MCS are shown (non-unique restriction sites are starred). Plasmid contains the ampicillin resistance gene (amp^R) and pBR322 *ori* from pKK223-3 (Stratagene). The *Acinetobacter ori* originated from pWH845 (78, 142). The *rrnB* operon region containing 5S rRNA region (5S) and *rrnB* T1 and T2 transcriptional terminators (*rrnB*T_1T_2) are also shown (2, 51, 83).

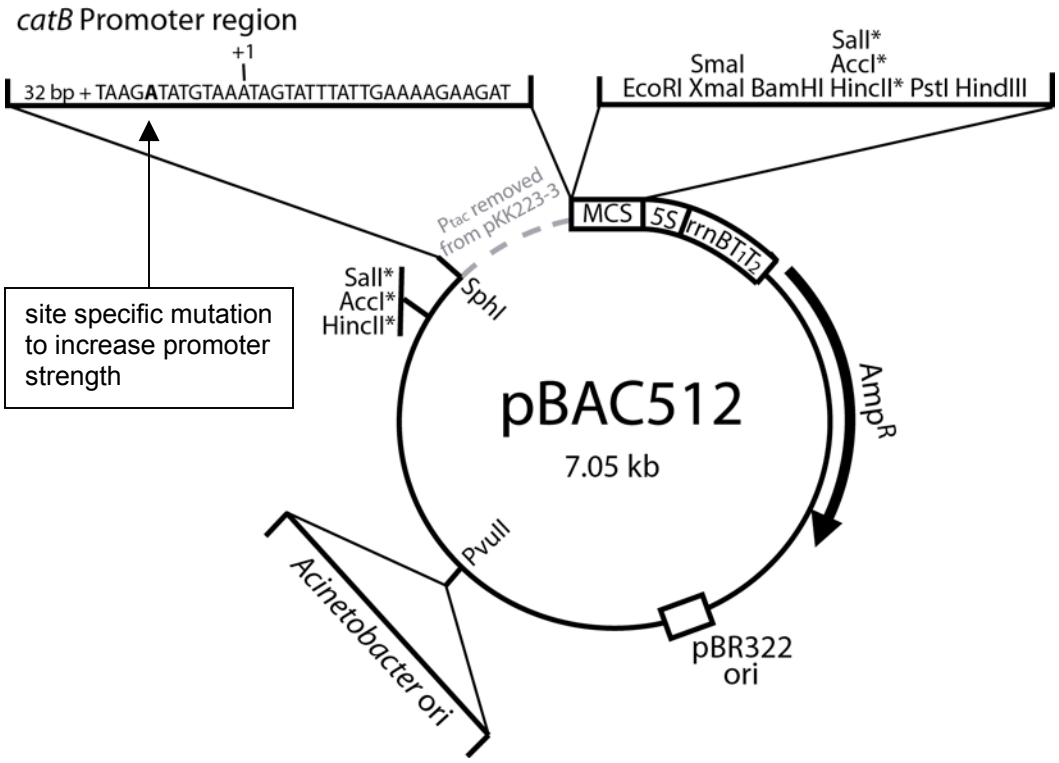
catB Promoter region
+1
32 bp + TAAGATATGTAAATAGTATTTATTGAAAAGAAGAT
SmaI
SalI*
AccI*
EcoRI XmaI BamHI HincII* PstI HindIII
Ptac removed from pKK223-3
MCS
5S
rrnBT1T2
site specific mutation to increase promoter strength
SalI*
AccI*
HincII*
SphI
pBAC512
7.05 kb
AmpR
PvuII
Acinetobacter ori
pBR322 ori

Figure 4.4. Schematic diagram of generating the PCR product of *catMB* intergenic region containing the G to A transition, 8 bp upstream of the transcriptional start of *catB*

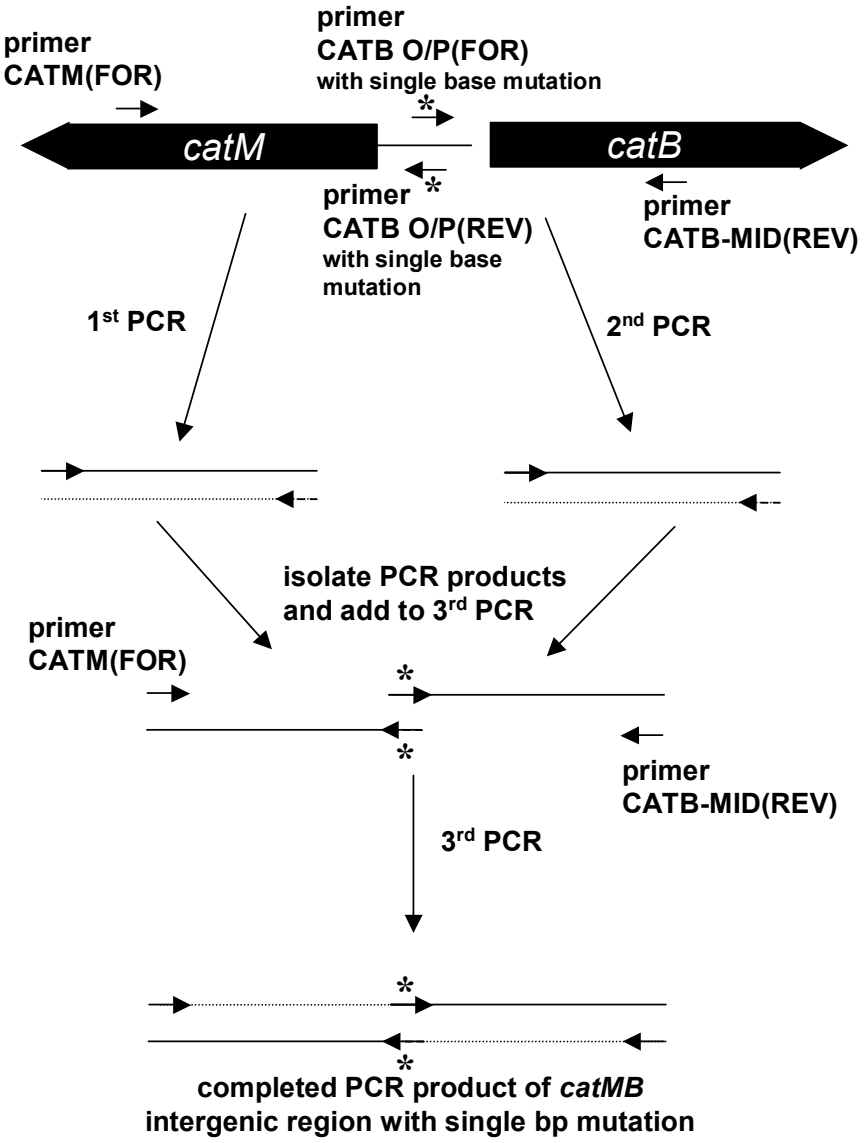
primer
CATM(FOR)
primer
CATB O/P(FOR)
with single base mutation
catM
catB
primer
CATB O/P(REV)
with single base
mutation
primer
CATB-MID(REV)
1st PCR
2nd PCR
isolate PCR products
and add to 3rd PCR
primer
CATM(FOR)
primer
CATB-MID(REV)
3rd PCR
completed PCR product of catMB
intergenic region with single bp mutation

Figure 4.5. Comparison of the intergenic region between the *benM* and *benA* genes and *catM* and *catB* genes. Transcriptional and coding start sites are shown for each gene, expect for *catM*. The nucleotide in the ben region that allows for BenM- and CatM-independent expression of *benA* is shown in red (27). The homologous nucleotide changed in the *cat* region is also shown in red (this study).

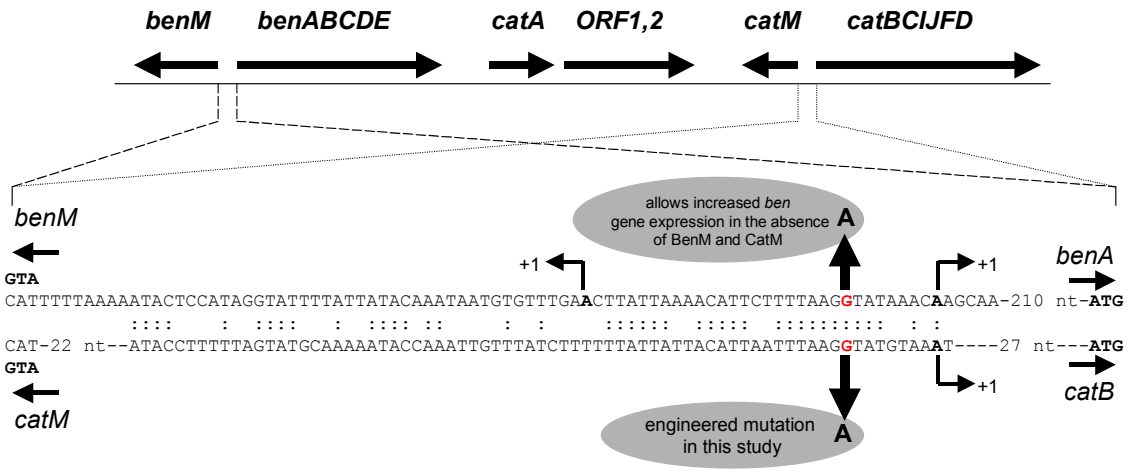
benM
benABCDE
catA
ORF1,2
catM
catBCIJFD
benM
allows increased ben
gene expression in the absence
of BenM and CatM
A
+1
+1
benA
GTA
CATTTTTAAAAATACTCCATAGGTATTTTATTATACAAATAATGTGTTTGAACTTATTAAAACATTCTTTTAAGGTATAAACAAGCAA-210 nt-ATG
CAT-22 nt--ATACCTTTTTAGTATGCAAAAATACCAAATTGTTTATCTTTTTTATTATTACATTAATTTAAGGTATGTAAAT----27 nt---ATG
GTA
+1
catB
catM
engineered mutation
in this study
A

Figure 4.6. Specific activity of PcaDO measured from cells grown in MM containing 3 mM protocatechuate as the sole carbon source, except for *E. coli*, which was grown in LB. Each culture was grown at 37^{o}C except for ACN462(pBAC538), which was grown at 25^{o}C. Each culture was grown in triplicate. See Materials and Methods for detailed explanation of the assay.

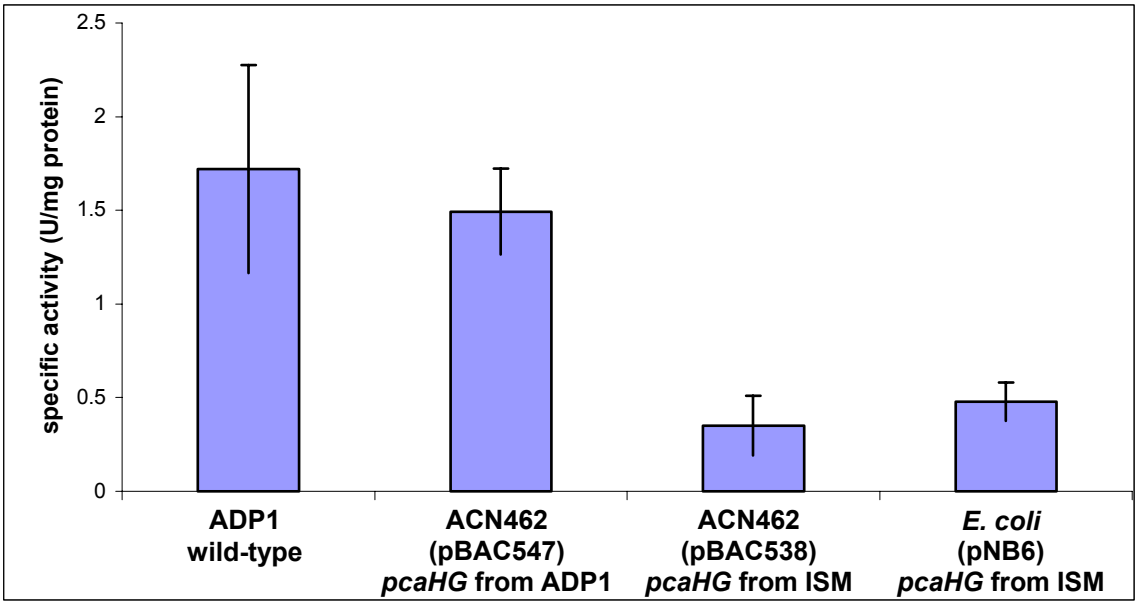
specific activity (U/mg protein)
2.5
2
1.5
1
0.5
0
ADP1 wild-type
ACN462 (pBAC547) pcaHG from ADP1
ACN462 (pBAC538) pcaHG from ISM
E. coli (pNB6) pcaHG from ISM

Figure 4.7. Specific activity of PcaDO from ACN462(pBAC547) cultures grown in MM and various carbon sources or LB. Each culture was grown at 37^{o}C and with either 30 mM acetate, 30 mM citrate, 30 mM pyruvate, or 10 mM succinate when grown in MM. Cultures were grown in triplicate. See Materials and Methods for detailed explanation of the assay.

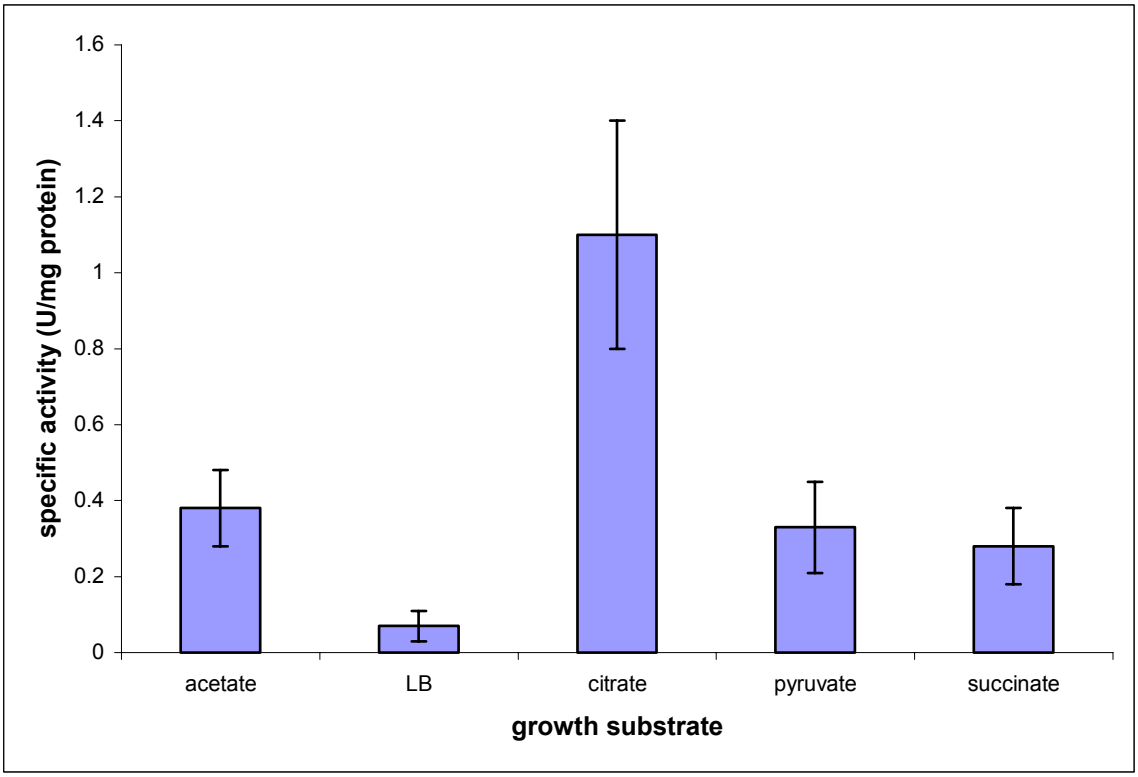
specific activity (U/mg protein)
1.6
1.4
1.2
1
0.8
0.6
0.4
0.2
0
acetate
LB
citrate
pyruvate
succinate
growth substrate

CONCLUSION

This dissertation describes the characterization of anthranilate 1,2-dioxygenase. This enzyme and other dioxygenases play an essential role in aromatic compound catabolism by *Acinetobacter* sp. strain ADP1. Two separate enzymes that constitute anthranilate 1,2-dioxygenase were expressed in *Escherichia coli* and purified to homogeneity: a reductase and a terminal dioxygenase. The electron-transferring and catalytic metal centers were identified and characterized. Furthermore, the size and quantity of anthranilate 1,2-dioxygenase subunits were analyzed, and deduced amino acid sequences were used to evaluate evolutionary relatedness among bacterial aromatic ring hydroxylating dioxygenases. Comprehensive activity measurements were completed for anthranilate 1,2-dioxygenase and a homolog, the benzoate 1,2-dioxygenase from ADP1.

In additional studies, an ADP1 derived mutant was used to measure the efficiency of generating random mutations and introducing them into the chromosomal *catA* gene that encodes catechol 1,2-dioxygenase. The conditions for mutagenesis were optimized using two different PCR-based approaches for incorporating random mutations. The optimization procedure took advantage of the natural transformability of ADP1-derived strains and the ability to select mutants directly in which mutations has generated non-functional catechol 1,2-

dioxygenase enzymes. These studies lay the foundation for continuing efforts to alter the substrate specificity of catechol 1,2-dioxygenase by random mutation.

This dissertation also reports investigations aimed at developing an *Acinetobacter* host system for the synthesis of dioxygenases encoded by genes from diverse microorganisms. An expression vector was constructed containing an engineered *Acinetobacter* promoter to facilitate high-level gene expression without the need for a transcriptional activator. To test the system, the wild-type *pcaHG* genes, encoding protocatechuate 3,4-dioxygenase, were deleted from the ADP1 chromosome. These genes were then expressed in trans from the vector, and the effects were determined with regards to growth on protocatechuate or *p*-hydroxybenzoate as the sole carbon source. Furthermore, the expression vector was used to demonstrate that the *pcaHG* genes from a marine *Roseobacter* isolate could complement the effect of the engineered deletion in the ADP1-derived host strain. Collectively, these studies constitute the beginning steps into engineering ADP1 as a host for altering the substrate specificity and catalytic activity of aromatic dioxygenases in the effort to generate novel growth phenotypes.

REFERENCES

1. **Altenschmidt, U., and G. Fuchs.** 1992. Novel aerobic 2-aminobenzoate metabolism. Eur. J. Biochem. **205**(721-727).
2. **Amann, E., J. Brosius, and M. Ptashne.** 1983. Vectors bearing a hybrid trp-lac promoter useful for regulated expression of cloned genes in Escherichia coli. Gene. **25**(2-3)**:**167-78.
3. **Assinder, S. J., and P. A. Williams.** 1990. The TOL plasmids: determinants of the catabolism of toluene and the xylenes. Adv. Microb. Physiol. **31:**1-69.
4. **Atlas, R. M., and R. Bartha.** 1993. Microbial Ecology, 3 ed. Benjamin/Cummings Publishing Co., Redwood City, CA.
5. **Averhoff, B., L. Gregg-Jolly, D. Elsemore, and L. N. Ornston.** 1992. Genetic analysis of supraoperonic clustering by use of natural transformation in Acinetobacter calcoaceticus. J Bacteriol. **174**(1)**:**200-4.
6. **Batie, C. J., E. LaHaie, and D. P. Ballou.** 1987. Putification and characterization of phthalate oxygenase and phthalate oxygenase reductase from *Pseudomonas cepacia.* J. Biol. Chem. **262**(4)**:**1510-1518.
7. **Beharry, Z. M.** 2002. University of Georgia, Athens, GA.
8. **Beil, S., J. R. Mason, K. N. Timmis, and D. H. Pieper.** 1998. Identification of chlorobenzene dioxygenase sequence elements involved

in dechlorination of 1,2,4,5-tetrachlorobenzene. J Bacteriol. **180**(21)**:**5520-8.

9. **Bertini, I., M. A. Cremonini, S. Ferretti, I. Lozzi, C. Luchionat, and M. S. Viezzoli.** 1996. Arene hydroxylases: metalloenzymes catalysing dioxygenation of aromatic compounds. Coord. Chem. Rev. **151:**145-160.
10. **Blattner, F. R., G. Plunkett, 3rd, C. A. Bloch, N. T. Perna, V. Burland, M. Riley, J. Collado-Vides, J. D. Glasner, C. K. Rode, G. F. Mayhew, J. Gregor, N. W. Davis, H. A. Kirkpatrick, M. A. Goeden, D. J. Rose, B. Mau, and Y. Shao.** 1997. The complete genome sequence of Escherichia coli K-12. Science. **277**(5331)**:**1453-74.
11. **Boyd, D. R., and G. N. Shedrake.** 1998. The dioxygenase-catalyzed Formation of Vicinal *cis*-diols. Natural Product Reports. **15**(3)**:**309-324.
12. **Bradford, M. M.** 1976. A rapid and sensitive method for the quantitation of microgram quantities of protein utilizing the principle of protein-dye binding. Anal. Biochem. **72:**248-254.
13. **Brugna, M., W. Nitschke, M. Asso, B. Guigliarelli, D. Lemesle-Meunier, and C. Schmidt.** 1999. Redox components of cytochrome bc-type enzymes in acidophilic prokaryotes. II. The Rieske protein of phylogenetically distant acidophilic organisms. J Biol Chem. **274**(24)**:**16766-72.
14. **Brzostowicz, P. C., A. B. Reams, T. J. Clark, and E. L. Neidle.** In Press. Transcriptional Cross-Regulation of the Catechol and Protocatechuate Branches of the β-ketoadpiate Pathway Contributes to Carbon-Source

Dependent Expression of the *Acinetobacter* sp. strain ADP1 *pobA* Gene. J. Bacteriol.

15. **Buchan, A.** 2001. University of Georgia, Athens, GA.
16. **Buchan, A., L. S. Collier, E. L. Neidle, and M. A. Moran.** 2000. Key aromatic-ring-cleaving enzyme, protocatechuate 3,4-dioxygenase, in the ecologically important marine Roseobacter lineage. Appl Environ Microbiol. **66**(11)**:**4662-72.
17. **Buchan, A., E. L. Neidle, and M. A. Moran.** 2001. Diversity of the ring-cleaving dioxygenase gene pcaH in a salt marsh bacterial community. Appl Environ Microbiol. **67**(12)**:**5801-9.
18. **Bundy, B. M.** 2001. University of Georgia.
19. **Bundy, B. M., A. L. Campbell, and E. L. Neidle.** 1998. Similarities between the *antABC*-encoded anthranilate dioxygenase and the *benABC*-encoded benzoate dioxygenase of *Acinetobacter* sp. strain ADP1. J. Bacteriol. **180**(17)**:**4466-4474.
20. **Bundy, B. M., L. S. Collier, T. R. Hoover, and E. L. Neidle.** 2002. Synergistic transcriptional activation by one regulatory protein in response to two metabolites. Proc Natl Acad Sci U S A. **99**(11)**:**7693-8.
21. **Butler, C. S., and J. R. Mason.** 1997. Structure-function analysis of the bacterial aromatic ring-hydroxylating dioxygenases. Adv. Micro. Physiol. **38:**47-84.
22. **Carey, F. A.** 1992. Organic chemistry, 2 ed. McGraw-Hill, Inc., New York.

23. **Carredano, E., A. Karlsson, B. Kauppi, D. Choudhury, R. E. Parales, J. V. Parales, K. Lee, D. T. Gibson, H. Eklund, and S. Ramaswamy.** 2000. Substrate binding site of naphthalene 1,2-dioxygenase: functional implications of indole binding. J Mol Biol. **296**(2)**:**701-12.

24. **Chua, C. H., Y. Feng, C. C. Yeo, H. E. Khoo, and C. L. Poh.** 2001. Identification of amino acid residues essential for catalytic activity of gentisate 1,2-dioxygenase from Pseudomonas alcaligenes NCIB 9867. FEMS Microbiol Lett. **204**(1)**:**141-6.

25. **Clark, T. J., C. Momany, and E. L. Neidle.** 2002. The benPK operon, proposed to play a role in transport, is part of a regulon for benzoate catabolism in Acinetobacter sp. strain ADP1. Microbiology. **148**(Pt 4)**:**1213-23.

26. **Coco, W. M., W. E. Levinson, M. J. Crist, H. J. Hektor, A. Darzins, P. T. Pienkos, C. H. Squires, and D. J. Monticello.** 2001. DNA shuffling method for generating highly recombined genes and evolved enzymes. Nat Biotechnol. **19**(4)**:**354-9.

27. **Collier, L. S.** 2000. Ph.D. University of Georgia.

28. **Collier, L. S., G. L. Gaines, III, and E. L. Neidle.** 1998. Regulation of benzoate degradation in *Acinetobacter* sp. strain ADP1 by BenM, a LysR-type transcriptional activator. J. Bacteriol. **180:**2493-2501.

29. **Collier, L. S., N. N. Nichols, and E. L. Neidle.** 1997. *benK* Encodes a Hydrophobic Permease-Like Protein Involved in Benzoate Degradation by *Acinetobacter* sp. Strain ADP1. J. Bacteriol. **179**(18)**:**5943-5946.

30. **Correll, C. C., C. J. Batie, D. P. Ballou, and M. L. Ludwig.** 1992. Phthalate dioxygenase reductase: a modular structure for electron transfer from pyridine nucleotides to [2Fe-2S]. Science. **258**(5088)**:**1604-10.

31. **Cosper, N. J., D. M. Eby, A. Kounosu, N. Kurosawa, E. L. Neidle, D. M. Kurtz, T. Iwasaki, and R. A. Scott.** In Press. Redox-dependent Structural Changes in Archaeal and Bacterial Rieske-type [2Fe-2S] Clusters. Protein Science.

32. **Coulter, E. D., and D. M. Kurtz, Jr.** 2001. A role for rubredoxin in oxidative stress protection in Desulfovibrio vulgaris: catalytic electron transfer to rubrerythrin and two-iron superoxide reductase. Arch Biochem Biophys. **394**(1)**:**76-86.

33. **Cowles, C. E., N. N. Nichols, and C. S. Harwood.** 2000. BenR, a XylS homologue, regulates three different pathways of aromatic acid degradation in Pseudomonas putida. J Bacteriol. **182**(22)**:**6339-46.

34. **Cowles, C. E., N. N. Nichols, and C. S. Harwood.** 2000. BenR, a XylS homologue, regulates three different pathways of aromatic acid degradation in *Pseudomonas putida*. J. Bacteriol. **182**(22)**:**6339-6346.

35. **Dagley, S.** 1986. Biochemistry of Aromatic Hydrocarbon Degradation in Pseudomonads, p. 527-555. *In* J. R. Sokatch (ed.), The Bacteria, vol. 10. Academic Press, Inc., New York.

36. **Dagley, S.** 1978. Microbial catabolism, the carbon cycle and environmental pollution. Naturwissenschaften. **65**(2)**:**85-95.

37. **Dal, S., I. Steiner, and U. Gerischer.** 2002. Multiple operons connected with catabolism of aromatic compounds in Acinetobacter sp. strain ADP1 are under carbon catabolite repression. J Mol Microbiol Biotechnol. **4**(4)**:**389-404.

38. **Danganan, C. E., R. W. Ye, D. L. Daubaras, L. I. Xun, and A. M. Chakrabarty.** 1994. Nucleotide-sequence and functional-analysis of the genes encoding 2,4,5-trichlorophenoxyacetic acid oxygenase in *Pseudomonas-cepecia* AC1100. Appl. Environ. Micro. **60**(11)**:**4100-4106.

39. **D'Argenio, D. A., A. Segura, W. M. Coco, P. V. Bunz, and L. N. Ornston.** 1999. The physiological contribution of Acinetobacter PcaK, a transport system that acts upon protocatechuate, can be masked by the overlapping specificity of VanK. J Bacteriol. **181**(11)**:**3505-15.

40. **Daubaras, D. L., C. E. Danganan, A. Hubner, R. W. Ye, W. Hendrickson, and A. M. Chakrabarty.** 1996. Biodegradation of 2,4,5-trichlorophenoxyacetic acid by *Burkholderia cepacia* strain AC1100: evolutionary insight. Gene. **179:**1-8.

41. **Devereaux, J., P. Haeberli, and O. Smithies.** 1984. A comprehensive set of sequence analysis programs for the VAX. Nuc. Acids Res. **12:**387-395.

42. **DiMarco, A. A., B. Averhoff, and L. N. Ornston.** 1993. Identification of the transcriptional activator *pobR* and characterization of its role in the expression of *pobA*, the structural gene for *p*-hydroxybenzoate hydroxylase in *Acinetobacter calcoaceticus*. J. Bacteriol. **175**(14)**:**4499-4506.

43. **Doten, R. C., K.-L. Ngai, D. J. Mitchell, and L. N. Ornston.** 1987. Cloning and Genetic Organization of the pca Gene Cluster from Acinetobacter calcoaceticus. J. Bact. **169**(7)**:**3168-3174.

44. **Dugad, L. B., G. N. La Mar, L. Banci, and I. Bertini.** 1990. Identification of localized redox states in plant-type two-iron ferredoxins using the nuclear Overhauser effect. Biochemistry. **29**(9)**:**2263-71.

45. **Eby, D. M., Z. M. Beharry, E. D. Coulter, D. M. Kurtz, Jr., and E. L. Neidle.** 2001. Characterization and evolution of anthranilate 1,2-dioxygenase from Acinetobacter sp. strain ADP1. J Bacteriol. **183**(1)**:**109-18.

46. **Edmondson, D. E., and D. B. McCormick (ed.).** 1987. Flavins and Flavoproteins. de Gruyter, Berlin, Germany.

47. **Elsemore, D. A., and L. N. Ornston.** 1994. The pca-pob supraoperonic cluster of Acinetobacter calcoaceticus contains quiA, the structural gene for quinate-shikimate dehydrogenase. J Bacteriol. **176**(24)**:**7659-66.

48. **Eraso, J. M., and S. Kaplan.** 1994. *prrA*, a putative response regulator involved in oxygen regulation of photosynthetic gene expression in *Rhodobacter sphaeroides*. J. Bacteriol. **176:**32-43.

49. **Fee, J. A., K. L. Findling, T. Yoshida, R. Hille, G. E. Tarr, D. O. Hearshen, W. R. Dunham, E. P. Day, T. A. Kent, and E. Munck.** 1984. Purification and characterization of the Rieske iron-sulfur protein from *Thermus thermophilus*. Evidence for a [2Fe-2S] cluster having non-cysteine ligands. J. Biol. Chem. **259**(1)**:**124-133.

50. **Fetzner, S., R. Müller, and F. Lingens.** 1992. Purification and Some Properties of 2-Halobenzoate 1,2-Dioxygenase, a Two-Component Enzyme System from *Pseudomonas cepacia* 2CBS. J. Bacteriol. **174**(1)**:**279-290.

51. **Frost, J. W., J. L. Bender, J. T. Kadonaga, and J. R. Knowles.** 1984. Dehydroquinate synthase from Escherichia coli: purification, cloning, and construction of overproducers of the enzyme. Biochemistry. **23**(19)**:**4470-5.

52. **Furukawa, K.** 2000. Engineering Dioxygenases for Efficient Degradating of Environmental Pollutants. Current Opinion in Biotechnology. **11:**244-249.

53. **Furukawa, K., J. Hirose, S. Hayashida, and K. Nakamura.** 1994. Efficient degradation of trichloroethylene by a hybrid aromatic ring dioxygenase. J Bacteriol. **176**(7)**:**2121-3.

54. **Gaines, G. L., III, L. Smith, and E. L. Neidle.** 1996. Novel nuclear magnetic resonance spectroscopy methods demonstrate preferential carbon source utilization by *Acinetobacter calcoaceticus*. J. Bacteriol. **178:**6833-6841.

55. **Gassner, G. T., D. P. Ballou, G. A. Landrum, and J. W. Whittaker.** 1993. Magnetic Circular Dichroism Studies on the Mononuclear Ferrous Active Site of Phthalate Dioxygenase from Pseudomonas cepacia show a Change of Ligation State on Substrate Binding. Biochemistry. **32:**4820-4825.

56. **Gassner, G. T., M. L. Ludwig, D. L. Gatti, C. C. Correll, and D. P. Ballou.** 1995. Structure and mechanism of the iron-sulfur flavoprotein phthalate dioxygenase reductase. FASEB J. **9:**1411-1418.

57. **Ge, Y., F. H. Vaillancourt, N. Y. Agar, and L. D. Eltis.** 2002. Reactivity of toluate dioxygenase with substituted benzoates and dioxygen. J Bacteriol. **184**(15)**:**4096-103.

58. **Gerischer, U.** 2002. Specific and global regulation of genes associated with the degradation of aromatic compounds in bacteria. J Mol Microbiol Biotechnol. **4**(2)**:**111-21.

59. **Gerischer, U., A. Segura, and L. N. Ornston.** 1998. PcaU, a transcriptional activator of genes for protocatechuate utilization in Acinetobacter. J Bacteriol. **180**(6)**:**1512-24.

60. **Gibson, D. T., and R. E. Parales.** 2000. Aromatic Hydrocarbon Dioxygenases in Environmental Biotechnology. Current Opinion in Biotechnology. **11:**236-243.

61. **Gibson, D. T., and V. Subramanian.** 1984. Microbial degradation of aromatic hydrocarbons, p. 181-252. *In* D. T. Gibson (ed.), Microbial degradation of organic compounds. Marcel Dekker, Inc., New York.

62. **Gorsky, L. D., D. R. Koop, and M. J. Coon.** 1984. On the stoichiometry of the oxidase and monooxygenase reactions catalyzed by liver microsomal cytochrome P-450. Products of oxygen reduction. J Biol Chem. **259**(11)**:**6812-7.

63. **Gralton, B., A. L. Campbell, A. L. English, and E. L. Neidle.** 1996. A physical and genetic map of *Acinetobacter calcoaceticus* strain ADP1(BD413), abstr. H-45. *In* Abstracts of the General Meeting of the American Society for Microbiology 1996. American Society for Microbiology, Washington D.C.

64. **Haak, B., S. Fetzner, and F. Lingens.** 1995. Cloning, Nucleotide Sequence, and Expression of the Plasmid-Encoded Genes for the Two-Component 2-Halobenzoate 1,2-Dioxygenase from *Pseudomonas cepacia* 2CBS. J. Bacteriol. **177**(3)**:**667-675.

65. **Harayama, S.** 1998. Artificial evolution by DNA shuffling. Trends Biotechnol. **16**(2)**:**76-82.

66. **Harayama, S., M. Kok, and E. L. Neidle.** 1992. Functional and evolutionary relationships among diverse oxygenases. Ann. Rev. Microbiol. **46:**565-601.

67. **Harayama, S., M. Rekik, A. Bairoch, E. L. Neidle, and L. N. Ornston.** 1991. Potential DNA slippage structures acquired during evolutionary divergence of *Acinetobacter calcoaceticus* chromosomal *benABC* and *Pseudomonas putida* TOL pWW0 plasmid *xylXYZ*, genes encoding benzoate dioxygenases. J. Bacteriol. **173**(23)**:**7540-7548.

68. **Harayama, S., M. Rekik, and K. N. Timmis.** 1986. Genetic analysis of a relaxed substrate specificity aromatic ring dioxygenase, toluate 1,2-dioxygenase, encoded by TOL plasmid pWW0 of *Pseudomonas putida*. Mol. Gen. Genet. **202:**226-234.

69. **Hartnett, C., E. L. Neidle, K. L. Ngai, and L. N. Ornston.** 1990. DNA sequences of genes encoding Acinetobacter calcoaceticus protocatechuate 3,4-dioxygenase: evidence indicating shuffling of genes and of DNA sequences within genes during their evolutionary divergence. J Bacteriol. **172**(2)**:**956-66.

70. **Harwood, C. S., N. N. Nichols, M. Kim, J. L. Ditty, and R. E. Parales.** 1994. Identification of the *pcaRKF* gene cluster from *Pseudomonas putida*: Involvement in chemotaxis, biodegradation, and transport of 4-hydroxybenzoate. J.Bacteriol. **176:**6479-6488.

71. **Harwood, C. S., and R. E. Parales.** 1996. The β-ketoadipate pathway and the biology of self-identity. Annu. Rev. Microbiol. **50:**In Press.

72. **Harwood, C. S., and R. E. Parales.** 1996. The ß-ketoadipate pathway and the biology of self-identity. Annu. Rev. Microbiol. **50:**553-590.

73. **Hayaishi, O., and R. Y. Stanier.** 1951. Bacterial oxidation of tryptophan. J. Bacteriol. **62:**691-709.

74. **Hayashi, T., K. Makino, M. Ohnishi, K. Kurokawa, K. Ishii, K. Yokoyama, C. G. Han, E. Ohtsubo, K. Nakayama, T. Murata, M. Tanaka, T. Tobe, T. Iida, H. Takami, T. Honda, C. Sasakawa, N. Ogasawara, T. Yasunaga, S. Kuhara, T. Shiba, M. Hattori, and H. Shinagawa.** 2001. Complete genome sequence of enterohemorrhagic Escherichia coli O157:H7 and genomic comparison with a laboratory strain K-12. DNA Res. **8**(1)**:**11-22.

75. **Hou, C. T., M. O. Lillard, and R. D. Schwartz.** 1976. Protocatechuate 3, 4-dioxygenase from Acinetobacter calcoaceticus. Biochemistry. **15**(3)**:**582-8.

76. **Hudlicky, T., D. Gonzalez, and D. T. Gibson.** 1999. Enzymatic Dihydroxylation of Aromatics in Enantioselective Synthesis: Expanding Asymmetric Methodiology. Aldrichimica Acta. **32**(2)**:**35-62.

77. **Hugo, N., J. Armengaud, J. Gaillard, K. N. Timmis, and Y. Jouanneau.** 1998. A novel [2Fe-2S] ferredoxin from *Pseudomonas putida* mt2 promotes the reductive reactivation of catechol 2,3-dioxygenase. J. Biol. Chem. **273**(16)**:**9622-9629.

78. **Hunger, M., R. Schmucker, V. Kishan, and W. Hillen.** 1990. Analysis and nucleotide sequence of an origin of DNA replication in *Acinetobacter calcoaceticus* and its use for *Escherichia coli*shuttle plasmids. Gene. **87:**45-51.

79. **Hurtubise, Y., D. Barriault, and M. Sylvestre.** 1998. Involvement of the terminal oxygenase beta subunit in the biphenyl dioxygenase reactivity pattern toward chlorobiphenyls. J Bacteriol. **180**(22)**:**5828-35.

80. **Ichihara, A., K. Adachi, K. Hosokawa, and Y. Takeda.** 1962. Enzymatic hydroxylation of aromatic carboxylic acids; substrate specificities of anthranilate and benzoate oxidases. J. Biol. Chem. **237:**2296-2302.

81. **Innis, M. A., D. H. Gelfand, J. J. Sninsky, and T. J. White.** 1990. PCR Protocols: A Guide to Methods and Applications. Academic Press, San Diego, CA.

82. **Iwasaki, T., Y. Isogai, T. Iizuka, and T. Oshima.** 1995. Sulredoxin: a novel iron-sulfur protein of the thermoacidophilic archaeon Sulfolobus sp. strain 7 with a Rieske-type [2Fe-2S] center. J Bacteriol. **177**(9)**:**2576-82.

83. **Jaffe, E. K., and G. D. Markham.** 1988. 13C NMR studies of methylene and methine carbons of substrate bound to a 280,000-dalton protein, porphobilinogen synthase. Biochemistry. **27**(12)**:**4475-81.

84. **Janion, C., and D. Shugar.** 1968. Studies on possible mechanisms of hydroxylamine mutagenesis. Acta Biochim Pol. **15**(1)**:**107-21.

85. **Jiang, H., R. E. Parales, and D. T. Gibson.** 1999. The alpha subunit of toluene dioxygenase from Pseudomonas putida F1 can accept electrons from reduced FerredoxinTOL but is catalytically inactive in the absence of the beta subunit. Appl Environ Microbiol. **65**(1)**:**315-8.

86. **Jones, R. M., L. S. Collier, E. L. Neidle, and P. A. Williams.** 1999. *areABC* Genes Determine the Catabolism of Aryl Esters in *Acinetobacter* sp. Strain ADP1. J. Bacteriol. **181**(15)**:**4568-4575.

87. **Jones, R. M., V. Pagmantidis, and P. A. Williams.** 2000. *sal* Genes Determining the Catabolism of Salicylate Esters Are Part of a Supraoperonic Cluster of Catabolic Genes in *Acinetobacter* sp. Strain ADP1. J. Bacteriol. **182**(7)**:**2018-2025.

88. **Jones, R. M., and P. A. Williams.** 2001. *areCBA* Is an Operon in *Acinetobacter* sp. Strain ADP1 and Is Controlled by AreR, a σ^{54}–Dependent Regulator. J. Bacteriol. **183**(1)**:**405-409.

89. **Juni, E.** 1972. Interspecies Transformation of Acinetobacter: Genetic Evidence for a Ubiquitous Genus. J. Bact. **112**(2)**:**917-931.

90. **Juni, E., and A. Janik.** 1969. Transformation of *Acinetobacter calco-aceticus (Bacterium anitratum)*. J. Bacteriol. **98:**281-288.

91. **Kadkhodayan, S., E. D. Coulter, D. M. Maryniak, T. A. Bryson, and J. H. Dawson.** 1995. Uncoupling oxygen transfer and electron transfer in the oxygenation of camphor analogues by cytochrome P450-CAM. Direct observation of an intermolecular isotope effect for substrate C-H activation. J Biol Chem. **270**(47)**:**28042-8.

92. **Karlsson, A., Z. M. Beharry, D. M. Eby, E. D. Coulter, E. L. Neidle, D. M. Kurtz, Jr., H. Eklund, and S. Ramaswamy.** 2002. X-ray crystal structure of benzoate 1,2-dioxygenase reductase from Acinetobacter sp. strain ADP1. J Mol Biol. **318**(2)**:**261-72.

93. **Karplus, P. A., and G. E. Schulz.** 1987. Refined structure of glutathione reductase at 1.54 A resolution. J Mol Biol. **195**(3)**:**701-29.

94. **Kauppi, B., K. Lee, E. Carredano, R. E. Parales, D. T. Gibson, H. Eklund, and S. Ramaswamy.** 1998. Structure of an aromatic-ring-hydroxylating dioxygenase- naphthalene 1,2-dioxygenase. Structure. **6:**571-586.

95. **Kimura, N., A. Nishi, M. Goto, and K. Furukawa.** 1997. Functional analyses of a variety of chimeric dioxygenases constructed from two biphenyl dioxygenases that are similar structurally but different functionally. J Bacteriol. **179**(12)**:**3936-43.

96. **Kirk, T. K., T. Higuchi, and H. Chang (ed.).** 1978. Lignin Biodegradation: Microbiology, Chemistry, and Potential Applications, vol. I. CRC Press Inc., Boca Raton, FL.

97. **Kirk, T. K., T. Higuchi, and H. Chang (ed.).** 1978. Lignin Biodegradation: Microbiology, Chemistry, and Potential Applications, vol. 2. CRC Press, Inc., Boca Raton, FL.

98. **Kok, R. G., D. A. D'Argenio, and L. N. Ornston.** 1997. Combining localized PCR mutagenesis and natural transformation in direct genetic analysis of a transcriptional regulator gene, pobR. J Bacteriol. **179**(13)**:**4270-6.

99. **Kok, R. G., D. A. D'Argenio, and L. N. Ornston.** 1998. Mutation analysis of PobR and PcaU, closely related transcriptional activators in acinetobacter. J Bacteriol. **180**(19)**:**5058-69.

100. **Kok, R. G., D. M. Young, and L. N. Ornston.** 1999. Phenotypic expression of PCR-generated random mutations in a Pseudomonas putida gene after its introduction into an Acinetobacter chromosome by natural transformation. Appl Environ Microbiol. **65**(4)**:**1675-80.

101. **Kuila, D., and J. A. Fee.** 1986. Evidence for a redox-linked ionizable group associated with the [2Fe- 2S] cluster of Thermus Rieske protein. J Biol Chem. **261**(6)**:**2768-71.

102. **Kurkela, S., H. Lehvaslaiho, E. T. Palva, and T. H. Teeri.** 1988. Cloning, nucleotide-sequence and characterization of genes encoding naphthalene dioxygenase of *Pseudomonas putida* strain NCIB9816. Gene. **73:**355-362.

103. **Kurtz, D. M.** 1998. Structure of an aromatic-ring-hydroxylating dioxygenase - naphthalene 1,2-dioxygenase. Chemtracts. **6:**571.

104. **Lee, K.** 1999. Benzene-induced uncoupling of naphthalene dioxygenase activity and enzyme inactivation by production of hydrogen peroxide. J. Bacteriol. **181**(9)**:**2719-2725.

105. **Link, T. A., W. R. Hagen, A. J. Pierik, C. Assmann, and G. von Jagow.** 1992. Determination of the redox properties of the Rieske [2Fe-2S] cluster of bovine heart bc1 complex by direct electrochemistry of a water-soluble fragment. Eur J Biochem. **208**(3)**:**685-91.

106. **Link, T. A., O. M. Hatzfeld, P. Unalkat, J. K. Shergill, R. Cammack, and J. R. Mason.** 1996. Comparison of the "Rieske" [2Fe-2S] center in the bc1 complex and in bacterial dioxygenases by circular dichroism spectroscopy and cyclic voltammetry. Biochemistry. **35**(23)**:**7546-52.

107. **Mampel, J., J. Ruff, F. Junker, and A. M. Cook.** 1999. The oxygenase component of the 2-aminobenzenesulfonate dioxygenase system from *Alcaligenes* sp. strain O-1. Microbiology. **145:**3255-3264.

108. **Martin, V. J. J., and W. W. Mohn.** 1999. A novel aromatic-ring-hydroxylating dioxygenase from the diterpeniod-degradating bacterium *Pseudomonas abietaniphila* BKME-9. J. Bacteriol. **181**(9)**:**2675-2682.

109. **Mason, J. R., and R. Cammack.** 1992. The Electron-transport proteins of hydroxylating bacterial dioxygenases. Annu. Rev. Microbiol. **46:**277-305.

110. **Minkin, V. I., M. N. Glukhovtsev, and B. Y. Simkin.** 1994. Aromaticity and Antiaromaticity. John Wiley & Sons, Inc., New York, NY.

111. **Mondello, F. J., M. P. Turcich, J. H. Lobos, and B. D. Erickson.** 1997. Identification and modification of biphenyl dioxygenase sequences that determine the specificity of polychlorinated biphenyl degradation. Appl Environ Microbiol. **63**(8)**:**3096-103.

112. **Moore, J. C., and F. H. Arnold.** 1996. Directed evolution of a para-nitrobenzyl esterase for aqueous-organic solvents. Nat Biotechnol. **14**(4)**:**458-67.

113. **Moore, J. C., H. M. Jin, O. Kuchner, and F. H. Arnold.** 1997. Strategies for the in vitro evolution of protein function: enzyme evolution by random recombination of improved sequences. J Mol Biol. **272**(3)**:**336-47.

114. **Neidle, E. L., C. Hartnett, and L. N. Ornston.** 1989. Characterization of *Acinetobacter calcoaceticus catM*, a repressor gene homologous in sequence to transcriptional activator genes. J. Bacteriol. **171**(10)**:**5410-5421.

115. **Neidle, E. L., C. Hartnett, L. N. Ornston, A. Bairoch, M. Rekik, and S. Harayama.** 1991. Nucleotide Sequence of the Acinetobacter calcoaceticus benABC genes for Benzoate 1,2-Dioxygenase reveal evolutionary relationships among Multicomponent Oxygenases. J. Bact. **173**(17)**:**5385-5395.

116. **Neidle, E. L., C. Hartnett, L. N. Ornston, A. Bairoch, M. Rekik, and S. Harayama.** 1991. Nucleotide sequences of the *Acinetobacter calcoaceticus benABC* genes for benzoate 1,2-dioxygenase reveal

evolutionary relationships among multicomponent oxygenases. J. Bacteriol. **173:**5385-5395.

117. **Neidle, E. L., and L. N. Ornston.** 1986. Cloning and Expression of the *Acinetobacter calcoaceticus* catechol 1,2-dioxygenase structural gene *catA* in *Escherichia coli*. J. Bacteriol. **165:**557-563.

118. **Neidle, E. L., M. Shapiro, and L. N. Ornston.** 1987. Cloning and expression in *Escherichia coli* of *Acinetobacter calcoaceticus* genes for benzoate degradation. J. Bacteriol. **169:**5496-5503.

119. **Nichols, N. N., and C. S. Harwood.** 1997. PcaK, a high-affinity permease for the aromatic compounds 4-hydroxybenzoate and protocatechuate from *Pseudomonas putida*. J Bacteriol. **179**(16)**:**5056-5061.

120. **Nomura, Y., M. Nakagawa, N. Ogawa, S. Harashima, and Y. Oshima.** 1992. Genes in PHT plasmid encoding the initial degradation pathway of phthalate in *Pseudomonas putida*. J. Ferment. Bioeng. **74:**333-344.

121. **Ornston, L. N., and E. L. Neidle.** 1991. Evolution of genes for the β-ketoadipate pathway in *Acinetobacter calcoaceticus*, p. 201-237. *In* K. J. Towner, E. Bergogne-Berezin, and C. A. Fewson (ed.), The biology of *Acinetobacter*. Plenum Press, New York.

122. **Ornston, L. N., and R. Y. Stanier.** 1966. The Conversion of Catechol and Protocatechuate to ß-Ketoadipate by Pseudomonas putida. JBC. **241**(16)**:**3776-3786.

123. **Pai, E. F., P. A. Karplus, and G. E. Schulz.** 1988. Crystallographic analysis of the binding of NADPH, NADPH fragments, and NADPH analogues to glutathione reductase. Biochemistry. **27**(12)**:**4465-74.

124. **Parales, J. V., R. E. Parales, S. M. Resnick, and D. T. Gibson.** 1998. Enzyme specificity of 2-nitrotoluene 2,3-dioxygenase from Pseudomonas sp. strain JS42 is determined by the C-terminal region of the alpha subunit of the oxygenase component. J Bacteriol. **180**(5)**:**1194-9.

125. **Parales, R. E., M. D. Emig, N. A. Lynch, and D. T. Gibson.** 1998. Substrate specificities of hybrid naphthalene and 2,4-dinitrotoluene dioxygenase enzyme systems. J Bacteriol. **180**(9)**:**2337-44.

126. **Parales, R. E., K. Lee, S. M. Resnick, H. Jiang, D. J. Lessner, and D. T. Gibson.** 2000. Substrate specificity of naphthalene dioxygenase: effect of specific amino acids at the active site of the enzyme. J Bacteriol. **182**(6)**:**1641-9.

127. **Parales, R. E., J. V. Parales, and D. T. Gibson.** 1999. Aspartate 205 in the catalytic domain of naphthalene dioxygenase is essential for activity. J Bacteriol. **181**(6)**:**1831-7.

128. **Parales, R. E., S. M. Resnick, C. L. Yu, D. R. Boyd, N. D. Sharma, and D. T. Gibson.** 2000. Regioselectivity and enantioselectivity of naphthalene dioxygenase during arene cis-dihydroxylation: control by phenylalanine 352 in the alpha subunit. J Bacteriol. **182**(19)**:**5495-504.

129. **Patel, R. N., C. T. Hou, A. Felix, and M. O. Lillard.** 1976. Catechol 1,2-dioxygenase from Acinetobacter calcoaceticus: purification and properties. J Bacteriol. **127**(1)**:**536-44.

130. **Petersen, E., J. Zuegg, D. W. Ribbons, and H. Schwab.** 1996. Molecular cloning and homology modeling of protocatechuate 3,4-dioxygenase from Pseudomonas marginata. Microbiol Res. **151**(4)**:**359-70.

131. **Pieper, D. H., and W. Reineke.** 2000. Engineering Bacteria for Bioremediation. Current Opinion in Biotechnology. **11:**262-270.

132. **Powlowski, J. B., S. Dagley, V. Massey, and D. P. Ballou.** 1987. Properties of anthranilate hydroxylase (deaminating), a flavoprotein from *Trichosporon cutaneum*. J. Biol. Chem. **262**(1)**:**69-74.

133. **Que, L., and R. Y. Y. Ho.** 1996. Dioxygen activation by enzymes with mononuclear non-heme iron active sites. Chem. Rev. **96:**2607-2624.

134. **Reams, A. B., and E. L. Neidle.** In Press. Genome Plasticity in Acinetobacter: New Degradative Capabilities Acquired by Spontaneous Amplification of Large Chromoosomal Segments. Molecular Microbiology.

135. **Reineke, W.** 1998. Development of hybrid strains for the mineralization of chloroaromatics by patchwork assembly. Annu Rev Microbiol. **52:**287-331.

136. **Riedel, A., S. Fetzner, M. Rampp, F. Lingens, U. Liebl, J. L. Zimmermann, and W. Nitschke.** 1995. EPR, electron spin echo envelope modulation, and electron nuclear double resonance studies of the 2Fe2S

centers of the 2-halobenzoate 1,2- dioxygenase from Burkholderia (Pseudomonas) cepacia 2CBS. J Biol Chem. **270**(52)**:**30869-73.

137. **Romero-Arroyo, C. E., M. A. Schell, G. L. Gaines III, and E. L. Neidle.** 1995. *catM* encodes a LysR-type transcriptional activator regulating catechol degradation in *Acinetobacter calcoaceticus*. J. Bacteriol. **177:**5891-5898.

138. **Sakamoto, T., J. M. Joern, A. Arisawa, and F. H. Arnold.** 2001. Laboratory evolution of toluene dioxygenase to accept 4-picoline as a substrate. Appl Environ Microbiol. **67**(9)**:**3882-7.

139. **Sambrook, J., E. F. Fritsch, and T. Maniatis.** 1989. Molecular Cloning: A Laboratory Manual. Cold Spring Harbor Laboratory Press, Cold Spring Harbor.

140. **Sambrook, J., E. F. Fritsch, and T. Maniatis.** 1989. Molecular cloning: a laboratory manual, 2nd ed. Cold Spring Harbor Laboratory Press, Cold Spring Harbor, N. Y.

141. **Schagger, H., and G. VonJagow.** 1987. Tricine sodium dodecyl-sulfate polyacrylamide gel electrophoresis for the separation of proteins in the range from 1-kDa to 100-kDa. Analytical Biochem. **166:**368-379.

142. **Schirmer, F., S. Ehrt, and W. Hillen.** 1997. Expression, Inducer Spectrum, Domain Structure, and Function of MopR, the Regulator of Phenol Degradation in *Acinetobacter calcoaceticus* NCIB8250. J. Bac. **179**(4)**:**1329-1336.

143. **Segura, A., P. V. Bunz, D. A. D'Argenio, and L. N. Ornston.** 1999. Genetic Analysis of a Chromosomal Region Containing vanA and vanB, Genes Required for Conversion of Either Ferulate or Vanillate to Protocatechuate in Acinetobacter. J. Bacteriol. **181**(11)**:**3494-3504.

144. **Shafikhani, S., R. A. Siegel, E. Ferrari, and V. Schellenberger.** 1997. Generation of large libraries of random mutants in Bacillus subtilis by PCR-based plasmid multimerization. Biotechniques. **23**(2)**:**304-10.

145. **Shanley, M. S., E. L. Neidle, R. E. Parales, and L. N. Ornston.** 1986. Cloning and expression of *Acinetobacter calcoaceticus catBCDE* genes in *Pseudomonas putida* and *Escherichia coli*. J. Bacteriol. **165**(2)**:**557-563.

146. **Stanier, R. Y., and J. L. Ingraham.** 1954. Protocatechuic acid oxidase. J . Biol. Chem. **210:**799-808.

147. **Subramanian, V., M. Sugumaran, and C. S. Vaidyanathan.** 1979. Anthranilate hydroxylase, an iron enzyme, from *Aspergillus niger*. Indian J. Biochem. Biophys. **16**(6)**:**370-374.

148. **Subramanian, V., and C. S. Vaidyanathan.** 1984. Anthranilate hydroxylase from *Aspergillus niger*: new type of NADPH-linked nonheme iron monooxygenase. J. Bacteriol. **160**(2)**:**651-655.

149. **Suyama, A., R. Iwakiri, N. Kimura, A. Nishi, K. Nakamura, and K. Furukawa.** 1996. Engineering hybrid pseudomonads capable of utilizing a wide range of aromatic hydrocarbons and of efficient degradation of trichloroethylene. J Bacteriol. **178**(14)**:**4039-46.

150. **Timmis, K. N., and D. H. Pieper.** 1999. Bacteria designed for bioremediation. Trends in Biotechnology. **17:**201-204.

151. **Trautwein, G., and U. Gerischer.** 2001. Effects exerted by transcriptional regulator PcaU from Acinetobacter sp. strain ADP1. J Bacteriol. **183**(3)**:**873-81.

152. **Trumpower, B. L.** 1990. Cytochrome bc_1 complexes of microorganisms. Microbiol. Rev. **54:**101-129.

153. **Tsang, H.-T., C. J. Batie, D. P. Ballou, and J. E. Penner-Hahn.** 1996. Structural characterization of the mononuclear iron site in Pseudomonas cepacia DB01 phthalate diocygenase using X-ray absorption spectroscopy. J. Biol. Inorg. Chem. **1:**24-33.

154. **Williams, P. A., and K. Murray.** 1974. Metabolism of benzoate and the methylbenzoates by *Pseudomonas putida (arvilla)* mt-2: Evidence for the existence of a TOL plasmid. J. Bacteriol. **120**(1)**:**416-423.

155. **Wolfe, M. D., D. J. Altier, A. Stubna, C. V. Popescu, E. Munck, and J. D. Lipscomb.** 2002. Benzoate 1,2-dioxygenase from Pseudomonas putida: single turnover kinetics and regulation of a two-component Rieske dioxygenase. Biochemistry. **41**(30)**:**9611-26.

156. **Wolfe, M. D., J. V. Parales, D. T. Gibson, and J. D. Lipscomb.** 2001. Single turnover chemistry and regulation of O2 activation by the oxygenase component of naphthalene 1,2-dioxygenase. J Biol Chem. **276**(3)**:**1945-53.

157. **Yamaguchi, M., and H. Fujisawa.** 1980. Purification and characterization of an oxygenase component in benzoate 1,2-oxygenase system from *Pseudomonas arvilla* C-1. J. Biol. Chem. **255**(11)**:**5058-5063.

158. **Yanisch-Perron, C., J. Vieira, and J. Messing.** 1985. Improved M13 phage cloning vectors and host strains: nucleotide sequences of the M13mp18 and pUC19 vectors. Gene. **33:**103-119.

159. **Young, D. M., R. G. Kok, and L. N. Ornston.** 2002. Phenotypic expression of polymerase chain reaction-generated random mutations in a foreign gene after its introduction into an Acinetobacter chromosome by natural transformation. Methods Mol Biol. **182:**103-15.

160. **Young, D. M., D. Parke, D. A. D'Argenio, M. A. Smith, and L. N. Ornston.** 2001. Evolution of a Catabolic Pathway. ASM News. **67**(7)**:**362-369.

161. **Zhang, C., M. Huang, and B. W. Holloway.** 1993. Mapping of *ben* genes of *Pseudomonas aeruginosa*. FEMS Micro. Letters. **112:**255-260.

162. **Zhang, C., M. Huang, and B. W. Holloway.** 1993. Mapping of the *ben, ant*, and *cat* genes of *Pseudomonas aeruginosa* and evolutionary relationship of the ben region of *P. aeruginosa* and *P. putida*. FEMS Micro. Letters. **108:**303-310.